2024-01-2096 Published 09 Apr 2024

Ultra-Downsizing of ICEs Based on True Atkinson Cycle Implementations. Thermodynamic Analysis and Comparison on the Indicated Fuel Conversion Efficiency of Atkinson and Classical ICE Cycles

Victor Gheorghiu Hamburg University of Applied Sciences

Citation: Gheorghiu, V., "Ultra-Downsizing of ICEs Based on True Atkinson Cycle Implementations. Thermodynamic Analysis and Comparison on the Indicated Fuel Conversion Efficiency of Atkinson and Classical ICE Cycles," SAE Technical Paper 2024-01-2096, 2024, doi:10.4271/2024-01-2096.

Received: 25 Oct 2023 Revised: 03 Feb 2024 Accepted: 04 Feb 2024

Abstract

Ultra-Downsizing (UD) was introduced as an even higher level of downsizing for Internal Combustion Engines ICEs, see [2] SAE 2015-01-1252.

The introduction of Ultra Downsizing (UD) aims to enhance the power, efficiency, and sustainability of ICEs while maintaining the thermal and mechanical strain within acceptable limits. The following approaches are utilized:

1. **True** Atkinson Cycles are implemented utilizing an asymmetrical crank mechanism called Variable Compression and Stroke Ratios (VCSR). This mechanism allows for extended expansion stroke and continuous adjustment of the Volumetric Compression Ratio (VCR).
2. Unrestricted two or more stage high-pressure turbocharging and intensive intercooling: This setup enables more complete filling of the cylinder and reduces the compression work on the piston, resulting in higher specific power and efficiency.
3. The new Load Control (LC) approach is based to continuous VCR adjustment. By adjusting the VCR without resorting to excessive throttling or external Exhaust Gas Recirculation (EGR), a stoichiometric Air Fuel Ratio (AFR) can be maintained. This facilitates easier exhaust gas aftertreatment using a three-way catalyst.
4. Fuel Flexibility: The continuous VCR adaptation capability enables the engine to operate in multi-fuel mode. In addition to gasoline or diesel, the engine can also run on alternative fuels like pure hydrogen (H_2) or H_2 blended with gases like CNG, Biogas, e-fuels, or even ammonia (NH_3). This versatility allows for reduced carbon emissions and increased sustainability.

By combining these approaches, the UD concept aims to achieve higher power output, improved efficiency, and reduced environmental impact in ICEs, all while ensuring the durability and strength of engine components remain within acceptable limits.

The thermodynamic analysis is done separately for **ideal** and **real** cycles in order to determine the Indicated Fuel Conversion Efficiency (IFCE), formulaically (for ideal cycles) and quantitatively (for real cycles).

AVL BOOST © is used to simulate the **real** cycles (within cylinder and turbocharger) and MATLAB © to process the simulation results.

Introduction

The conventional reciprocating engine, also known as the internal combustion engine (ICE), has undergone significant advancements and refinements over the past century, particularly in terms of efficiency. However, as the engine has evolved, the incremental gains in efficiency have become smaller, approaching the limits set by the theoretical ideal processes.

Currently, the challenge is to achieve significant efficiency improvements in the area of conventional combustion engines in order to reduce CO_2 emissions, with further significant CO_2 reductions to be achieved using carbon-free fuels. To achieve significantly higher efficiency levels, it is necessary to reevaluate the current working processes employed by ICEs. This reevaluation may involve exploring alternative working cycles, such as the

Atkinson cycle or other advanced combustion concepts, as well as incorporating new technologies like hybridization of the vehicle drive systems. However, by rethinking the fundamental work processes of internal combustion engines, significant progress can be made in improving their efficiency, fuel flexibility and thus sustainability.

The concept of using an Atkinson cycle in internal combustion engines as an alternative to the classic Otto cycle is not a new idea for improving the indicated fuel conversion efficiency (IFCE). Throughout the development of internal combustion engines, there has been a long-standing goal of expanding the combustion gases as much as possible to ambient pressure (state 5* in Fig. 1) to maximize the work output during the expansion stroke and ultimately achieve the highest IFCE.

When analyzing the **true** Atkinson **ideal** cycle, it is found that the true Atkinson cycle results from the overlapping of classical ideal Otto ICE and gas turbine Brayton cycles, where the common parts of both cycles merge.

In the **true** Atkinson cycle, a significant portion of the specific work released by the turbine to drive the compressor to compress the air from the ambient state to the pre-compression state can be recovered. This specific work acts as internal heat recovery, effectively recovering some of the energy and improving overall efficiency. The geometrical compression stroke in the **true** Atkinson cycle is shortened and commences from this pre-compression state. This compression stroke reduction is significant because it reduces the piston mechanical work consumed for compression. The part of the piston stroke dedicated to pre-compression in classical ICEs can be eliminated if **true** Atkinson cycles are used instead, resulting in significant improvements in efficiency and engine performance.

FIGURE 1 Pressure-volume diagrams above for overexpanded engine cycle (1234561) and classical Atkinson cycle (1235*61) according to [1] as well as the two other variants shown below.

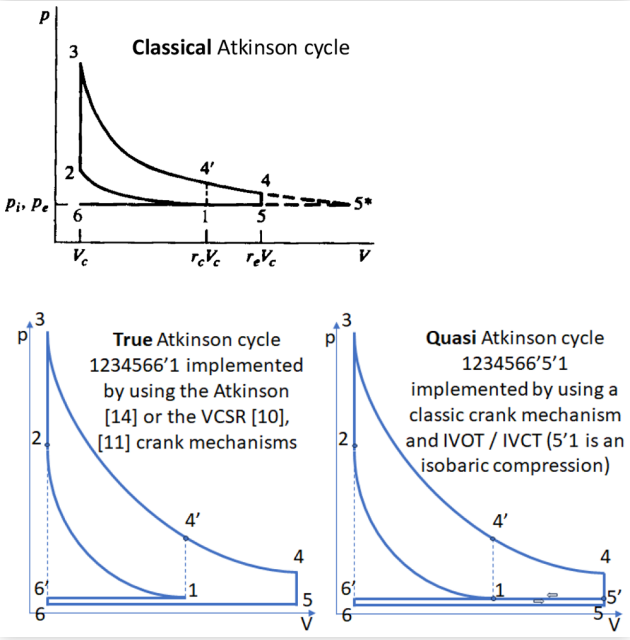

The designation **true** Atkinson cycle is underpinned by the identical piston strokes (i.e. short for intake & compression respective long for expansion & exhaust) of the crank drives patented by Atkinson and the author, in which the pre-compression stroke 51 from Fig. 1 is missing. For a simple comparison, see the animations [15, 16].

In order to make a proper comparison of the efficiencies of the **ideal** Otto (O) and **true** Atkinson (A) cycles, certain parameters such as VCR, isentropic exponent κ, stoichiometric AFR, and pressure rise ratio δ_p during combustion should be kept identical in both cycles. As a result, on the one hand, the compression and expansion curves of the cycles will overlap, but on the other hand, different amounts of heat will be released during combustion in each cycle.

The variations in heat release have a direct impact on the overall efficiency of the A cycles. Therefore, when comparing the efficiencies of the O and A cycles, it is important to remark both the overlapping curves and the differences in heat release during combustion.

The thermodynamic analysis of **real** cycles additionally takes into account the gas mass variation during the cycles and has the following objectives:

1. Verification of IFCE estimates from the analysis of **ideal** cycles.
2. Demonstration of the ultra downsizing UD load control LC, based in particular on the adjustment of the volumetric compression ratio VCR.
3. Because of the gas mass variation in the **real** cycles, the classical temperature, specific entropy T,s -diagram is not meaningful during the gas exchange processes.
4. Temperature, entropy flow, T,dS/dt-diagram, as a new analysis tool, is introduced instead of classical T,s-diagram, thermodynamically justified, evaluated and applied accordingly.

According to Heywood [1] (1988), the pressure-volume diagram for the overexpanded engine cycle (1234561) and the Atkinson cycle (1235*61, full expansion state is 5*) for unthrottled operation of a naturally aspirated engine with isochoric heat release are shown above in the top of Fig. 1 (original Fig. 5-11 from [1] page 184).

In this r_c and r_e are the volumetric compression and expansion ratios, respectively. In the Atkinson cycle shown in the top of Fig. 1, full expansion occurs within the cylinder up to the exhaust pressure p_e (state resp. point 5*) equal to the ambient pressure.

Note that the crank mechanism patented by Atkinson [14] as well as the crank mechanisms patented by the author [10, 11] cannot guarantee full expansion up to the ambient pressure (state 5*, see top of Fig. 1), but only geometrically true overexpanded motor cycles.

While the Atkinson cycle or overexpanded cycles have the potential to improve efficiency, they also come with certain drawbacks. One disadvantage is the reduced specific power output, measured in [kW/dm^3], due to the

shortened intake stroke (in Fig. 1 from point 6 to 1) and the resulting lower intake mass, as well as the extended expansion stroke, which increases the dimensions and weight of the engines. In addition, these cycles usually require a higher mechanical complexity of the crank mechanism. The same situation is known from Stirling engines. For these reasons, the implementation of Atkinson cycles in NA engines, as presented in the top of Fig. 1, does not make sense. Turbocharging (TC) of these engines is absolutely necessary to increase the specific power particularly strongly without degrading IFCE as shown in the bottom of Fig. 1 for **True** Atkinson cycles. See IFCE and IMEP curves from Fig. A2-EOPs-01-15 in Appendix 2.

At this point, the notion of displacement volume and the comparison criteria for IFCE of ICE cycles need to be defined to avoid ambiguity. These specifications are necessary because the compression and expansion strokes as well as the compression and expansion ratios are different.

The displacement volume should indeed indicate the available volume for the aspirated gas mass. For example, the specific engine output in [kW/dm^3], [kW/liter] etc. is based on this.

An alternative definition of the displacement volume via the largest piston stroke, in this case the expansion, has no basis in engine technology.

The definition of displacement volume serves multiple purposes, including vehicle taxation, engine categorization, and performance comparisons. However, it is important to recognize that the notion of displacement volume is more than an agreement or convention. This definition must apply to all engines, regardless of whether they use the classic, true Atkinson or overexpanded cycle.

The term “classic Atkinson cycles” refers to the Atkinson (1235*61), where 5* denotes the state of full expansion up to the ambient pressure and overexpanded (1234561) engine cycles from the upper part of Fig. 1 according to Heywood, which is also referred to here as (H) Atkinson cycle, or H cycle for short. The classic Atkinson cycle according to Heywood corresponds to that of an unthrottled **naturally aspirated** engine, so that the pressures in states 1, 5, 6 are identical to the ambient pressure. This cycle is treated here because its IFCE formula (5.55) appears in the bellow IFCE discussion. Although Heywood does not specify whether he developed the formula (5.55) for an ICE with a classical or an Atkinson crank mechanism, the basic formula (5.54) of formula (5.55) shows that the work consumed for the isobaric partial compression 51 is subtracted, i.e. is present. That means that the formula (5.55) has been developed for an ICE with a classic crank mechanism and therefore also applies to the Quasi Atkinson cycle of a **supercharged** ICE, which is shown in Fig. 1 bottom right and described below.

This terminology is used to distinguish it from the two current variants shown in the lower part of Fig. 1 and described below:

a. **Quasi** Atkinson cycles refer to the simulated cycles that attempt to replicate the characteristics of an overexpanded cycle by adjusting the intake valve closing time (IVCT) while using classic crankshafts. In these cycles, the piston strokes have equal lengths, but the overexpansion effect is achieved by delaying the IVCT. In the quasi-Atkinson cycles, the intake valve is kept open during the initial 5’1 phase of the compression stroke (see Fig.1 bottom right) i.e. when the piston begins to ascend, some of the air that had entered the cylinder is returned to the intake manifold, delaying the start of compression. In this way, the expansion ratio is increased without increasing the effective compression ratio. Sophisticated variable valve timing is used to carefully adjust the intake valve timing to operating conditions in order to reach maximum efficiency. For a more in-depth analysis and further details on these quasi Atkinson cycles, including their thermodynamic analysis, Appendix 3 of [2] provides valuable information. The appendix discusses the simulation and examination of these real cycles, helping to understand their performance and efficiency characteristics from a thermodynamic standpoint. Please note: That IVCT is denoted to there as IVOT!

b. **True** Atkinson A ideal cycles are also overexpanded cycles but without piston stroke part (51, s. Fig. 1 bottom left) and especially for high turbocharged engines. **True** Atkinson ideal cycle referred to Fig. 1 consists of two parts: the first (1234) takes place in the cylinder, the second for closing from 4 to 1 via, 4A=3TC-4TC-1TC-1A=1 s. Figs. 5 to 7, in the turbocharger (TC). This means that the pre-compression 1TC-1A in the compressor, which is ensured by the full expansion 3TC-4TC via the turbine of TC, is explicitly required for closing the cylinder part of the **true** A ideal cycle. This condition is specific only to **true** A but does not apply to the **quasi** Atkinson ideal cycles. Full expansion, i.e. up to the ambient pressure (p_1), is not efficient to achieve in a pure piston engine due to the extremely long expansion stroke (therefore dimensions and weight) required. The ratio IMEP/p_1 always decreases with the lengthening of the expansion (see Fig. 5-12 from [1] page 185. For full expansion as shown in Fig. 5, an expansion stroke ca. three times as long is required.

The situation is different for a double helical screw internal combustion engine, its thermodynamic is presented in [7] (1996) and design in [12] (1997). This engine, named as DHSICE, consists of two pairs of positive displacement helical screws, one pair of which is responsible for compressing the working fluid and the other pair for expanding it. Between these helical screws pairs there are two plate valves and a central plate with the combustion chamber.

Heywood’s formula (5.55) for the indicated fuel conversion efficiency IFCE of the classical H Atkinson cycle from Fig. 1 as developed in [1] is denoted here as η_{thHv}.

The subscript (v) denotes an isochoric type of heat release in the cycle, i.e. identical to the classical Otto O cycle. The Heywood's IFCE formula (5.55) is rewritten using the variable definitions from this work (see below in section 1).

The long bracket in the Heywood's formula (5.55) considers the assumed isobaric compression 5-1 or 5*-1 according Fig. 1, which causes the difference from the true Atkinson (A cycle) formula η_{thAv} developed in this work.

The parameters in all these formulas are defined as follows: γ is the ratio between the volumetric expansion ratio VER ε_e and volumetric compression ratio VCR ε_c, and κ is the mean isentropic exponent on the cycles. The subscript (v) indicates that the heat Q* is released isochorically and causes the pressure rise ratio δ_p in A and O cycles.

The numerical values of IFCE according to classic Atkinson (H) cycle according to Heywood η_{thH_v}, true Atkinson (A) η_{thA_v}, and classical Otto (O) η_{thO_v} cycles are shown below for the used parameters from Fig. 2. (see section 1. below or/and Appendix 1 for a thermodynamically based justification of their formulas). The piston strokes for exhaust and intake are not shown because the ideal cycle are closed, i.e. the internal gas mass remains constant and chemically unchanged. The combustion is simulated by heat release that produces the pressure rise δp. The exhaust is simulated by heat discharge that produces the state changes 4O-1O in O cycle and 4A-1A in A cycle using the TC cycle. The complete p,v-diagram is presented in Figs 5 and 7. This detailed pressure-volume diagram shown the positioning of the cylinder inner part of the A cycle and indicates its closure over the TC Brayton/Joule cycle. The TC cycle part (see Fig. 6 for completion) serves as cylinder outer part of the A cycle.

The calculation of the IFCE (η_{th}) values for the cycles A, O, H using the formulas from section 1 and using the parameters from Fig. 2 results in the following numerical values, where the subscript (v) indicates an isochoric heat release and (p) indicates an isobaric heat release.

$$\eta_{thH_v} = 0.559 \; \eta_{thO_v} = 0.471 \; \eta_{thA_v} = 0.655 \; \eta_{thA_p} = 0.586$$

Note that even for the case where the classic Otto (O) cycle would operate with a hypothetical VCR = $\varepsilon_c \cdot \gamma$ = 30, i.e. with a VCR equal to the VER of the true Atkinson (A) cycle, its IFCE η_{thO_v} remains lower than that of the true Atkinson cycle η_{thA_v} with VCR = ε_c = 10. The difference of ca. 7% between these values results from the shortened compression stroke of the true Atkinson (A) cycle. The reason for this is the omission of the piston stroke part for precompression 5-1 according to Fig. 1 resp. 1O-1A according to Fig. 2, which is no longer present in the A cycle. See Fig. 4 for the displacement volume, crank angle V,CA diagram of classical Otto or Diesel, generalized named here Seiliger cycle, compared to the same diagram for the A cycle.

The thermodynamic analysis of the classical Atkinson (H) cycle has been extensively studied by various researchers over the years, including Heywood (1988) [1], Chan et al. (1996) [7], Schutting et al. (2014) [6], and others. These studies have contributed to understanding the characteristics, weak points and performance of the classical Atkinson H cycle.

The IFCE curves from Fig. 3 clearly show the influence of VCR and of the parameter γ, i.e. of the ratio between the volumetric expansion ratio VER ε_e and volumetric compression ratio VCR ε_c, which also corresponds to the ratio between expansion and compression strokes.

The IFCE of the A cycle increases with an increase of γ, so a brief analysis of the possible design of γ values is necessary.

For γ =1, the A cycle degenerates to the classic O cycle, since the strokes for expansion and compression become identical.

FIGURE 2 Detail of p,v-diagram from Fig. 5 a of true Atkinson (A) and classic Otto (O) ideal cycles, with the used parameters.

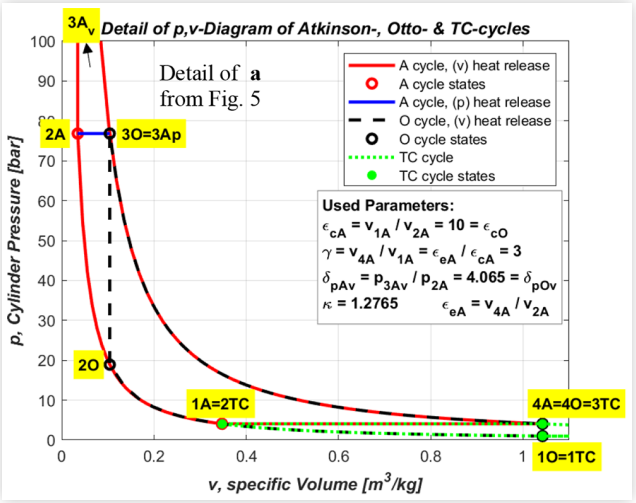

FIGURE 3 IFCE dependencies for true Atkinson cycle with isochoric heat release Av and with isobaric heat release Ap (the curve for Ap represents the IFCE lower limit for γ =3).

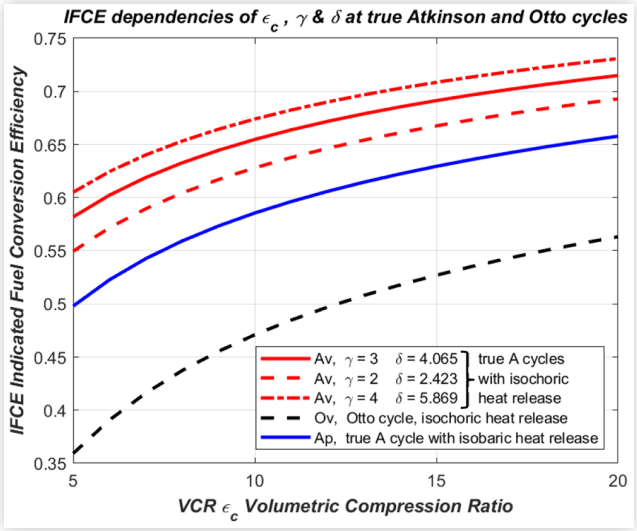

It can be seen from Fig. 2 that the pressures in the states 4A and 1A should be almost the same. This objective places high demands on the efficiency of high-pressure turbocharging. On the one hand, the boost pressure should be maximized to enable the selection of high γ -values, and on the other hand, this should be achieved without creating excessive cylinder backpressure in the exhaust manifold ahead of the turbine. Therefore, the choice of the γ parameter should be based on the efficiency of the available turbocharger. Multi-stage turbocharging is therefore recommended as well as new designs.

The author has dedicated a significant amount of time to advancing the classic Atkinson (H) cycle into the true Atkinson (A) cycle as presented in 2011 [4], 2013 [3] and more important 2015 [2]. As part of this development, the author has invented new crank mechanisms, named VCSR, specifically designed for this purpose. These innovative crank mechanisms feature different stroke lengths for compression and expansion (s. Fig. 4, [5, 10, 11], section 2 and Appendix 2) and allow stepless adjustment of the VCR, which play a crucial role in achieving the desired characteristics and performance of the true Atkinson A cycle.

The course of the displacement volume over crank angle from Fig. 4 respective eccentric crank angle illustrates the clear differences in the piston strokes. The condition of the same VCR forces the shift of the displacement volume curve of the A cycle closer to the cylinder head.

In the Seiliger (S) cycle, the heat release happens proportionally isochoric and isobaric, although one proportion can also be zero. The Seiliger cycle is thus the generalization of the Otto and Diesel cycles.

In addition to the crank mechanism development, the author has also focused on the development of a new load control approach. This load control approach is an integral part of realizing the ultra-downsizing (UD) concept, which aims to further enhance the efficiency and performance of the engine (see details in Appendix 2).

The author has patented the new matching crank mechanisms VCSR and the appropriate ultra-downsizing (UD) load control (LC) to implement true Atkinson A cycles and UD concept as [10, 11].

In [5], the design change from a classic 3-cylinder in-line to a VCSR ICE is shown, whereby the VCR and the load are varied by slightly turning the ring gear of the planetary gears used. In [5, 9], some design concepts of 3-cylinder VCSR-ICE in-line 3L and star 3Y cylinder arrangements and corresponding animations of two variants of crank mechanisms are short presented, see slides 5 to 7 of [9].

By combining the advancements in crank mechanisms and load control, the author has successfully advanced the classical Atkinson H cycle, resulting in the true Atkinson A cycle with improved characteristics and potential for ultra-downsizing UD. This research could represent a significant contribution to the field of ICEs and offers new possibilities for achieving higher efficiency and performance in practical applications.

It is important to note that the thermodynamics of the true Atkinson A cycles, specifically for modern high-turbocharged ICEs, have been described in detail in this paper. The evidence supporting the IFCE formulas η_{thA_v} and η_{thA_p} has been provided and analyzed exclusively within this work, contributing to a comprehensive understanding of the A cycle's thermodynamic characteristics in the context of high-turbocharged ICEs.

The A cycle is characterized by its operational division on two different components: on the cylinder and on the turbocharger (TC).

The cylinder part of the A cycle encompasses the traditional processes of intake, compression, combustion, expansion, and exhaust, which occur within the engine cylinder. These processes are responsible for generating power and converting fuel into useful mechanical work.

Characteristic of the A cycle is that the compression consists of two parts, an unbounded (i.e. without limiting by waste gate, VTG, etc.) external pre-compression in the compressor of the TC, followed by an internal compression with adapted VCR in the cylinder. This allows the compression stroke in the cylinder to be shortened, since the internal compression starts from the final state of pre-compression. The higher the pre-compression, the better the efficiency of the engine. The stepless VCR adjustment provided by the VCSR crank mechanism ensures that the durability and strength of engine components remain within acceptable limits. This is in contrast to the idea from [8], which attempts to extend these limits.

The papers [18, 19] present investigations using engine simulations of two turbocharged SI engines with modified crank mechanisms to implement true over-expanded Atkinson cycles.

The basic over-expansion ratio in both papers is set to γ =1.5 and the fixed VCR are set to10 and 9.2

FIGURE 4 V, CA- of the Seiliger and V, Eccentric CA-diagrams of true Atkinson (A) cycles. Note: "Gasex." stands for gas exchange. The VCR = 10 is identical in both cycles, the same is true for the length of the expansion strokes. The compression stroke is half as long as expansion stroke in the A cycle, i.e. $\gamma = 2$. The designations 1A to 6A are added here to establish a simple correlation with the cycles shown in Fig. 1.

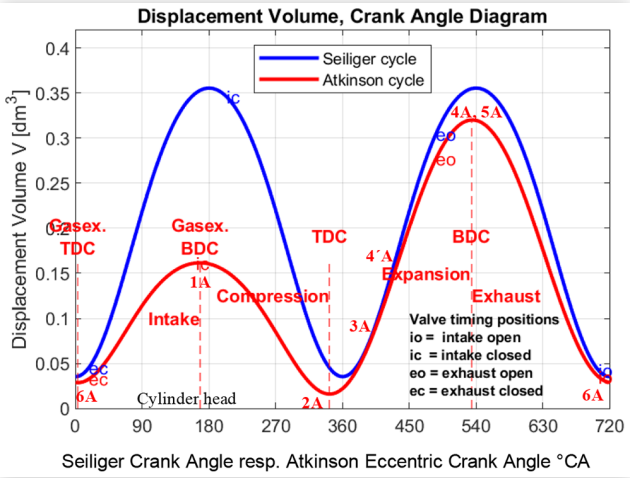

respectively. Since VCR cannot be adjusted for these over-expanded engines, this means that:

a. at low loads, the engines incline to generate negative work due to over-expansion and only an increase of ca. 2% in the IFCEnet is achieved. A growth of VCR would help to increase it probably over 10%.
b. At middle and high loads, the knocking must be prevented and that implies either the spark must be retarded, which diminish the efficiency, or γ enhanced to 1.8. A reduction of VCR would help to prevent the knocking and increase the IFCEnet probably by 10% supplementary.

The turbocharger (TC) plays a crucial role in the A cycle by effectively harnessing the enthalpy of the exhaust gases to pre-compress the intake air. The concept of multi-stage turbocharging with intercooling is particularly beneficial, as it enhances the efficiency of the A cycle by providing an upper pre-compression state of the intake air and thus increase engine power output.

By integrating the cylinder and turbocharger processes, the A cycle optimizes the recovery and utilization of energy, resulting in overall engine efficiency and performance. The in-depth thermodynamic analysis presented in this paper provides insights into the specific processes and interactions within the A cycle, emphasizing its advantages and potential applicability in contemporary supercharged internal combustion engines (ICEs).

The work not only presents the Indicated Fuel Conversion Efficiency (IFCE) formula but also rigorously substantiates its validity through an extensive thermodynamically analysis. By concentrating exclusively on the A cycle and its potential use in highly supercharged internal combustion engines (ICEs), the author aims to make a substantial contribution to the comprehension of the thermodynamic aspects associated with this particular engine configuration.

1. Thermodynamic analysis and comparison of the Indicated Fuel Conversion Efficiency of true Atkinson and classical ICE ideal cycles

In order to facilitate a meaningful comparison of the efficiencies between the ideal Otto (O) and true Atkinson (A) cycles, the following conditions and considerations were taken into account:

a. Key parameter such as the Volumetric Compression Ratio (VCR, ε_c), the isentropic exponent (κ), the stoichiometric Air-Fuel Ratio (AFR, λ), and the pressure-rise ratio (δ_p) during isochoric
heat release were kept identical in both cycles.
b. As a consequence of the identically kept parameters, the compression and expansion curves of the two cycles overlap, which inevitably leads to different amounts of heat released isochorically during the respective cycles.
c. Within the A cycle, the fresh charge (air) for intake into Variable Compression and Stroke Ratios (VCSR) ICE cylinders undergoes pre-compressed through high-pressure Turbocharging (TC). The processes originated from TC are simulated using the Brayton/Joule (TC) cycle in this analysis.
d. The compression and expansion curves of the A and O cycles overlap according to points a) and b). However, the initial and final states of compression and the initial states of expansion are different, but the final states of expansion are identical in the A and O cycles.
e. All cycles, are considered as ideal, designed in such a way that the temperature upon entering the turbine (T), specifically at the beginning of exhaust process of A and O cycles, reaches approximately 1200°C.
f. The objective was to select an exhaust gas temperature that aligns with the current tolerance of turbine blades, without necessitating special cooling measures.

This approach ensures a systematic and controlled comparison between the two cycles, shedding light on their respective efficiencies and thermodynamic characteristics.

It is a well-established fact that the Indicated Fuel Conversion Efficiency (IFCE) of the O cycle (i.e. of the ideal cycle of gasoline-powered ICEs) is primarily dependent on two key factors: the VCR here denoted as ε_c and the isentropic exponent κ of the working gas, typically air. Its thermodynamic efficiency is independent of the charging level (as formula η_{thO_v} from section 1 shown). Consequently, when applied to a turbocharged Otto cycle, the states within the cycle merely shift to higher temperatures and pressures, leaving the thermodynamic efficiency of the cycle unchanged. This limitation is a significant disadvantage of the Otto cycle, as it lacks a direct mechanism for heat recovery through turbocharging (TC).

The internal processes of the true Atkinson (A) cycle (1A–2A–3A–4A) and of classical Otto (O) cycle (1O–2O–3O–4O–1O) within cylinder are illustrated in Figures 2, 5 to 8. In the case of isochoric (v) heat release, 3A is denoted as 3Av, while for isobaric (p) heat release, it becomes 3Ap.

Note:

- In the figures that follow, the parameter γ, representing the ratio between the Volumetric Expansion Ratio (VER) ε_e and Volumetric Compression Ratio (VCR) ε_c (or the ratio between the expansion and compression stroke lengths) in A cycle, is set as an example to $\gamma = 3$.
- Ideal cycles assume constant gas masses, typically air, meaning they do not account for piston strokes related to exhaust and intake (i.e., without gas exchange).

As previously mentioned, the true Atkinson (A) ideal cycle consists of two parts: the first occurs within the cylinder, the second take place in the turbocharger (TC). Therefore, this cycle unfolds within both a piston and a flow machine.

The Gas Turbine, Brayton or TC cycle 1TC–2TC–3TC–4TC–1TC is introduced here as represent the processes within the turbocharger (TC) to complete the true Atkinson (A) cycle. Note that the piston stroke 4A-1A does not exist.

The closure of the A cycle is only hypothetical and can be achieved either via 4A-1O-1A in approach a) or via 4A–1A in approach b). This hypothetical closure is necessary to develop the formula for thermal efficiency IFCE, as explained in more details below. In reality, the closure of the A cycle occurs over TC cycle, specifically part 4A=3TC–4TC–1TC–2TC=1A.

The heat discharged in the A cycle, represented as q_{4A_1A}, serves the role of the heat released as q_{2TC_3TC} in the TC cycle. This relationship is visually depicted in the lower part of diagram **a** and its detailed view in **c** from Fig. 5, although this is better scaled and shown in detailed view in **d** from Fig. 6.

FIGURE 5 The p,v pressure, specific volume diagram of true Atkinson (A), Otto (O) and Brayton (TC) cycles. Part **a** shows the full presentation of this diagram, with the low-pressure region blurred due scaling. Detail **c** of **a** fixes this blur into cylinder and denotes the exchanged heats. The values for VCR and pressure ratio δ during combustion are identical for both A and O cycles.

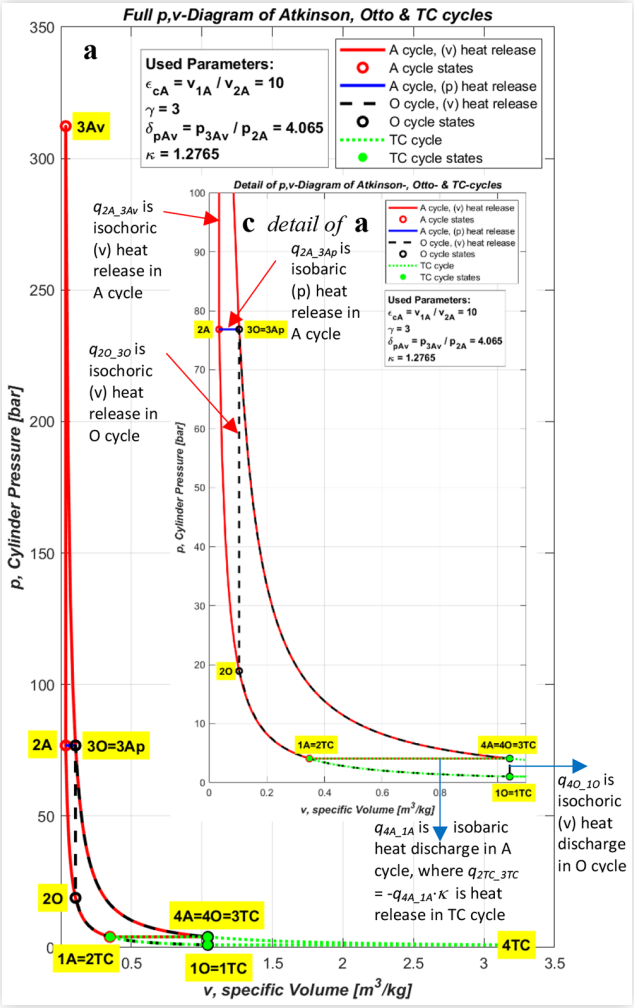

FIGURE 6 Detailed pressure-volume diagram for the positioning of the cylinder inner part of the true Atkinson cycle and its closure over the TC Brayton/Joule cycle.

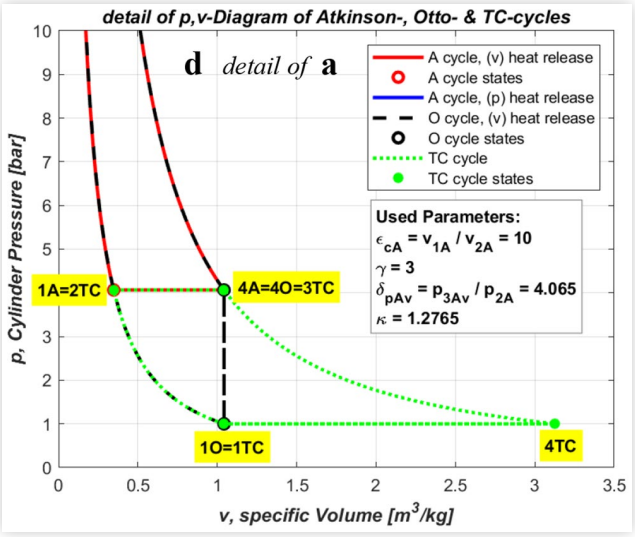

Specifically, the state changes 4A–1A in A cycle respectively 2TC–3TC in TC cycle are considered virtual because there is no piston stroke for 4A-1A. These work as internal boundary between cylinder and TC systems and are assumed only for the thermodynamic closure of their cycles.

The three cycles (A, O, and TC) are more effectively visualized through their shared logarithmic representation in a pressure, specific volume (p,v) diagram in Figure 7. This representation provides a clearer understanding of the relationships between these cycles and how they interact from the thermodynamic perspective.

The Brayton (TC) cycle completes the cylinder inside part of expansion in A cycle up to ambient pressure and assure the pre-compression of the intake air.

Note: The impact of the type of heat release - isochoric (v) or isobaric (p) - in the A cycle on thermal efficiency IFCE is depicted in Fig. 3 and is further elaborated in Appendix 1. The blue line (2A – 3O=3Ap) representing the isobaric (p) heat release in the A cycle is displayed in Figures 2, 5 to 8. This (p) heat release mode provides the IFCE comparison of the A and O cycles at identical maximum cylinder pressures. At the same time, the IFCE values for (p) and (v) heat release in A cycle form the lower and upper IFCE limits.

The **true** Atkinson (A) Cycle results as an overlapping of classic Otto (O) and Brayton Gas Turbine (TC) Cycles, with the common parts of both cycles merging or, more precisely, disappearing together.

One way to interpret this is that the processes of the true Atkinson A cycle, occurring in the cylinders 1A – 2A – 3A – 4A, effectively replace the isobaric heat release process 2TC – 3TC of the Brayton TC cycle. Conversely, the Brayton cycle, when excluding its isobaric heat release process 2TC – 3TC (i.e., 3TC=4A – 4TC – 1TC – 2TC=1A), essentially functions as the gas exchange processes within the true Atkinson A cycle.

FIGURE 7 The logarithmic fully scaled p,v pressure, specific volume-Diagram of the true Atkinson cycle. Expanding exhaust gases to ambient pressure is unrealistic with a very long piston stroke.

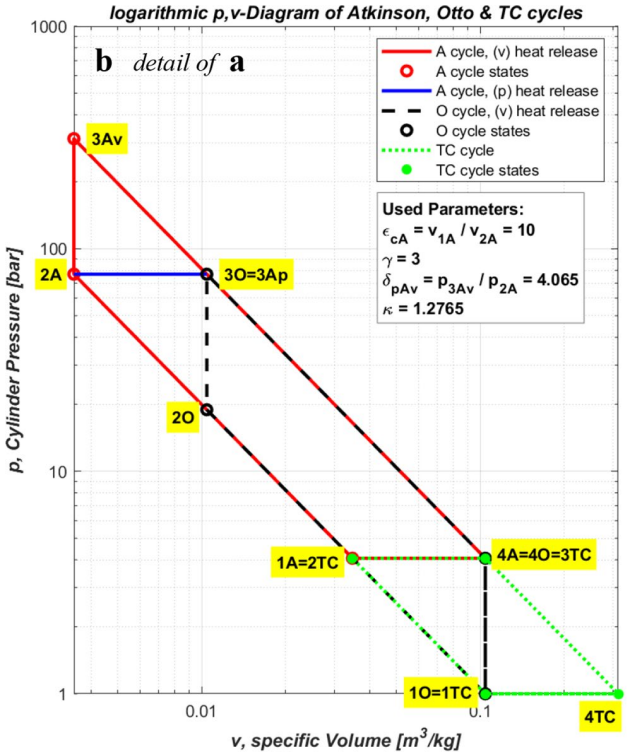

In the true Atkinson (A) cycle, the closing process (from 4A to 1A) effectively occurs within the turbocharger (TC) rather than in the cylinder, as depicted in figures 5 to 8. This means that the turbocharger is responsible for pre-compressing the air to the 1A state utilizing the exhaust gas enthalpy from the 4A state. Consequently, the part of the piston stroke 1O to 1A, which represents air pre-compression, and the apparent piston stroke from 4A to 1A, intended to close the cycle, do not actually exist within the true Atkinson A cycle.

The complementarity of the true Atkinson and Brayton (TC) cycles can be better seen from the logarithmic scaled pressure, specific volume diagram from Figure 7.

The enclosed areas in diagram **d** from Fig. 6 have following meaning: The enclosed area under (3TC, 4TC) to the p-axis is proportional (~) to the specific technical work w_{t3TC_4TC} performed by the turbine (T) and the enclosed area under (1TC, 2TC) to the p-axis is ~ to the specific technical work w_{t1TC_2TC} consumed by the compressor (C) to pre-compress the air. The specific volume change work w_{v1O_1A} that the piston would consume for air pre-compression (1O-1A) is ~ to the trapped area (1O-1A) to **v**-axis. The feasibility of true Atkinson A cycle is given if following assignment holds: $w_{t3TC\_4TC} > w_{t1TC\_2TC} > w_{v1O\_1A}$, what is clearly true here (see also their numerical values in Appendix 1).

The TC cycle part serves as cylinder outer part of the true Atkinson cycle.

Therefore, much of the expansion takes place in the TC's turbine, which is suitable for this purpose.

Two approaches for obtaining the thermal efficiency formula of the true Atkinson A cycle based on the plot in Figures 2, 5 to 8 are provided. All specific work (w*) and specific amounts of heat released or discharged (q*) are related to the specific internal energy (u_{1O}) in the 1O state. The deduction and calculation of these specific quantities is presented in detail in Appendix 1.

Each of these two approaches are explained in more detail:

Approach a)

Consider only the cylinder part 1A–2A–3A–4A–1O–1A of the true Atkinson cycle, which is indeed not closed via 1O–1A, because there is no such piston stroke for this pre-compression. The volume change work (thus energy) required for the pre-compression 1O–1A is provided by the Turbine (T) and used to drive the compressor (C) in the TC cycle and feed back to the cylinder as heat/energy recovery. Consequently, the discharged heat on the cycle between the states 4O–1O must be reduced by this amount. See evidences 1st and 2nd for approach a) for the IFCE of the true Atkinson cycle with isochoric heat release in Figure A1-3 of Appendix 1.

Approach b)

Consider the cylinder part of the closed true Atkinson cycle 1A–2A–3A–4A–1A. Here, the isobaric change of states 4A-1A is intended only to formally complete the true Atkinson A cycle and provides the heat discharging on the cycle without necessitating a piston stroke. As a result, no volume change work is done on 4A-1A, i.e. only the internal energy changes, and the efficiency formula derived from this approach considers this. See evidences 1st and 2nd for approach b) for IFCE of the true Atkinson cycle with isochoric heat release in Figure A1-3 of Appendix 1.

These two approaches offer different perspectives on the thermodynamics of the true Atkinson cycle and the work involved in different stages of the cycle. The specific formula for the thermal efficiency (IFCE) can be derived based on the chosen approach and the consideration of volume change work and technical work in the different parts of the cycle.

The T,s – diagrams from Fig. 8 help to understand the differences between the IFCE magnitudes given in the Introduction for Otto (O) η_{thO_v} and true Atkinson (A) η_{thA_v} cycles.

The meaning of most of the enclosed areas in the T,s – diagrams from Fig. 8 is given bellow and also in Appendix 1. (sp. means specific)

a. sp. heat released within isochoric (v) combustion in Otto cycle is ~ to the trapped area (a-2O-3O-b-a)
b. sp. heat discharged within isochoric (v) exhausting in Otto cycle is ~ to the trapped area (b-4O-1O-a-b)
c. sp. heat released within isochoric (v) combustion in true Atkinson cycle is ~ to the trapped area (a-2A-3Av-b-a) and matches to the maximum possible heat released in that cycle.

FIGURE 8 The T,s temperature, specific entropy-diagram of the true Atkinson (A), Otto (O) and Brayton (TC) cycles.

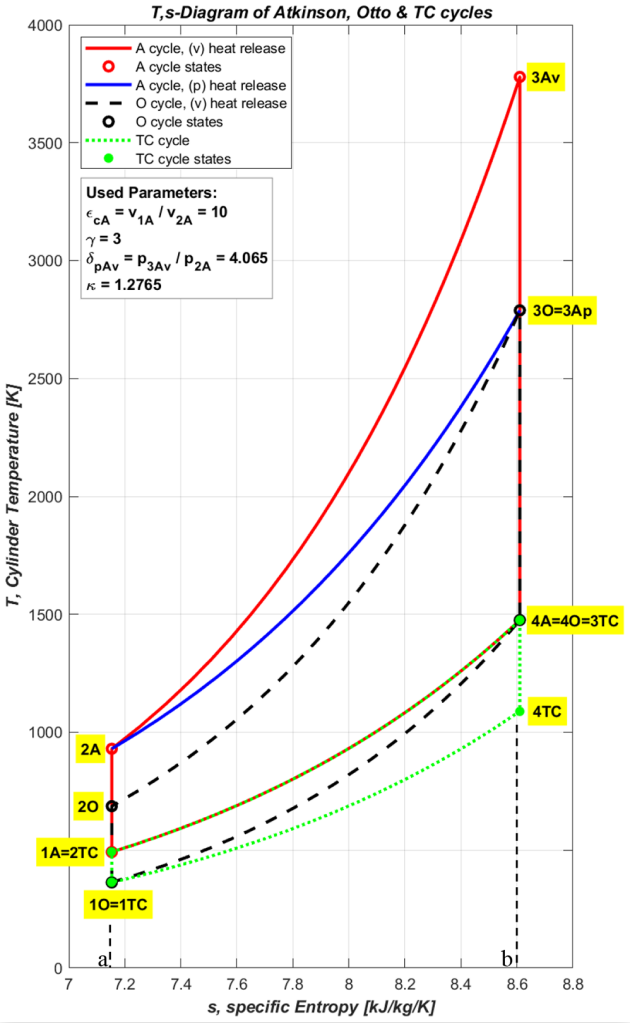

d. sp. heat released within isobaric (p) combustion in true Atkinson cycle is ~ to the trapped area (a-2A-3Ap-b-a) and matches to the minimum possible heat released in that cycle.

e. sp. heat discharged within isobaric (p) exhausting in true Atkinson cycle is ~ to the trapped area (b-4A-1A-a-b). This is in amount equivalent to the necessary released heat on Brayton respective TC cycle, taken alone as an independent cycle.

f. sp. technical work w_{t3TC_4TC} carried out by the turbine T is proportional (~) to the trapped area of (1TC-3TC-4TC-1TC).

g. sp. technical work w_{t1TC_2TC} consumed by compressor C is ~ to the trapper area of (1TC-2TC-3TC-1TC).

h. sp. heat discharged within isobaric (p) exhausting in Brayton, TC cycle is ~ to the trapped area (b-4TC-1TC-a-b).

The dotted state change 2TC-3TC or 4A-1A is only an internal energy system boundary for the heat exchange between cylinder (discharged) and turbocharger (introduced/released). This is required for the closure of the cylinder part of the A cycle and TC cycle for the development of their IFCE formulas (see below Appendix 1).

The variation of the Indicated Fuel Conversion Efficiency IFCE as function of (VCR, γ, κ) plotted in Fig. 3 and presented formulaically below and in Appendix 1, where κ means the isentropic exponent. Fig. 3 clearly shows the efficiency improvement potential if true Atkinson cycles are used instead of classic gasoline cycles (Otto, e.g. with VCR = 10). A thermodynamic demonstration of the IFCE formulas is presented in Appendix 1. The offered continuous variation of the VCR in the true Atkinson cycle of VCSR ICEs allows the Ultra Downsizing UD load control LC even when the Air-Fuel Ratio is kept stoichiometric, i.e. AFR = 1, see a proof by simulations of **real** cycles using the AVL Boost Tool in Appendix 2.

Justification of the treatment of two heat release variants in the diagrams from Figures 5 to 8:

In practice, there is no pure isochoric (v for max IFCE) or isobaric (p for min IFCE) heat release. The best replication to real heat releases is described in [2], as v,p,T heat release.

The true Atkinson Cycle results as an overlapping of Gas Turbine and Otto Cycles, where the common parts of both cycles merge. In the true Atkinson cycle, a big part of the released specific work of the Turbine is fed back on the cycle as specific work for air pre-compression. As a result, the compression stroke can be significantly shortened and, thus, it starts from the pre-compression state 1A, i.e. the compression stroke part from environment state 1O=1TC to the pre-compression state 1A can be omitted. However, the expansion strokes of the Atkinson and Otto cycles end in the same state 4A=4O=3TC (s. Figs 5 to 8). The thermodynamic substantiation is presented below in Figures A1-1 to A1-4 of Appendix 1.

For a suitable comparison of the efficiencies of the **Otto & Atkinson Cycles**, some more conditions need to be discussed below:

In a **1st Comparison Variant**, the **pressure-rise ratios** $\delta_{pA\_v} = \delta_{pO\_v}$ during the **isochoric** (v) heat release are kept **identical** in Atkinson & Otto Cycles. This leads to a) very high-pressure peak p_{3A} and b) much higher released heat on the Atkinson Cycle (s. area a-2A-**3Av**-b-a) compared to the Otto Cycle (s. area a-2O-3O-b-a in T,s-diagram of Fig. 8). Although the isochoric amount of heat released is not explicitly present in the IFCE formulas, the **1st Comparison Variant** could be debatable because of the different high pressure peaks! Thus, the IFCE of the Atkinson cycle in this 1st Variant can be interpreted as its **upper** limit. In this variant, the IFCE value of Atkinson cycle is over 30% higher compared to the IFCE value of the Otto cycle.

In a **2nd Comparison Variant**, the **maximal pressure** values are kept **identical** in both cycles, which implies an **isobaric** (p) heat release on the Atkinson cycle (s. [2] for more real heat release variants). That leads to moderate heat release on the Atkinson Cycle (s. area a-2A-**3O=3Ap**-b-a in T,s-diagram of Fig. 8) compared to the Otto Cycle. The δ_{pO_v} during the isochoric heat release

of the Otto cycle appears this time explicitly in the IFCE formula of Atkinson cycle, because δ_{pO_v} governs the maximal pressure level on both cycles. Thus, the IFCE of the Atkinson cycle in this 2nd Variant can be interpreted as its **lower** limit. Even in this worst-case heat release variant, the IFCE value of Atkinson cycle is over 24% higher compared to the IFCE value of the Otto cycle (s. Figure A1-4).

Just a reminder: **All three cycles are designed to reach a temperature of around 1200°C at the start of exhaust**, i.e. upon entering the turbine (T). See above for comparison conditions e), f) and Figs. 5 to 8.

IFCE Formulas of H, O an A Cycles

Used parameters:

ϵ_c = VCR κ = mean isentropic exponent

ϵ_e = VER $\delta_p = \frac{p_3}{p_2}$ δ_p is the pressure rise ratio due to the released heat Q^* on the isochoric state change 2-3 (combustion)

$\gamma = \frac{\epsilon_e}{\epsilon_c}$ η_{th} = indicated fuel conversion efficiency IFCE

$q^* = \frac{Q^*}{c_v \cdot T_1}$ $q^* = q^*_{23}$ is the specific released heat i.e. Q* referred to specific internal energy u_1 in state 1

For comparison used numerical values: ϵ_c = 10, γ = 3, κ = 1.277, δ_p = 4.065

$$\eta_{thH_v} = 1 - \frac{1}{\left(\epsilon_c \cdot \gamma\right)^{\kappa-1}} \cdot \left[1 + \frac{1}{q^*} \cdot \epsilon_c^{\kappa-1} \cdot \left(1 - \kappa \cdot \gamma^{\kappa-1} + \left(\kappa - 1\right) \cdot \gamma^{\kappa}\right)\right]$$

Heywood (5.55)

1st Law of Thermodynamics (1.LoT) on isochoric combustion 2-3 yields: $q^*_{23} = \epsilon_c \kappa^{-1} \cdot (\delta_p - 1)$ and after using of

$\gamma^{\kappa} = 1 + \frac{q^*}{\epsilon_c^{\kappa-1}}$ according to Heywood [1] (5.56), and $q^* = q^*_{23}$

it results for $\delta_p = \gamma^{\kappa}$, which produces $q^* = 5.793$

Finally, after substituting of (5.56) into (5.55), we obtain for IFCE of the classical Atkinson H cycle according to Heywood [1]

$$\eta_{thH_v} = 1 - \frac{1}{\left(\epsilon_c \cdot \gamma\right)^{\kappa-1}} \cdot \left[1 + \frac{1}{\gamma^{\kappa} - 1} \cdot \left(1 - \kappa \cdot \gamma^{\kappa-1} + \left(\kappa - 1\right) \cdot \gamma^{\kappa}\right)\right]$$

The IFCE of the classical Otto O cycle depends as known only on VCR and κ, so its value is independent of δ_p.

$$\eta_{thO_v} = 1 - \frac{1}{\epsilon_c^{\kappa-1}}$$

The IFCE of the true Atkinson A cycle with isochoric heat release depends on VCR and κ but also on δ_p and γ.

$$\eta_{thA_v} = 1 - \frac{1}{\left(\epsilon_c \cdot \gamma\right)^{\kappa-1}} \cdot \frac{\delta_p - \gamma^{\kappa-1}}{\delta_p - 1}$$

Further formula is obtained after eliminating of δ_p using the relation $\delta_p = \gamma^{\kappa}$. The proof of this relation is provided by the p,v-diagrams from Figs. 2 and 6 and following thermodynamic correlations:

The state changes 1A-2A and 3A-4A occur isentropically, thus

$\epsilon_c = \frac{V_{2A}}{V_{1A}}$ $\epsilon_e = \frac{V_{4A}}{V_{2A}}$ $\gamma = \frac{\epsilon_e}{\epsilon_c} = \frac{V_{4A}}{V_{1A}}$

$p_{2A} = p_{1A} \cdot \epsilon_c^{\kappa}$, $p_{3A} = p_{2A} \cdot \delta_p$, i.e. $p_{3A} = p_{1A} \cdot \epsilon_c^{\kappa} \cdot \delta_p$,

$p_{3A} = p_{4A} \cdot (\epsilon_c \cdot \gamma)^{\kappa}$, $p_{4A} = p_{1A}$, i.e. $p_{3A} = p_{1A} \cdot \epsilon_c^{\kappa} \cdot \gamma^{\kappa}$

Equating both expressions for p_{3A} yields the relationship we are looking for $\delta_p = \gamma^{\kappa}$. The IFCE of A cycle thus becomes:

$$\eta_{thA_v} = 1 - \frac{1}{\left(\epsilon_c \cdot \gamma\right)^{\kappa-1}} \cdot \left[1 + \frac{1}{\gamma^{\kappa} - 1} \cdot \left(1 - \gamma^{\kappa-1}\right)\right]$$

If the heat is released purely isobarically (p) after the pressure p2A = p3O has been reached, i.e. in such a way that no further increase in pressure occurs. The IFCE in this case becomes:

$$\eta_{thA_p} = 1 - \frac{1}{\kappa \cdot \epsilon_c^{\kappa-1}}$$

Summary of the Comparison of Ideal Cycles

Depending on the estimated heat release type in the Atkinson cycle, the improvement of IFCE between the Atkinson and Otto cycles, are as follows:

Isochoric heat release in A cycle **Isobaric** heat release in A cycle

$\frac{\eta_{thA\_v} - \eta_{thO\_v}}{\eta_{thO\_v}} = 39\%$ $\frac{\eta_{thA\_p} - \eta_{thO\_v}}{\eta_{thO\_v}} = 24.3\%$

The IFCE comparison between the Atkinson cycle and the Gas Turbine (TC) cycle is very much stronger, but distorted because of the different VCR values:

$\frac{\eta_{thA\_v} - \eta_{thTC\_p}}{\eta_{thTC\_p}} = 149.9\%$ $\frac{\eta_{thA\_p} - \eta_{thTC\_p}}{\eta_{thTC\_p}} = 123.5\%$

Even the IFCE comparison between the Otto cycle and the Gas Turbine (TC) cycle is very unfavorable for the TC cycle:

$$\frac{\eta_{thO\_v} - \eta_{thTC\_p}}{\eta_{thTC\_p}} = 79.8\%$$

All these IFCE (efficiency) comparisons show that the Gas Turbine cycle of aircraft engines, such as turboprop and turbofan, have to be rigorously reconsidered. Their lower VCR is imposed from T_{4TC} = 1200°C and stoichiometric AFR, λ = 1, at ambient intake pressure.

Using a VCSR engine, as the CORE instead of the burn chamber of the turbofan or turboprop aero engines will enables the following:

a. A huge increase in efficiency, thus drastically reducing the specific fuel consumption,
b. A much greater bypass flow, e.g. well over 20%,
c. A simpler compensation of the altitude flight by the variable VCR,
d. The use of various fuels, such as gaseous or liquefied H_2 or NH_3, biofuels, CNG, LPG or even Kerosene, either pure or in any mixture.

2. Thermodynamic analysis and comparison of the IFCE of true Atkinson A and classical O ICE real cycles

In Appendix 2, the comparison of the A and O cycles in 15 engine operating points (EOPs) is performed to illustrate the ultra-downsizing (UD) load control (LC) behavior. In these EOPs the VCR is varied between 4.4 and 21.5 and kept identical in both cycles, Because the size of the diagrams of all EOPs far exceed the size of this paper, they can be found in Appendix 2. All simulations of real cycles are done using the AVL tool Boost.

Apart of Appendix 2, 2 true Atkinson (A) cycles and 3 Seiliger (S) cycles are selected here based on the EOP 5, varying the aspirated gas mass and VCR, but leaving the parameter γ ≅ 2 of A cycles unchanged. The characteristic parameters of the 5 cycle variants are listed in the Table 1. In all 5 cycles, cooling via cylinder walls is not taken into account, i.e. these cycles are adiabatic and reversible in order to avoid influences due to different stroke lengths and VCR values. It is up to the reader to assess these influences for themselves. Some considerations about this can be found in [6].

TABLE 1 Parameter of the simulation variants. QF means the fuel energy, i.e. fuel mass m_f multiplied by the lower calorific value. HR* is the heat release calculated over integration (see the formula below and its course over crank angle CA in Fig. 12).

Variant	VCR	VER	QF	HR*	air mass	IFCE
\Unit	-	-	J	J	g	-
A1	5.5	9.9	1979	2015	0.589	0.459
A2	10	20	1106	1079	0.325	0.528
S1	9.9	9.9	1095	1078	0.326	0.414
S2	20.2	20.2	1113	1040	0.326	0.486
S3	9.9	9.9	1991	1937	0.589	0.425

The classic T,s diagram as used in Fig. 8, which is useful for comparing the IFCE for **ideal** cycles, is not at all suitable for **real** cycles due to the change in gas mass during gas exchange processes.

Fig. 9 demonstrates that, and shows that no important differences between the 5 cycles from Table 1 result, despite the fact that cycle type, VCR, IFCE and gas mass are very different.

Free and forced exhaust (cylinder empting) occurs isentropically (i.e. adiabatically and reversibly) from (eo) up to opening of intake valve (io) and only causes a temperature T reduction there, without variations of the specific entropy s.

The reduction in specific entropy s between (io) and (ic) is not caused by the heat or enthalpy discharged from the cylinder but by the dilution of hot exhaust gas with cold fresh air. The areas under the (io)-(ic) curves up to the abscissa and the areas within the cycles from Fig. 9 are not proportional to the heat released or the mechanical work done in these cycles, as is the case for ideal cycles shown in Fig. 8.

All these facts show that the T,s diagram from Fig. 9 is unsuitable for real cycles.

To illustrate the unsuitability of the T,s diagram from Fig. 9, Figure 10 shows the pressure curves over the cylinder volume, i.e. the p,V diagram, focusing on the gas exchange processes.

Accordingly, in Figure 11 a new diagram type is introduced here, which shows the temperature (T) depending

FIGURE 9 The T,s temperature, specific entropy diagram of the true Atkinson (A) and Seiliger (S) **real** cycles. The valves timing: exhaust open (eo), intake open (io), exhaust close (ec) and intake close (ic), as well as, the dead centers: TDC and BDC, and the positions: for start of combustion (SoC) and end of combustion (EoC) are shown.

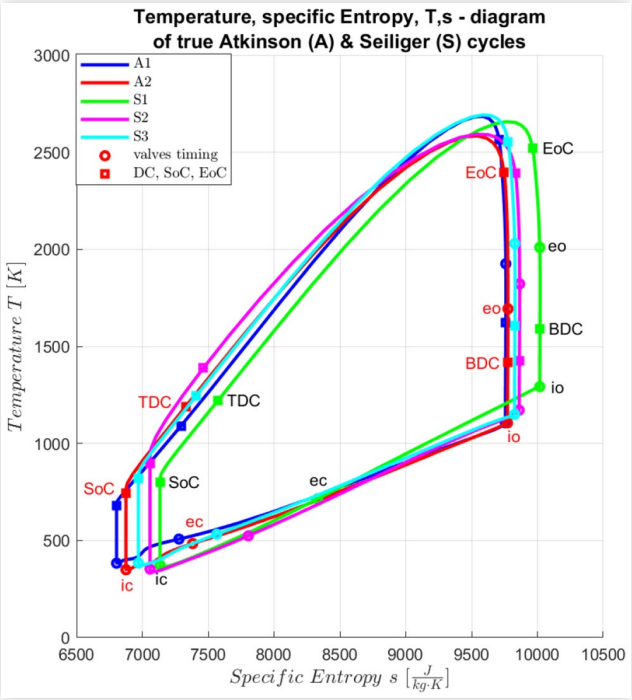

FIGURE 10 p,V pressure, displacement volume diagram of all 5 cycles. This diagram shows the gas exchange processes in detail.

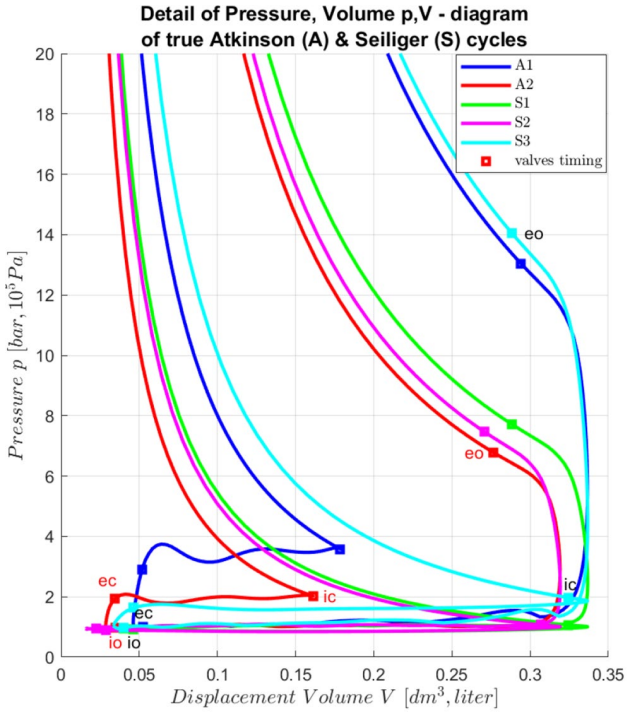

FIGURE 11 T,dS/dt temperature, absolute entropy flow diagram of all 5 cycles. This diagram is below detailed commented and explained.

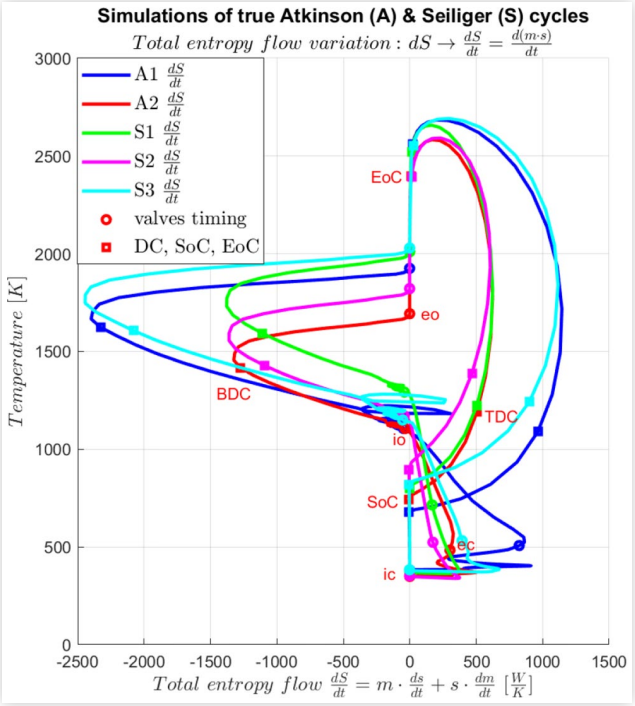

on the entropy flow (dS/dt), which also takes into account the variation of the gas mass due to the mass flows and the resulting entropy flows.

The large differences between the cycles from Table 1 can be seen in the low pressure portion of the p,V pressure-volume diagram from Fig. 10.

The entropy flow dS/dt, more correctly expressed as:

$$\frac{dS}{dt} = m \cdot \frac{ds}{dt} + s \cdot \frac{dm}{dt}$$

is taken as abscissa in Fig. 11 instead of the specific entropy s, used in Figs 8 and 9, in order to include also the influence of the exchanged gas mass (i.e. of the mass flows).

Entropy accompanies heat and mass flows, so it can increase or decrease with them.

Only the irreversible processes (such as friction, mixing, etc.) always cause entropy increase.

In this investigation, all cycles are reversible.

The T,dS/dt diagram from Fig. 11 shows on the positive abscissa side above the start of combustion (SoC) to the end of combustion (EoC) the contribution in entropy and temperature increase of the released heat in the cycles.

The area in the T,dS/dt diagram, i.e. the integral

$$HR^* = \int_{SoC}^{EoC} \left(T - T_{SoC}\right) \cdot \left(\frac{dS}{dt}\right) dt$$

gives the numerical value of the heat released HR* from Table 1 as shown in Fig. 12 using the cumulative integration.

If one neglects the mass increase due to fuel supply at integration, i.e. the term $s \cdot \frac{dm}{dt}$, this slightly reduces the values for QR* and results in the lower QR values from Fig. 13. This occurs because of low fuel mass fraction.

In contrast, the term $s \cdot \frac{dm}{dt}$ significantly determines the entropy flow during the gas exchange processes, i.e. after the (eo) point, as shown in Fig. 11 on the negative side of abscissa presented.

The special achievement of the T,dS/dt diagram is to make visible the enthalpy unused in the cylinder for the extraction of volume change (mechanical) work, which is lost with the exhaust gas discharge.

A part of this exhausted enthalpy is used in the turbocharger TC for pre-compression of the intake air, and thus is partly in A cycles recover.

The enclosed areas in the T,dS/dt diagram during exhaust gas discharge are proportional to, but not limited to, the magnitude of the exhausted enthalpies discharged. A list of all T·dS/dt decomposition terms and interpretation of their integrals is presented below.

In addition to the enclosed areas in the T,dS/dt diagram during exhaust gas discharge, the different average temperatures of these areas, i.e. at which the exhaust gas is pushed-out from cylinder, indicate the exergy losses. These can be easily estimated visually.

The higher the temperature at which the heat / energy is discharged, the more exergy is also lost. Exergy is the fraction of energy (here heat or enthalpy) that can be completely converted into other useful forms of energy, such as mechanical work. The diagram T,dS/dt shows that the classical Seiliger cycle expels too much

FIGURE 12 Released heat course over crank angle for the 5 cycles from Table 1. In this plot, the increase of gas mass during combustion due to addition of fuel is also taken into account. Its maxima correspond to HR* from Table 1.

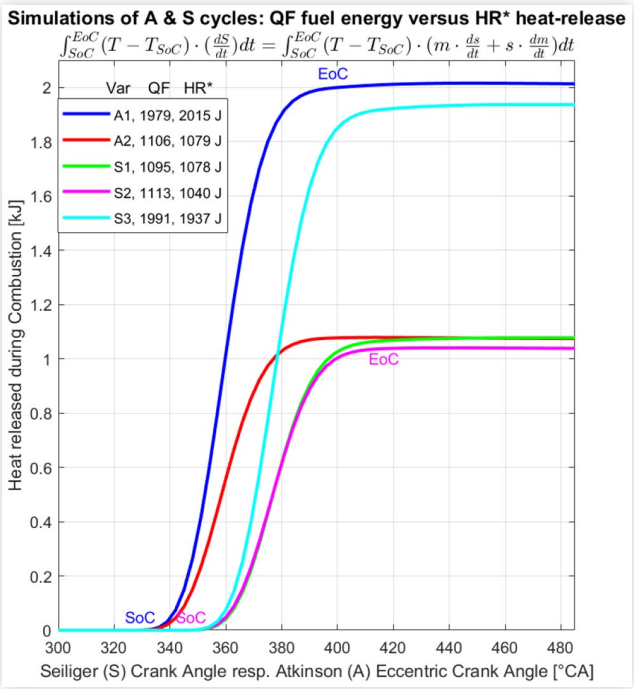

exergy from the released heat instead of effectively converting it into mechanical work. These facts also explain the difference in the final values of IFCE.

FIGURE 13 Released heat course over crank angle for the 5 cycles from Table 1. In this plot, the increase of gas mass during combustion due to addition of fuel is not more taken into account. Its maxima is denoted as HR.

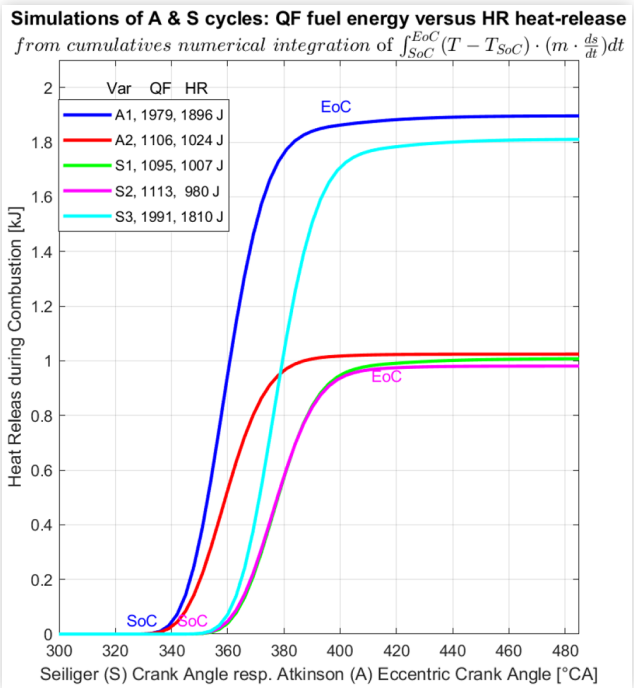

From Fig. 11 it can be seen that due to the higher VER in the cycles, a much larger portion of the nearly equal amount of heat released is converted into mechanical work. The prolonged expansion of the A cycle at identical VCR and gas mass values as S cycles is clearly visible as distance between (EoC) and (eo), e.g. for A2 and S1 cycles. This means that the burned gases after expansion are exhausted at significantly lower temperatures in A cycle.

These simulations of true Atkinson and Seiliger cycles are done for **adiabatic** engines. The losses produced by heat transfer in a nonadiabatic i.e. in a real engine can be estimated from Fig. A2-00 from Appendix 2. These amounts to ca. 5% for Seiliger cycle. For the A-cycle, these losses will be somewhat different because of the shortened compression or extended expansion (see [6] for details, considerations and evaluations).

FIGURE 14 Schematic of the glow plug assisted ignition of hydrogen direct injection with two variants of thermodynamic system boundaries (SysB): a) only inside the cylinder and b) inside cylinder extended to its connecting pipes up to measuring points MP3 and MP5

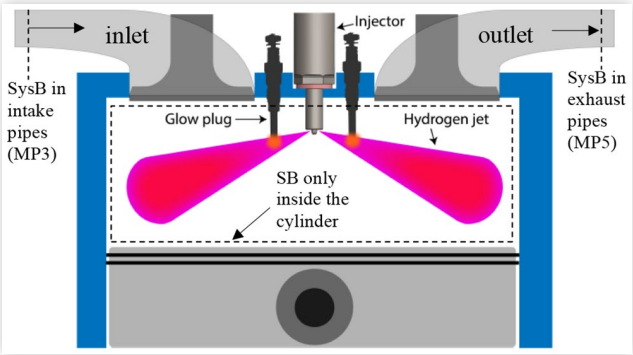

Proof of T·dS/Dt Decomposition Terms and Interpretation of their Integrals

Note: All full differentials of the kind dX or the inexact differential δX mean for simplicity further an infinitesimal amount change of X that happens within the elementary time dt, forming their time derivative $\frac{dX}{dt}$ or the flow rate $\dot{X}$ of the X.

For example, the mass flow rate passing through the inlet (in) or outlet (out) boundaries of the thermodynamic system from Fig. 14 is explicitly denoted by $\dot{m}$.

The first law of thermodynamics for transient processes in open systems, as shown in Fig. 14, is given in formula (1).

$$\frac{dU}{dt} = \frac{dQ}{dt} + \frac{dW_{rev}}{dt} + \frac{dW_{irr}}{dt} + \dot{m}_{in}\cdot h_{in} - \dot{m}_{out}\cdot h_{out} \qquad (1)$$

Where the differentials are for simplicity variations over the time, i.e.

The second law of thermodynamics for transient processes in open systems is (2) as follows:

$$\frac{dS}{dt} = \frac{1}{T}\frac{dQ}{dt} + \frac{1}{T}\frac{W_{irr}}{dt} + \dot{m}_{in} \cdot s_{in} - \dot{m}_{out} \cdot s_{out} \tag{2}$$

The mass balance is done by (3)

$$\frac{dm}{dt} = \dot{m}_{in} - \dot{m}_{out} \tag{3}$$

The entropy $S = m \cdot s$ is a full differential state variable, as given in (4), where s the specific entropy means.

$$\frac{dS}{dt} = m \cdot \frac{ds}{dt} + s \cdot \frac{dm}{dt} \tag{4}$$

Following definitions of internal energy U, enthalpy H and their differentials as well as of the volume changing work dW_v and the pressure changing work dW_p from (5) are furthermore needed:

$$\begin{aligned} H &= U + p{\cdot}V & H &= c_p{\cdot}m{\cdot}T \\ dH &= h{\cdot}dm + m{\cdot}d & U &= c_v{\cdot}m{\cdot}T \\ dH &= dU + p{\cdot}dV + V{\cdot}dp & dH &= c_p{\cdot}m{\cdot}dT + c_p{\cdot}T{\cdot}dm \\ dW_v &= dW_{rev} = -p{\cdot}dV & dW_p &= V{\cdot}dp \end{aligned} \tag{5}$$

After eliminating the terms for irreversible work dW_{irr} and heat dQ between equations (1) and (2) using the definitions (5) for eliminating dU and dW_{rev}, we obtain (6):

$$\begin{aligned} T\cdot\frac{dS}{dt} = \frac{dH}{dt} - \frac{dW_p}{dt} - \dot{m}_{in}\cdot\left(h_{in} - T{\cdot}s_{in}\right) \\ +\dot{m}_{out}\cdot\left(h - T{\cdot}s\right) + \left(T - T_{SoC}\right){\cdot}m{\cdot}\frac{ds}{dt} \end{aligned} \tag{6}$$

We assume that specific entropy s, Temperature T and specific enthalpy h at the exit of the system boundary are identical to that from interior of the system, e.g. $s_{out} = s$, this corresponds to a system boundary in the cylinder before the exhaust valve (see Fig. 14).

The last term on the right side of equation (6) is a source term indicating the influence of the short-time heat release on the cycle. This only occurs between the start of combustion *SoC* and the end of combustion *EoC* and increases the thermodynamic states based on the final compression temperature T_{SoC}. For these reasons, this term must be introduced additionally.

The product of temperature and entropy flow, T·dS/dt, i.e. the left side term of eq. (6) and the sum its decomposition terms from right side of eq. (6) are plotted during the cycles over the crank angle as shown in Fig. 15. Their 2-D cross-correlation is almost perfect.

The analysis of the curves from Fig. 15 shows the following influences:

The substantial increase of T·dS/dt during combustion because due to the heat released, as well as its significant decrease during the free expulsion of the exhaust gases are clearly visible.

The strong influence of the degree of filling of the cylinder, i.e. of the intake air plus the added fuel mass, i.e.

FIGURE 15 Evolution and correlation of the product of temperature and entropy flow, T·dS/dt (solid lines) and the sum its decomposition terms (dashed lines) during the cycles over the crank angle.

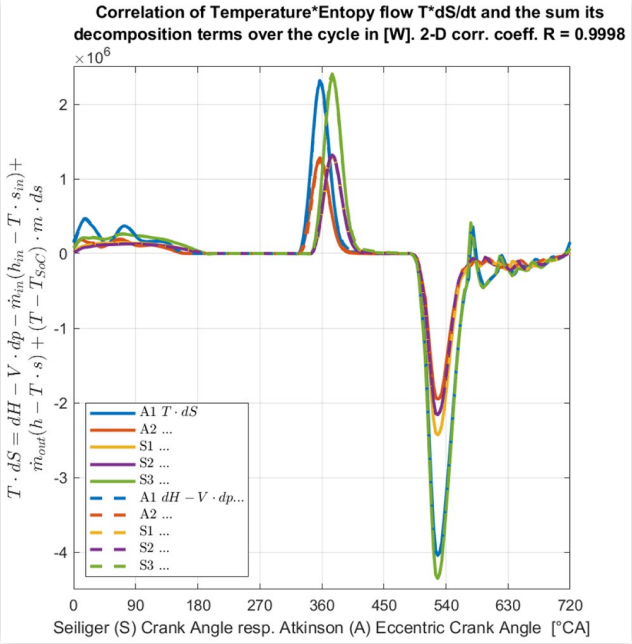

of the total gas mass, can be seen for cycle variants A1 and S3 with double mass compared to the other 3 (A2, S1, S2).

The other cycle parameters from Table 1 cause only minor differences between the curves.

Further information about the cycles and their different efficiencies, i.e. IFCEs, can be obtained after their cumulative integration.

The cumulative integrals of the product of temperature and entropy flow, T·dS/dt and its decomposition terms over the cycles are shown in Fig. 15, optimal (i.e. maximal) scaled in their subplots.

The same is shown in Fig. 16, but this time scaled uniformly to allow easy visual comparison of their magnitudes.

Figs 15 and 16 show that in cycle A2 the highest proportion of thermal energy is converted into mechanical work, so the cumulative exhausted energy $\dot{m}_{out}\cdot\left(h - T{\cdot}s\right)$ until the end of the cycle are the lowest. The cycle A2 has the highest IFCE value. Although the VCR in cycle S2 is twice as large as in cycle A2, S2 IFCE is significantly smaller than that of A2 cycle. See Fig. 20 for an extended comparison of these.

The comparison of A2 and S1 cycles, with identical VCR, is even more disadvantageous for S1. See a detailed comparison in Fig. 19.

This shows that actually the VER is decisive for the IFCE height.

The lack of pre-compression piston stroke of the A cycles is obviously beneficial even at identical VER, as shown by comparing A2 with S2 with single (i.e., at

FIGURE 16 Cumulative integrals of the product of temperature and entropy flow, T·dS/dt and of its decomposition terms during the cycles over the crank angle, optimal (i.e. maximal) scaled in their subplots.

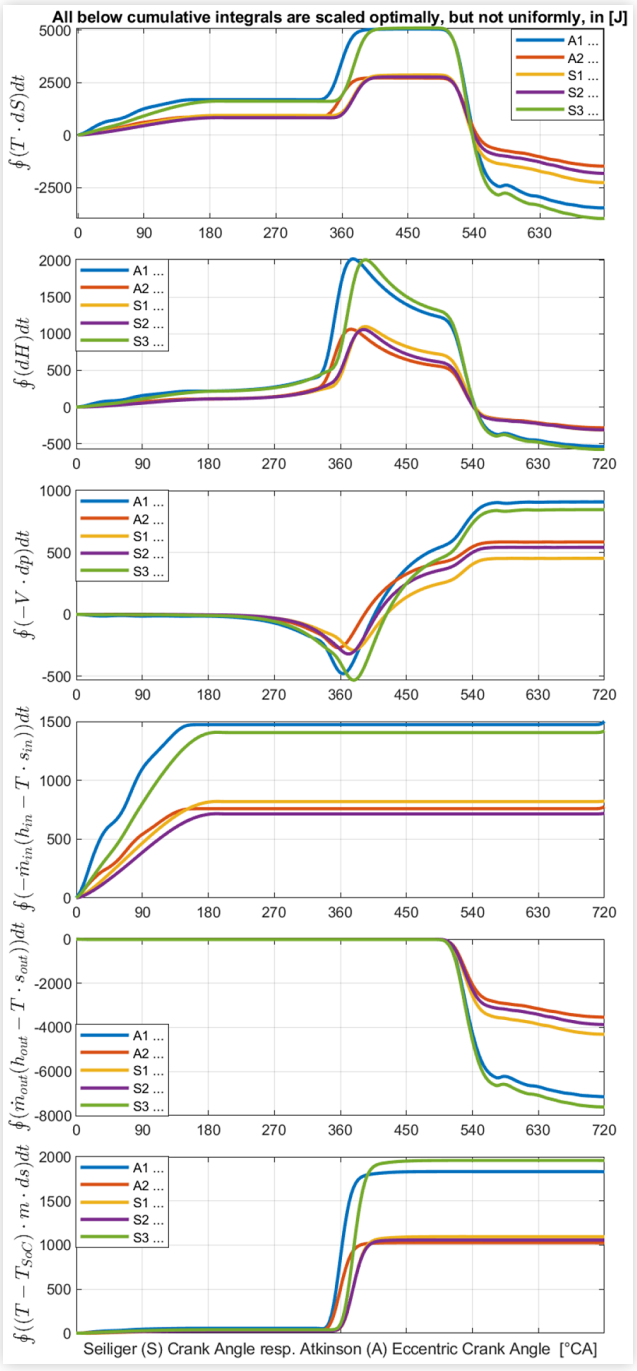

FIGURE 17 Cumulative integrals of the product of temperature and entropy flow, T·dS/dt and of its decomposition terms during the cycles over the crank angle, uniformly scaled in their subplots to allow visual comparison of their magnitudes.

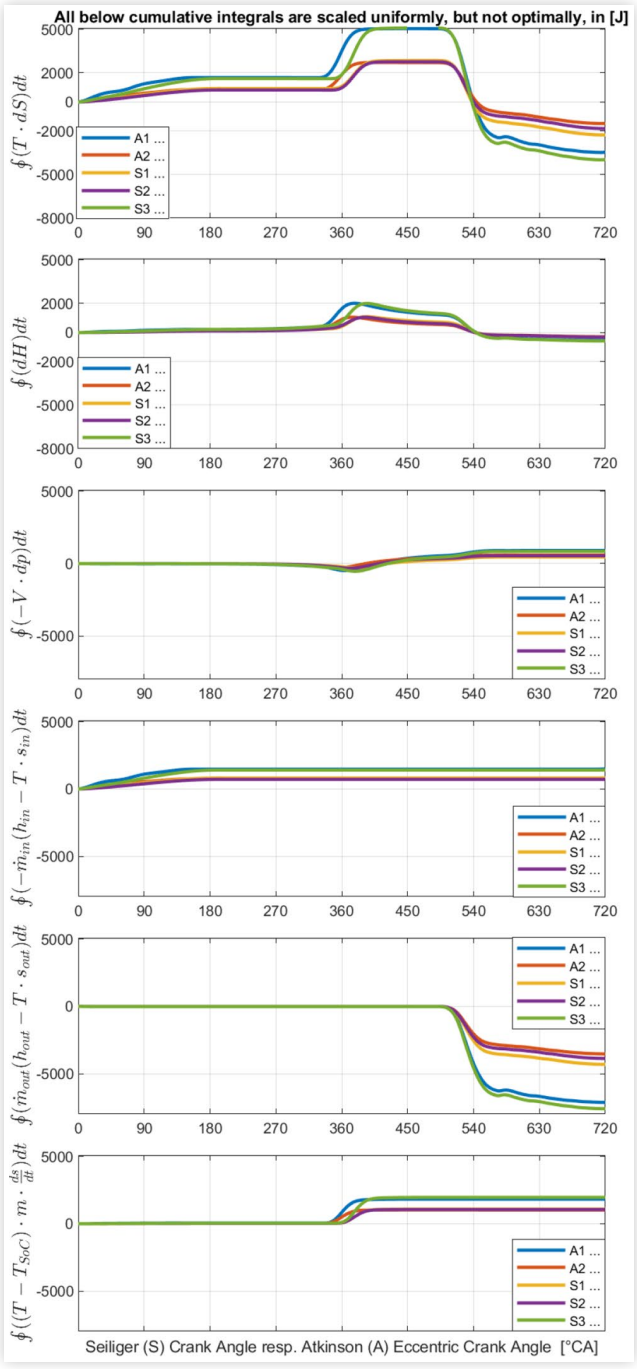

medium load from Fig. 20) and A1 and S3 with double gas mass (i.e., at high load of ICE from Fig. 21).

In the Figures 19 to 22, the differences between the classical Seiliger (S) cycle and true Atkinson (A) cycles, as combination of the cases from Table 1, are shown and briefly addressed or explained.

Equation (6) can be simplified for the adiabatic, $\frac{ds}{dt} = 0$, exhaust-only, $\dot{m}_{in} = 0$, phase, and reestablished, i.e., only for the cycle part between (eo) and (io). That means also $\left(T - T_{SoC}\right) \cdot m \cdot \frac{ds}{dt} = 0$.

After some calculations with the above settings the result is

$$\frac{dS}{dt} = s \cdot \frac{dm}{dt} = \frac{s}{c_p} \cdot \left(\frac{dH}{dt} - \frac{dW_p}{dt} \right)$$

FIGURE 18 "pure exhaust". Evolution and correlation of the product of temperature and entropy flow, T·dS/dt (solid lines) and the sum its decom- position terms (dashed lines) during the pure exhaust phase over the CA.

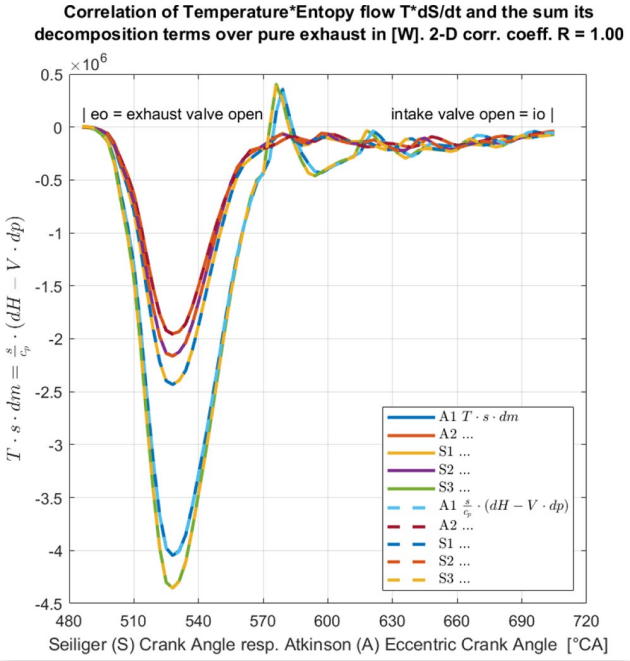

which illustrate the energy lost in the exhaust without gaining any mechanical work on the piston.

The graphical representation is seen as a detail of Figure 18 and therefore this is referred to as Figure 18 "pure exhaust".

The Figures 19 to 22 are intended to illustrate the influences of VCR, VER and load (here simulated by the amount of aspirated gas mass in the cylinder) on the efficiency, IFCE of A and S cycles. This study is performed in addition to all other simulation cases presented in Appendix 2.

For better comparing and understanding of the differences between the S and A adiabatic cycles, the parameter γ of A cycle is kept unchanged, $\gamma \cong 2$, where γ is the ratio between the volumetric expansion ratio VER ε_e and volumetric compression ratio VCR ε_c, or the ratio between the expansion and compression stroke lengths.

In addition to this, the expansion stroke lengths and the aspirated gas masses are identical in pairs for A an O cycle comparisons. The variation of the aspirated gas mass from single, as in Figs. 19 and 20, to double, as in Figs. 21 and 22 shown, is to simulate and to allow the comparison between two load points.

The course of the displacement volume over crank angle respective eccentric crank angle illustrates the clear differences in the piston strokes. The condition of the same VCR in both A and S cycles forces the displacement volume curve of the A cycle to be shifted closer to the cylinder head, as shown in Fig. 19. However, the lengths of the expansion strokes are identical in both cycles.

Brief description of the Figs 19 to 22, which also correspond for the Figures from Appendix 2.

1. The top-left subplot, i.e. (row, column) position (1,1) of each Figs depicts the variations of the displacement volume (V) versus crank angle (CA). Because of the kinematic of the VCSR crank mechanism, the angular positions of the TDC of A cycle can migrate in relation to the TDC of the S cycle. That produces a slow translation of the curves in the diagrams of other EOPs.
   - The VCR is defined as the quotient of the displacement Volume (V) in Gasex. BDC to V in TDC (Gasex. is the abb. for gas exchange, s. Fig. 3 for these BDC and TDC locations).
   - The VER is defined as the quotient of the V in BDC to V in TDC.
   - The Parameter γ is defined as the quotient of VER to VCR and thus of V in BDC to V in Gasex. BDC.
   - The expansion stroke lengths are identical in the A and S cycles, i.e. only the compression stroke lengths of the A cycles are γ-time shorter than the expansion stroke length of the A and S cycles.
2. The top-right subplot, position (1,2) of each Figs depicts the variations of the cylinder pressure (p) versus displacement volume (V) in natural logarithmic coordinates. With the exception of the gas exchange area, this subplot corresponds to Fig. 7 for ideal cycles, where the heat release is modeled here by means of a Vibe function. Note here the different boost pressure levels required to achieve the same intake gas mass in both cycles, and the maximum pressures achieved in the cylinder.
3. The middle-left subplot, position (2,1) of each Figs depicts the variations of the cylinder gas mass (m) versus V. The maximum values on the cycles are nearly identical and indicated there for an easy comparison.
4. The middle-right subplot, position (2,2) of each Figs depicts the variations of the indicated fuel conversion efficiency IFCE (i.e. of the volumetric work cumulative integral divided by the released heat on the cycle) versus V. These diagrams depict the losses and gains in volumetric work along the strokes. The end values are included. The advantage of a γ-time longer expansion stroke referred to compression stroke of the A cycle is obvious.
5. The bottom-left subplot, position (3,1) of each Figs depicts the variations of the cylinder gas Temperature (T) versus absolute (S = m*s) entropy flow dS/dt. The areas within the diagrams are energy flows in Watt released into the cylinder or exchanged between the gas from the cylinder and the exterior. The lower consumed power on the compression strokes and the greater released power on the expansion strokes

FIGURE 19 Comparison between the cases A2 and S1 from Table 1. VCR is almost the same in both cycles, thus the displacement volume course must be shifted toward the cylinder head in the A cycle. Therefore, the VER result differently. IFCE final values are also very different. IFCE win of A cycle is ca. 30% referred to S cycle.

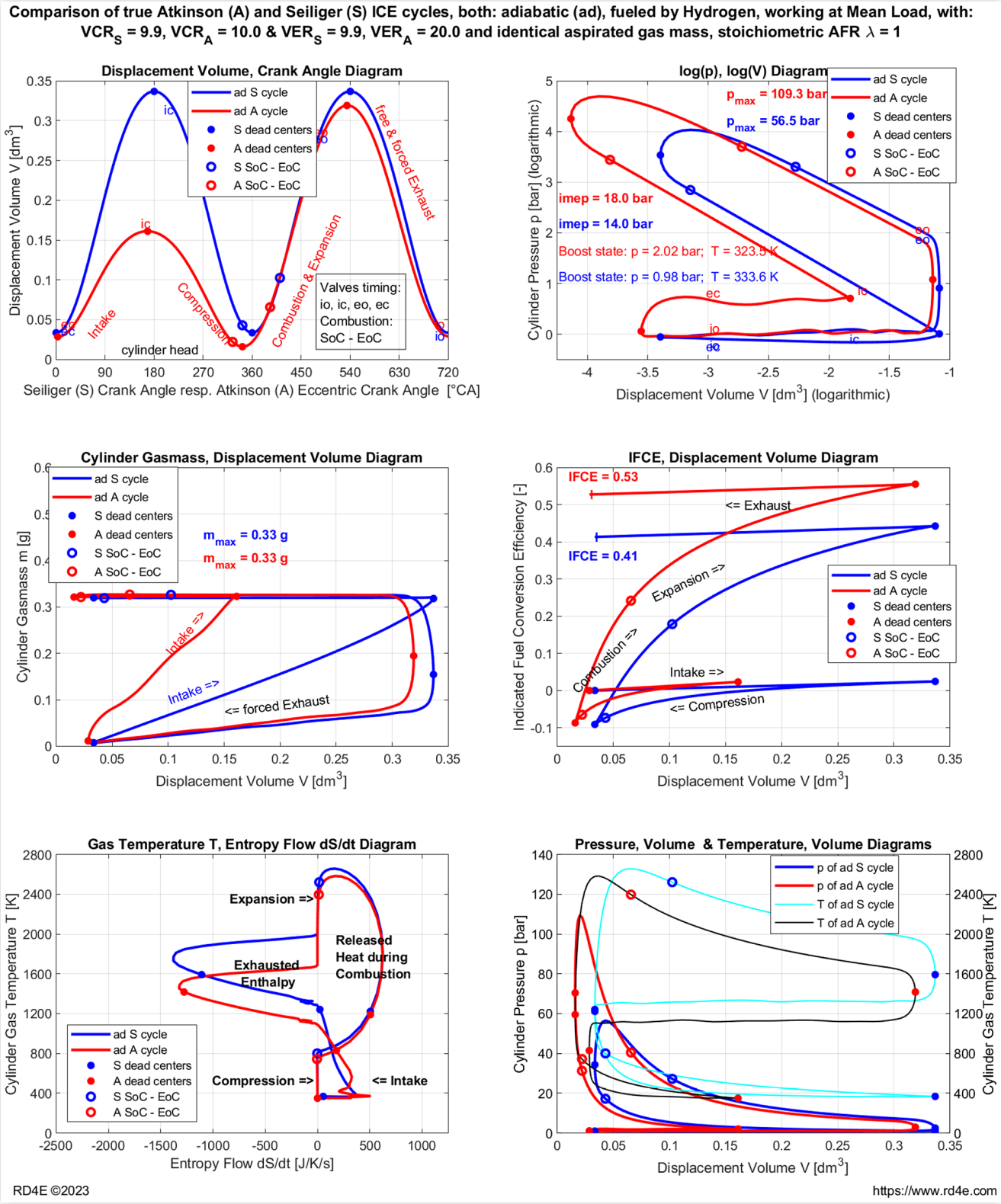

FIGURE 20 Comparison between cases A2 and S2 from Table 1. VER is almost identical in both cycles. Thus, the VCR result differently. Only the lack of pre- compression piston stroke, i.e. the shorted comp. stroke, of the A cycles leads to the differences in IFCE values. IFCE win of A cycle is ca. 8.5% referred to S cycle.

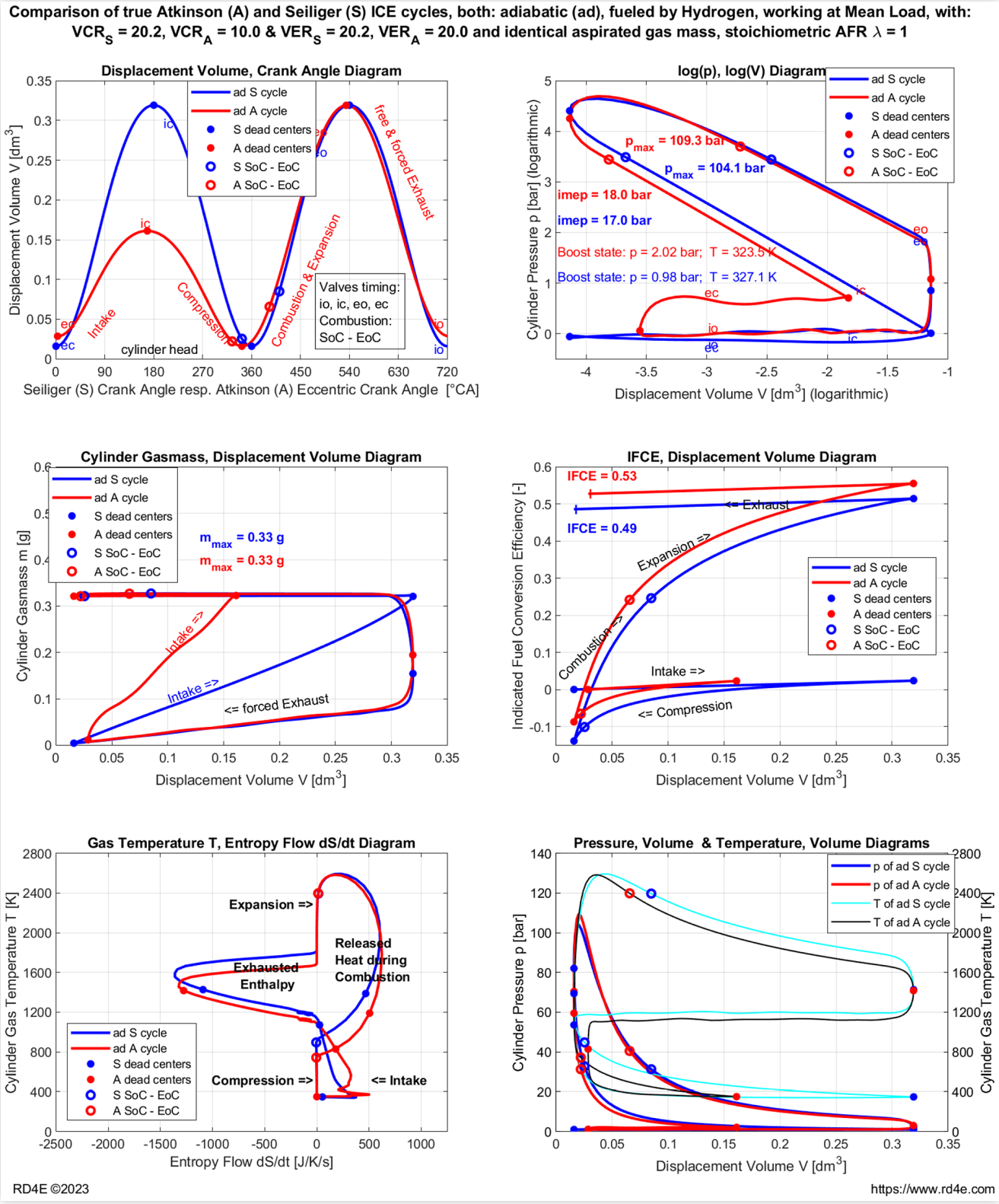

FIGURE 21 Comparison between cases A1 and S3 from Table 1. VER is almost identical in both cycles. VCR of the S cycle is about twice that of A cycle. The comparison is similar to that of Fig. 20, but the cylinder gas mass is twice as large, i.e., a high load is simulated. IFCE win of A cycle is ca. 8% referred to S cycle.

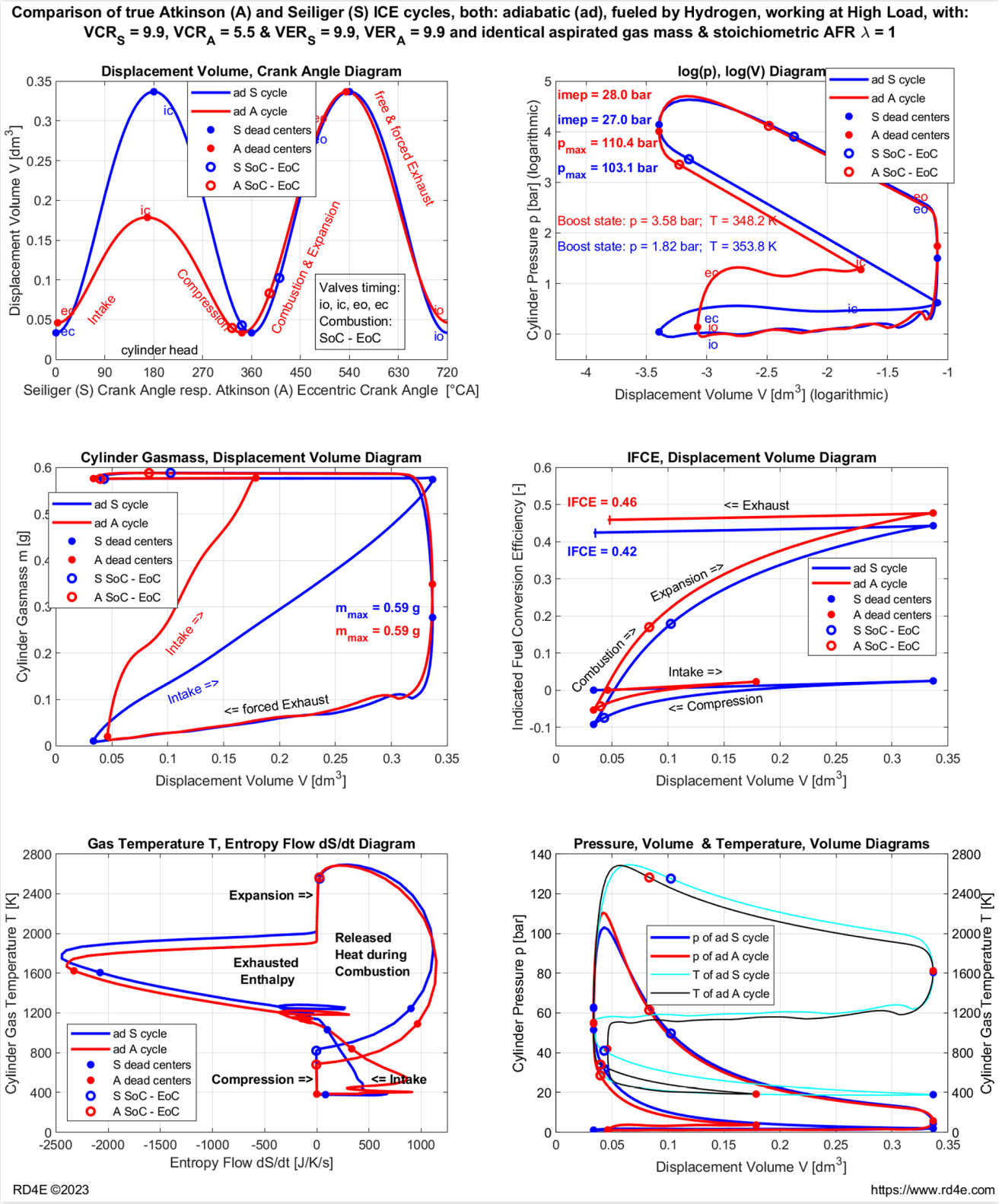

FIGURE 22 Comparison between cases S1 and S3 from Table 1. VCR and VER are identical in both cycles. Only the gas mass in cylinder differs from simple (for mean load simulation) to double, i.e., for the high load simulation. IFCE is almost identical in both cycles. The T,dS/dt diagram clearly shows the load difference.

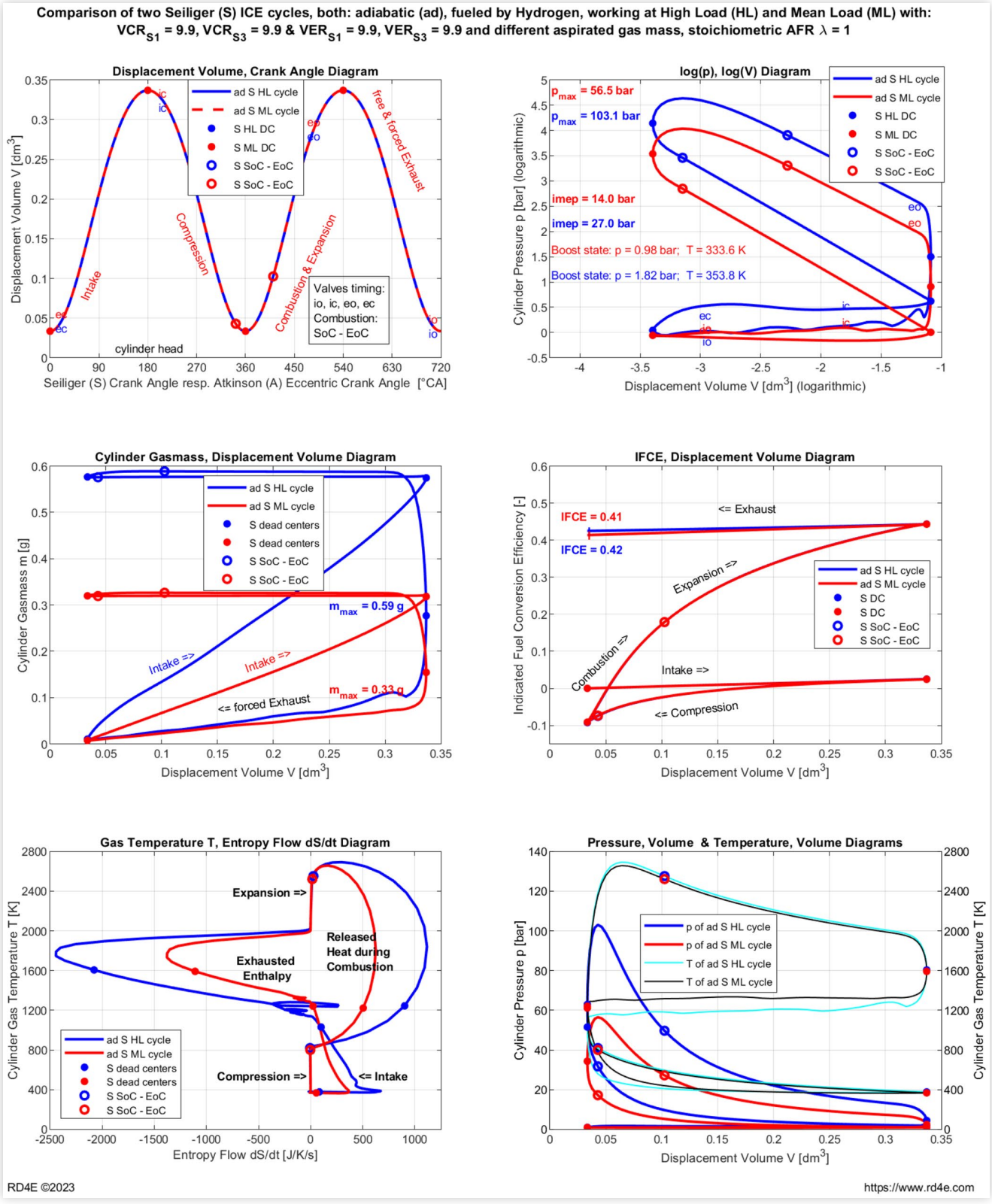

of the A cycles are clearly shown. The enthalpy flow during exhaust is clearly depicted. This energy flow does not produce volumetric work at the piston, but it drives the TC-compressor. In the A cycle the exergy part of the exhausted enthalpy flow is much lower (indicated also by its lower mean temperature) because of their conversion on the extended expansion for producing of volumetric work, compared with the S cycle.

6. The bottom-right subplot, position (3,2) of each Figs depicts the variations of the cylinder pressure p versus V and the cylinder temperature (T) versus V in the usual coordinates.
7. In Appendix 2. The summary (text) files A and S of true Atkinson and Seiliger cycles which contain the mean values of most cycle parameters, are linked in the captions of all EOPs! For example, the above A and S are linked to the summary files of the 8th EOP.

Conclusions

Internal combustion engines with VCSR crank mechanisms can be operated according to the **true** Atkinson cycle (A) and UD load control. This would allow a higher efficiency, expressed by IFCE, of over 25% compared to combustion engines classically operating according to the Seiliger cycle (S) for identical VCR values.

The performance of the TC system determines the maximal selectable value of the parameter γ, i.e. the ratio of VER to VCR or of the overexpansion when designing the ICE.

New turbocharger systems, e.g. with a multi-stage axial compressor driven by a two-stage turbine and capable of achieving boost pressures of around 10 bar, would be very interesting due to the VCR adaptation. E.g., a VCSR engine used as a core instead of the annular combustion chamber of a turbofan engine with such a high boost pressure, would therefore allow γ values close to 3, and thereby: (a) significantly increase efficiency and therefore reduce BSFC, (b) a significantly higher bypass throughput, e.g. well over 20%, (c) easier compensation for altitude flight by adjusting the VCR, (d) the use of different fuels, such as gaseous or liquefied H_2 or NH_3, biofuels, CNG, LPG or kerosene, either pure or in any mixture.

An outlook on operating strategies for internal combustion engines operated with pure H_2 or H_2-CNG mixtures can be found in [17]. This applies both to classic internal combustion engines and to internal combustion engines with VCSR crank mechanism operated according to the **true** Atkinson cycle and with UD load control.

The results from the over-expanded Atkinson cycles implementations from [18, 19] show that crank drives that only offer an extended expansion do not meet the requirements for high efficiency at all operating load points and that a simultaneous VCR adjustment is absolutely necessary. This applies all the more if multi-fuel operation of these engines is the aim.

By combining these approaches, the UD concept aims to achieve higher power output, improved efficiency, and reduced environmental impact in ICEs, all while ensuring the durability and strength of engine components remain within acceptable limits.

This important increase in efficiency is confirmed both by thermodynamic analysis of **ideal** cycles and by analysis of simulations (performed with AVL Boost Tool) of **real** cycles.

Acknowledgments

My special thanks to Mr. Dave Roth for his review and very valuable comments.

References

1. Heywood, J. and B., *Internal Combustion Engine Fundamentals* (McGraw-Hill international editions, 1988) ISBN 0-07-100499-8
2. Gheorghiu, V., "Ultra-Downsizing of Internal Combustion Engines," SAE Technical Paper 2015-01-1252 (2015), https://doi.org/10.4271/2015-01-1252.
3. Gheorghiu, V. "Ultra-Downsizing of Internal Combustion Engines," in *1st ICEP, International Conference on Engine Processes*, Berlin, June, 2013.
4. Gheorghiu, V. "Ultra-Downsizing of Internal Combustion Engines," in *APAC16 16th, M20100119*, Chennai, India, October 2011.
5. Gheorghiu, V. "VCSR aided Ultra Downsizing of ICEs," Presentation, 2018.
6. Schutting, E., Dumböck, O., Eichlseder, H., Graz, T.U., et al. "Diagnostics of Spark an Ignition Engine with Extended Expansion – Challenges and Approaches," in *International Symposium for Burn Diagnostics*, Baden-Baden, 2014.
7. Chan, S.H., and Goh, S.C., "An Overview of Otto / Atkinson / Diesel / Brayton Cycles in IC Engine Applications," Nanyang Technological University Singapore, csh-gsc\jdhsice1 / 22.10.96
8. Turner, J., Popplewell, A., Patel, R., Johnson, T. et al., "Ultra Boost for Economy: Extending the Limits of Extreme Engine Downsizing," *SAE Int. J. Engines* 7, no. 1 (2014): 387-417, https://doi.org/10.4271/2014-01-1185.
9. Gheorghiu, V. "Sustainable Mobility & Sustainable Energy System Transition against Global Warming, "Thesis_00", Presentation, 2020-2022.
10. Patent DE102013003682B4 (filed 2013, granted 2018).
11. Patent EP 2 772 624 B1 (filed 2014, granted 2020).
12. Chan, S. and Goh, S., "The Design of a Double Helical Screw Internal Combustion Engine," SAE Technical Paper 970064 (1997), https://doi.org/10.4271/970064.

13. Gheorghiu, V. "Comparison of the thermal efficiencies for the real cycles of the true Atkinson (A) and the classic gasoline Otto (O) ICE Seiliger (S), both turbocharged & hydrogen fueled, while maintaining the same VCR values, expansion stroke lengths, maximum gas mass and stoichiometric AFR", outsourced as Appendix 2.
14. Atkinson, J. US Patent 367496.
15. Animation of Atkinson crank mechanism from [14]
16. Animation of VCSR crank mechanism from [10] and [11] in variants 1 or 2
17. Eichlseder, H., and Klell, M., "Wasserstoff in der Fahrzeugtechnik," "Hydrogen in vehicle technology," Springer Link, 2018, doi:10.1007/978-3-658-20447-1
18. Anandhan, M. and Cheng, W., "Performance Assessment of Extended Stroke Spark Ignition Engine," SAE Technical Paper 2018-01-0893 (2018), https://doi.org/10.4271/2018-01-0893.
19. Yang, Z., Miganakallu Narasimhamurthy, N., Miller, T., and Naber, J., "Investigation and Optimization of Cam Actuation of an Over-Expanded Atkinson Cycle Spark-Ignited Engine," *SAE Int. J. Adv. & Curr. Prac. In Mobility* 1, no. 2 (2019): 639-653, https://doi.org/10.4271/2019-01-0250.

Contact Information

Victor Gheorghiu
Prof. Emeritus PhD ME
Hamburg University of Applied Sciences, Faculty TI
Dpt. of Mechanical Engineering
Berliner Tor 2, 20099 Hamburg, Germany
victor.gheorghiu@haw-hamburg.de
https://www.victor-gheorghiu.de/
mail@victor-gheorghiu.de
https://www.rd4e.com
grg@rd4e.com

Abbreviations also for Appendices 1 and 2

Internal Combustion Engines - **ICE**
Electrical Vehicle - **EV**
Fuel Cell Electrical Vehicle - **FCEV**
Variable Compression and Stroke Ratios - **VCSR**
Ultra-Downsizing - **UD**
Load Control - **LC**
Air Fuel Equivalence Ratio - **AFR**
Volumetric Compression Ratio - **VCR**
Volumetric Expansion Ratio - **VER**
Indicated Fuel Conversion Efficiency - **IFCE**
Indicated Mean Pressure - **IMEP**
GreenHouse Gas emissions - **GHG**
Specific (i.e. related to mass) - **sp.**
stoichiometric - **stoich.**
relative (non-dimensional) - **rel.**
Calorical Equation - **CE**
State Equation - **SE**
Law of Thermodynamics - **LoT**
First Law of Thermodynamics - **1.LoT**
Second Law of Thermodynamics - **2.LoT**
Turbocharger - **TC**
Turbine of TC - **T**
Compressor of TC - **C**
True Atkinson cycle - **A cycle**
Otto (Gasoline engine) cycle - **O cycle**
Gas Turbine cycle - **TC cycle**
proportional - **~**
Top Dead Center - **TDC**
Bottom Dead Center - **BDC**
Gas exchange TDC - **gasex. TDC**
Gas exchange BDC - **gasex. BDC**
intake valve open - **io**
intake valve closed - **ic**
exhaust valve open - **eo**
exhaust valve closed - **ec**
VCSR Basic Working Principle - **BWP**
Planet Gear - **PG**
Eccentric Crank - **EC**
Crank Disc - **CD**
Sun Gear - **S**
Planet Carrier - **PC**
Planet - **P**
Ring Gear - **RG**

Foot / Head Indices

p - isobaric
v - isochoric
t - technical
c - compression
e - expansion
0 - environment state
A - Atkinson cycle
O - Otto cycle
TC - Gas Turbine (TC) cycle
1, 2, 3, 4 - thermodynamic states
°(head index) - Ideal Gas Behavior

Definitions

Symbol	Meaning	Unit
v	specific Volume	m^3/kg
T	absolute (Kelvin) Temperature	K
p	Pressure	Pa, bar, MPa
m	Mass	kg
c^o_v	specific isochoric Heat Capacity	kJ/kg/K
c^o_p	specific isobaric Heat Capacity	kJ/kg/K
c	flow Speed	m/s
s	specific Entropy	kJ/kg/K
u	specific internal Energy	kJ/kg
h	specific Enthalpy	kJ/kg
q	specific Heat	kJ/kg
w_v	specific volume change Work	kJ/kg
w_p or y	specific pressure change Work	kJ/kg
w_t	specific technical Work	kJ/kg
j	specific irreversible Work	kJ/kg
R	Gas Constant of Air as Ideal Gas	kJ/kg/K
κ	isentropic Exponent	-
ε_c	**VCR** (Volumetric Compression Ratio)	-
ε_e	**VER** (Volumetric Expansion Ratio)	-
λ	Air Fuel Equivalence Ratio **AFR**	-
δ	Pressure-Rise Ratio during the heat release = combustion	-
γ	Compression to Expansion Volumetric Ratios, **VCR**/**VER**	-
S_{exp}	Expansion stroke length	m
S_{comp}	Compression stroke length	m
r_{CS}	Crank shaft radius	m
r_{EC}	Eccentric crank radius	m
$\Delta\alpha_R$	Twist angle of the ring gear for setting the VCR	° degree
n	speed	rpm
CA	Crank angle	°CA
CDA	Crank disc angle	°CDA

Appendix 1

Comparison of the thermal efficiencies of the **true** Atkinson (**A**) and gasoline classic Otto (**O**) ICE cycles, both with Brayton/Joule Gas Turbine cycle (particular **TC**), while maintaining the same Temperature at the Exhaust beginning in all three **ideal** cycles (i.e. under the same conditions)

FIGURE A1-1 Thermodynamic background and proof of the Efficiency formulas. Part 1.

Thermodynamic properties of the air, reference state and other common values

Environment state (Index 0)

$T_0 := 273.15 \cdot K$ Temperature

$p_0 := 1 \cdot bar$ Pressure

$s_0 := 6.7763 \cdot \frac{kJ}{kg \cdot K}$ air specific entropy

$\kappa := 1.2765$ Isentropic Exponent averaged per engine cycles, a more realistical value than 1.4 of air in environment state

$R := 287.2 \cdot \frac{J}{kg \cdot K}$ Gas Constant of Air (as Ideal Gas)

Further conventions:
All three cycles are ideal, i.e.:
$dj = 0$ thus reversible, and
$d\left(\frac{c^2}{2}\right) = 0$ the variation of specific kinetic energy is neglected here

Foot Indices:
p = isobaric
v = isochoric
c = compression
e = expansion
t = technical
Head Index:
° = Ideal Gas

Some usefull thermodynamical formulas:

Specific Heat Capacities

$c^\circ_v = \frac{R}{\kappa - 1}$ $c^\circ_p = c^\circ_v + R$ $c^\circ_p = \frac{\kappa \cdot R}{\kappa - 1}$ $\frac{c^\circ_p}{c^\circ_v} = \kappa$

$c^\circ_v := \frac{R}{\kappa - 1}$ $c^\circ_v = 1.039 \frac{kJ}{kg \cdot K}$ $c^\circ_p := \frac{\kappa \cdot R}{\kappa - 1}$ $c^\circ_p = 1.326 \frac{kJ}{kg \cdot K}$

Specific Entropy Equations

$s(T,p) = s_0 + c^\circ_p \cdot \ln\left(\frac{T}{T_0}\right) - R \cdot \ln\left(\frac{p}{p_0}\right)$ $s(T,v) = \left(s_0 + c^\circ_v \cdot \ln\left(\frac{T}{T_0}\right)\right) + R \cdot \ln\left(\frac{v}{v_0}\right)$

State Equation (**SE**)
$p \cdot v = R \cdot T$ or
$p \cdot V = m \cdot R \cdot T$

Calorical Equations (**CE**)
$du = c^\circ_v \cdot dT$
$dh = c^\circ_p \cdot dT$

Specific Enthalpy definition, and it differential
$h = u + p \cdot v$
$dh = du + p \cdot dv + v \cdot dp$
$dh = du - dw_v + dy$
$dw_t = dy + dj + d\left(\frac{c^2}{2}\right)$
$dw_t = dy$ in agreement with the left conventions

1.LoT Energy balance differential & integral, First law of thermodynamic
$du = dq + dw_v + dj$ $u_2 - u_1 = q_{12} + w_{v12} + j_{12}$

2.LoT Entropy balance differential, Second law of thermodynamic
$ds = \frac{dq + dj}{T} = \frac{du - dw_v}{T} = \frac{dh - dy}{T}$

True Atkinson Cycle (Index A)

Otto Cycle (Index O)

Brayton Cycle (Index TC) for Turbocharger (TC) states

identical VCR volumetric compression ratios in Atkinson & Otto cycles

$\varepsilon_{cA} = \varepsilon_{cO}$ $\varepsilon_{cA} = \varepsilon_{cO}$

Brayton cycle has a different VCR!!!!

$\varepsilon_{cA} = \frac{v_{1A}}{v_{2A}}$ VCR of Atkinson cycle

$\varepsilon_{eA} = \frac{v_{4A}}{v_{2A}} = \frac{v_{4O}}{v_{2A}}$ Volumetric Expansion Ratio VER of Aktinson cycle, i.e.

$\gamma = \frac{\varepsilon_{eA}}{\varepsilon_{cA}} = \frac{v_{4A}}{v_{2A}} \cdot \frac{v_{2A}}{v_{1A}} = \frac{v_{4A}}{v_{1A}}$ VER to VCR ratio also expansion to compression strokes ratio of Atkinson cycle

$\gamma = \frac{v_{4O}}{v_{1A}} = \frac{\varepsilon_{cO} \cdot v_{2O}}{\varepsilon_{cA} \cdot v_{2A}} = \frac{v_{1O}}{v_{1A}} = \frac{v_{2O}}{v_{2A}}$ other derived dependencies

$\varepsilon_{eA} = \varepsilon_{cA} \cdot \gamma$ $v_{1A} = \frac{v_{4A}}{\gamma} = \frac{v_{4O}}{\gamma} = \frac{v_{2O} \cdot \varepsilon_{cO}}{\gamma} = \frac{v_{1O}}{\gamma}$

$\varepsilon_{cO} = \frac{v_{1O}}{v_{2O}} = \frac{v_{4O}}{v_{2O}}$ VCR of Otto cycle

$v_{4O} = v_{4A}$ identical cylinder displacemal in both Otto- and Atkinson-cycles

identical states 1 in both Otto and Brayton cycles, thus:

$p_{1O} = p_{1TC}$ $T_{1O} = T_{1TC}$ $v_{1O} = v_{1TC}$

Because state 1A lie on the isentropic state changing 1O-2O, it follows

$m_{1A} = m_{1O} = m_{1TC}$ the proof is presented below to states 1A, 1O, 1TC

$\varepsilon_{cTC} = \frac{v_{1TC}}{v_{2TC}} = \frac{v_{4TC}}{v_{3TC}}$ and with:
$v_{2TC} = v_{1A}$
$v_{1TC} = v_{1O}$

$\varepsilon_{cTC} = \frac{v_{1O}}{v_{1A}} = \gamma$

True Atkinson Cycle (Index A)

Otto Cycle (Index O)

Brayton Cycle (Index TC) for Turbocharger (TC) cycle part

Description of the state changes on all three cycles, referred to 1O as reference state

1A-2A	isentropic Compression:	$s_{1A} = s_{2A}$,
2A-3A	isochoric Heat Release:	$v_{2A} = v_{3A}$ Combust. simulation
3A-4A	isentropic Expansion,	$s_{3A} = s_{4A}$
4A-1A	Atkinson-cycle is closed over the Turbocharger (TC) cycle i.e. the Atkinson cycle substitues the heat release on the Brayton here TC cycle.	

1O-2O	isentropic Compression:	$s_{1O} = s_{2O}$
2O-3O	isochoric Heat Release:	$v_{2O} = v_{3O}$
3O-4O	isentropic Expansion:	$s_{3O} = s_{4O}$
4O-1O	isochoric Exhaust to entvir.	$v_{4O} = v_{1O}$

1TC-2TC	isentropic Compression:	$s_{1TC} = s_{2TC}$
2TC-3TC	**assumed** isobaric Heat Release:	$p_{2TC} = p_{3TC}$
3TC-4TC	isentropic Expansion:	$s_{3TC} = s_{4TC}$
4TC-1TC	isobaric Exhaust to entvir.	$p_{4TC} = p_{1TC}$

State 1A in Atkinson-cycle $p_{1A}, T_{1A}, v_{1A}, V_{1A}, m_{1A}, s_{1A}$

State 1O in Otto-cycle, all states are given: $p_{1O}, T_{1O}, v_{1O}, V_{1O}, m_{1O}, s_{1O}$

$p_{1O} \cdot V_{1O}^{\kappa} = p_{1A} \cdot V_{1A}^{\kappa}$

State 1TC in TC-cycle $p_{1TC}, T_{1TC}, v_{1TC}, m_{1TC}, s_{1TC}$

$p_{1O} = p_{1TC}$ $T_{1O} = T_{1TC}$ $v_{1O} = v_{1TC}$

The gas mass is in all cycles equal. Proof:

1O-1A-2O-2A isentropic compression

it applies: $p_{1A} = p_{1O} \cdot \left(\frac{V_{1O}}{V_{1A}}\right)^{\kappa}$ $T_{1A} = T_{1O} \cdot \left(\frac{V_{1O}}{V_{1A}}\right)^{\kappa - 1}$

with $\gamma = \frac{V_{1O}}{V_{1A}}$ it results $p_{1A} = p_{1O} \cdot \gamma^{\kappa}$ $T_{1A} = T_{1O} \cdot \gamma^{\kappa - 1}$

$m_{1A} = \frac{p_{1A} \cdot V_{1A}}{R \cdot T_{1A}} = \frac{p_{1O} \cdot \gamma^{\kappa} \cdot \frac{V_{1O}}{\gamma}}{R \cdot T_{1O} \cdot \gamma^{\kappa - 1}} = \frac{p_{1O} \cdot V_{1O}}{R \cdot T_{1O}} = m_{1O}$

from state equation **SE** in the states 1A and 1O it results identical gas mass:

$m_{1O} = \frac{p_{1O} \cdot V_{1O}}{R \cdot T_{1O}}$ and because the state 1O and 1TC are identical, it results:

$m_{1TC} = m_{1O} = m_{1A}$

1.LoT on 1O-1A $u_{1A} - u_{1O} = w_{v1O\_1A} + q_{1O\_1A}$

where $q_{1O\_1A} = 0$ isentropic => adiabatical

CE $u_{1A} - u_{1O} = c^\circ_v \left(T_{1A} - T_{1O}\right)$ $u_{1O} = c^\circ_v \cdot T_{1O}$

specific volume change work related to u_{1O}

$w_{v1O\_1A} = c^\circ_v \cdot \left(T_{1A} - T_{1O}\right)$

$w^*_{v1O\_1A} = \gamma^{\kappa - 1} - 1$ $w^*_{v1O\_1A} = \frac{w_{v1O\_2A}}{u_{1O}}$

FIGURE A1-2 Thermodynamic background and proof of the Efficiency formulas. Part 2.

State 2A, Isentropic Compression (1A-2A), 1A & 2A lie on (1O-2O)

$p_{2A} = p_{1A}\cdot\varepsilon_{cA}^{\kappa} = p_{1O}\cdot(\varepsilon_{cA}\cdot\gamma)^{\kappa}$ $\quad v_{2A} = \frac{v_{1A}}{\varepsilon_{cA}} = \frac{v_{1A}}{\varepsilon_{cA}}$

$T_{2A} = T_{1A}\cdot\varepsilon_{cA}^{\kappa-1} = T_{1O}\cdot(\varepsilon_{cA}\cdot\gamma)^{\kappa-1} = T_{1O}\cdot\varepsilon_{eA}^{\kappa-1}$ $\quad s_{2A} = s_{1A} = s_{1O}$

1.LoT on 1A-2A $u_{2A} - u_{1A} = w_{v1A\_2A} + q_{1A\_2A}$

where $q_{1A\_2A} = 0$ isentropic => adiabatical

CE $u_{2A} - u_{1A} = c^{\circ}_{v}(T_{2A} - T_{1A})$

specific volume change work $w_{v1A\_2A} = c^{\circ}_{v}\cdot(T_{2A} - T_{1A})$

related to u_{1O} $w^{*}_{v1A\_2A} = \gamma^{\kappa-1}\cdot\left(\varepsilon_{cA}^{\kappa-1} - 1\right)$

State 3A, Isochoric Heat Release (2A-3A)

The pressure Increase δ_{pA_v} due to isochoric combustion is identical in both A & O cycles

$\delta_{pA\_v} = \frac{p_{3A}}{p_{2A}} = \frac{T_{3A}}{T_{2A}}$ it folows with respect of: $\quad \delta_{pA\_v} = \delta_{pO\_v}$ $\quad \delta_{pTC\_p} = 1$

$v_{3A} = v_{2A}$ $\quad p_{3A} = p_{2A}\cdot\delta_{pA\_v}$ $\quad \varepsilon_{cA} = \varepsilon_{cO}$ $\quad \varepsilon_{cTC} = \gamma$

$p_{2A}\cdot v_{2A} = R\cdot T_{2A}$ $\quad p_{3A}\cdot v_{3A} = R\cdot T_{3A}$

$T_{3A} = T_{2A}\cdot\delta_{pA\_v} = T_{1O}\cdot(\varepsilon_{cA}\cdot\gamma)^{\kappa-1}\cdot\delta_{pA\_v}$

1.LoT on 2A-3A $u_{3A} - u_{2A} = w_{v2A\_3A} + q_{2A\_3A}$

where $w_{v2A\_3A} = 0$ isochoric, no volume variation

CE $u_{3A} - u_{2A} = c^{\circ}_{v}(T_{3A} - T_{2A})$

specific released heat $q_{2A\_3A} = c^{\circ}_{v}\cdot(T_{3A} - T_{2A})$

$q_{2A\_3A} = c^{\circ}_{v}\cdot T_{1A}\cdot\varepsilon_{cA}^{\kappa-1}\cdot(\delta_{pA\_v} - 1)$

related to u_{1O} $q^{*}_{2A\_3A} = (\varepsilon_{cA}\cdot\gamma)^{\kappa-1}\cdot(\delta_{pA\_v} - 1)$

$s_{3A} = s_0 + c^{\circ}_{p}\cdot\ln\left(\frac{T_{3A}}{T_0}\right) - R\cdot\ln\left(\frac{p_{3A}}{p_0}\right)$

State 4A, Isentropic Expansion (3A-4A), 4A lies on (3O-4O)

$p_{4A} = \frac{p_{3A}}{\varepsilon_{eA}^{\kappa}} = \frac{p_{3A}}{(\varepsilon_{cA}\cdot\gamma)^{\kappa}}$ $\quad v_{4A} = v_{3A}\cdot\varepsilon_{eA} = v_{1A}\cdot\gamma$

$T_{4A} = \frac{T_{3A}}{\varepsilon_{eA}^{\kappa-1}} = \frac{T_{2A}\cdot\delta_{pA}}{(\varepsilon_{cA}\cdot\gamma)^{\kappa-1}} = T_{1O}\cdot\delta_{pA\_v}$ $\quad s_{4A} = s_{3A} = s_{3O}$

1.LoT on 3A-4A $u_{4A} - u_{3A} = w_{v3A\_4A} + q_{3A\_4A}$

where $q_{3A\_4A} = 0$ isentropic => adiabatical

CE isochoric $u_{4A} - u_{3A} = c^{\circ}_{v}(T_{4A} - T_{3A})$

specific volume change work $w_{v3A\_4A} = c^{\circ}_{v}\cdot(T_{4A} - T_{3A})$

related to u_{1O} $w^{*}_{v3A\_4A} = \delta_{pA\_v}\cdot\left[1 - (\varepsilon_{cA}\cdot\gamma)^{\kappa-1}\right]$

State 1A, Complete Atkinson cycle: Isentropic expantion in TC Turbine (4A-4TC), Isobaric Exhaust and Heat Discharge over TC Turbine (4TC-1TC), Isentropic compression (1TC-2TC) in TC Compressor and Filling the cylinders (2TC-1A)

1.LoT on 4A-1O $u_{1O} - u_{4A} = w_{v4A\_1O} + q_{4A\_1O}$

where $w_{v4A\_1O} = 0$ no piston work needed for that state change

CE isochoric $u_{1O} - u_{4A} = c^{\circ}_{v}(T_{1O} - T_{4A})$ thus

specific isochoric discharged heat $q_{4A\_1O} = c^{\circ}_{v}(T_{1O} - T_{4A})$

related to u_{1O} $q^{*}_{4A\_1O} := (1 - \delta_{pA\_v})$

State 2O, Isentropic Compression (1O-2O)

$p_{2O} = p_{1O}\cdot\varepsilon_{cO}^{\kappa} = p_{1O}\cdot\left(\frac{v_{1O}}{v_{2O}}\right)^{\kappa}$ $\quad v_{2O} = \frac{v_{1O}}{\varepsilon_{cO}}$

$T_{2O} = T_{1O}\cdot\varepsilon_{cO}^{\kappa-1}$ $\quad s_{2O} = s_{1O}$

1.LoT on 1O-2O $u_{2O} - u_{1O} = w_{v1O\_2O} + q_{1O\_2O}$

where $q_{1O\_2O} = 0$ isentropic => adiabatical

CE $u_{2O} - u_{1O} = c^{\circ}_{v}(T_{2O} - T_{1O})$

specific volume change work $w_{v1O\_2O} = c^{\circ}_{v}\cdot(T_{2O} - T_{1O})$

related to u_{1O} $w^{*}_{v1O\_2O} = \varepsilon_{cO}^{\kappa-1} - 1$

State 3O, Isochoric Heat Release (2O-3O)

The pressure Increase δ_{pO_v} due to isochoric combustion

$\delta_{pO\_v} = \frac{p_{3O}}{p_{2O}} = \frac{T_{3O}}{T_{2O}}$ $\quad \delta_{pA\_v} = \delta_{pO\_v}$ $\quad \delta_{pTC\_p} = 1$

$\varepsilon_{cA} = \varepsilon_{cO}$ $\quad \varepsilon_{cTC} = \gamma$

$v_{3O} = v_{2O}$ $\quad p_{3O} = p_{2O}\cdot\delta_{pO\_v}$

$p_{2O}\cdot v_{2O} = R\cdot T_{2O}$ $\quad p_{3O}\cdot v_{3O} = R\cdot T_{3O}$

$T_{3O} = T_{2O}\cdot\delta_{pO} = T_{1O}\cdot\varepsilon_{cO}^{\kappa-1}\cdot\delta_{pO\_v}$

1.LoT on 2O-3O $u_{3O} - u_{2O} = w_{v2O\_3O} + q_{2O\_3O}$

where $w_{v2O\_3O} = 0$ isochoric

CE $u_{3O} - u_{2O} = c^{\circ}_{v}(T_{3O} - T_{2O})$

specific released heat $q_{2O\_3O} = c^{\circ}_{v}\cdot(T_{3O} - T_{2O})$

$q_{2O\_3O} = c^{\circ}_{v}\cdot T_{1O}\cdot\varepsilon_{cO}^{\kappa-1}\cdot(\delta_{pO\_v} - 1)$

related to u_{1O} $q^{*}_{2O\_3O} = \varepsilon_{cO}^{\kappa-1}\cdot(\delta_{pO\_v} - 1)$

$s_{3O} = s_0 + c^{\circ}_{p}\cdot\ln\left(\frac{T_{3O}}{T_0}\right) - R\cdot\ln\left(\frac{p_{3O}}{p_0}\right)$

State 4O, Isentropic Expansion (3O-4O)

$p_{4O} = \frac{p_{3O}}{\varepsilon_{cO}^{\kappa}} = p_{3O}\cdot\left(\frac{v_{3O}}{v_{4O}}\right)^{\kappa}$ $\quad v_{4O} = v_{1O}$

$\varepsilon = \varepsilon_{eO}$

$T_{4O} = \frac{T_{3O}}{\varepsilon_{cO}^{\kappa-1}} = T_{1O}\cdot\delta_{pO\_v}$ $\quad s_{4O} = s_{3O}$

1.LoT on 4O-3O $u_{4O} - u_{3O} = w_{v4O\_3O} + q_{4O\_3O}$

where $q_{4O\_3O} = 0$ isentropic => adiabatical

CE isochoric $u_{4O} - u_{3O} = c^{\circ}_{v}(T_{4O} - T_{3O})$

specific volume charge work $w_{v4O\_3O} = c^{\circ}_{v}\cdot(T_{4O} - T_{3O})$

related to u_{1O} $w^{*}_{v3O\_4O} = \delta_{pO\_v}\cdot\left(1 - \varepsilon^{\kappa-1}\right)$

State 1O, Complete Otto cycle: Isochoric Heat Discharge (4O-1O) and Exhaust to ambient

The pressure Increase δ_{pO_v} due to Combustion 2O-3O is the same for pressure decrease on Exhaust 4O-1O

$\delta_{pO\_v} = \frac{p_{4O}}{p_{1O}} = \frac{p_{3O}}{p_{1O}\cdot\varepsilon_{cO}^{\kappa}} = \frac{p_{3O}}{p_{2O}}$ $\quad \delta_{pO\_v} = \frac{T_{4O}}{T_{1O}}$

where $T_{1O} = \frac{T_{2O}}{\varepsilon_{cO}^{\kappa-1}}$ $\quad T_{4O} = \frac{T_{2O}\cdot\delta_{pO\_v}}{\varepsilon_{cO}^{\kappa-1}}$

specific isochoric discharged heat $q_{4O\_1O} = c^{\circ}_{v}(T_{1O} - T_{4O})$

related to u_{1O} $q^{*}_{4O\_1O} := (1 - \delta_{pO\_v})$

State 2TC, Isentropic flow Compression (1TC-2TC) in TC compressor (C), identical with (1O-2A)

$p_{2TC} = p_{1TC}\cdot\varepsilon_{cTC}^{\kappa} = p_{1TC}\cdot\left(\frac{v_{1TC}}{v_{2TC}}\right)^{\kappa}$ $\quad v_{2TC} = \frac{v_{1TC}}{\varepsilon_{cTC}}$

$T_{2TC} = T_{1TC}\cdot\varepsilon_{cTC}^{\kappa-1}$ $\quad s_{2TC} = s_{1TC}$

1.LoT on 1O-2A $h_{2TC} - h_{1TC} = w_{t1TC\_2TC} + q_{1TC\_2TC}$

where $q_{1TC\_2TC} = 0$ isentropic = adiabatical

CE $h_{2TC} - h_{1TC} = c^{\circ}_{p}(T_{2TC} - T_{1TC})$

specific technical work of C $w_{t1TC\_2TC} = c^{\circ}_{p}\cdot(T_{2TC} - T_{1TC})$

related to u_{1O} $w^{*}_{t1TC\_2TC} = \kappa\cdot\left(\varepsilon_{cTC}^{\kappa-1} - 1\right)$

State 3TC, Isobaric Heat Release (2TC-3TC)

No pressure increase δ_{pTC_p} due to the assumed isobaric combustion

$p_{3TC} = p_{2TC}$ isobaric $\quad \delta_{pTC\_p} = 1$

For a suitable comparison of the efficiencies of the Otto & Atkinson Cycles, is necessary to respect some conditions: All three cycles are designed so that the temperature on entering the turbine (T) i.e. at the Exhaust beginning reaches about 1000°C. See e) comparison condition.

$T_{3TC} = T_{4O} = T_{4A}$ $\quad \delta_{pTC} = \delta_{pA\_v} = \delta_{pO\_v}$

The sates 3TC, 4O & 4A are identical $\quad \varepsilon_{cTC} = \gamma$

1.LoT on 2TC-3TC $h_{3TC} - h_{2TC} = w_{t2TC\_3TC} + q_{2TC\_3TC}$

where $w_{t2TC\_3TC} = 0$ isobaric

CE $h_{3TC} - h_{2TC} = c^{\circ}_{p}(T_{3TC} - T_{2TC})$

specific released heat $q_{2TC\_3TC} = c^{\circ}_{p}\cdot(T_{3TC} - T_{2TC})$

$q_{2TC\_3TC} = c^{\circ}_{p}\cdot\left(T_{3TC} - T_{1TC}\cdot\varepsilon_{cTC}^{\kappa-1}\right)$

related to u_{1O} $q^{*}_{2TC\_3TC} = \kappa\cdot\left(\delta_{pTC} - \varepsilon_{cTC}^{\kappa-1}\right)$

$s_{3TC} = s_0 + c^{\circ}_{p}\cdot\ln\left(\frac{T_{3TC}}{T_0}\right) - R\cdot\ln\left(\frac{p_{3TC}}{p_0}\right)$

State 4TC, Isentropic flow Expansion (3TC-4TC) in T

$p_{4TC} = \frac{p_{3TC}}{\varepsilon_{cTC}^{\kappa}} = p_{1TC} = p_{1O} = p_0$ $\quad v_{4TC} = \frac{v_{3TC}}{\varepsilon_{cTC}}$

with $\quad \delta_{pTC} = \delta_{pA\_v} = \delta_{pO\_v}$

$T_{4TC} = \frac{T_{3TC}}{\varepsilon_{cTC}^{\kappa-1}}$ $\quad s_{4TC} = s_{3TC}$

1.LoT on 1TC-2TC $h_{4TC} - h_{3TC} = w_{t3TC\_4TC} + q_{3TC\_4TC}$

where $q_{3TC\_4TC} = 0$ isentropic = adiabatical

CE isobaric $h_{4TC} - h_{3TC} = c^{\circ}_{p}(T_{4TC} - T_{3TC})$

specific technical work of T $w_{t3TC\_4TC} = c^{\circ}_{p}\cdot(T_{4TC} - T_{3TC})$

related to u_{1O} $w^{*}_{t3TC\_4TC} = \kappa\cdot\delta_{pTC}\cdot\left(\frac{1}{\varepsilon_{cTC}^{\kappa-1}} - 1\right)$

State 1TC, Complete TC cycle part: Isobaric Exhaust and Heat Discharge (4TC-1TC) over TC Turbine (T)

$p_{4TC} = p_{1TC} = p_{1O}$ isobaric

In the Brayton cycle the released heat is only assumed for an adequate comparison to the Atkinson & Otto cycles. All cycles are designed so that the temperature on entering the turbine, at the start of Exhaust, reaches about 1000°C.

$\varepsilon_{cTC} = \gamma$ $\quad T_{3TC} = T_{4A} = T_{4O}$ $\quad T_{1TC} = T_{1O}$

specific isobaric discharged heat $q_{4TC\_1TC} = c^{\circ}_{p}\cdot(T_{1O} - T_{4TC})$

rel. to u_{1O} $q^{*}_{4TC\_1TC} = \kappa\cdot\left(1 - \frac{\delta_{pTC}}{\varepsilon_{cTC}^{\kappa-1}}\right) = \kappa\cdot\left(1 - \frac{\delta_{pTC}}{\gamma^{\kappa-1}}\right)$

FIGURE A1-3 Thermodynamic background and proof of the Efficiency formulas for **isochoric** heat release. Part 3.

Numerical value results for the folowing parameter: $\varepsilon_{cA}=10$ $\gamma=3$ $\delta_{pA\_v}=4.065$ $\varepsilon_{cO}=10$ $\delta_{pO\_v}=4.065$ $\kappa=1.277$ $\varepsilon_{cTC}=3$ $\varepsilon_{cTC}=\gamma$ $\delta_{pTC}:=\delta_{pO\_v}$

$q^*_{4A\_1O}:=(1-\delta_{pA\_v})$ $q^*_{4A\_1O}=-3.065$

$q^*_{2A\_3A}:=(\varepsilon_{cA}\cdot\gamma)^{\kappa-1}\cdot(\delta_{pA\_v}-1)$ $q^*_{2A\_3A}=7.849$

$w^*_{v1O\_1A}:=\gamma^{\kappa-1}-1$ $w^*_{v1O\_1A}=0.355$

$w^*_{v1A\_2A}:=\gamma^{\kappa-1}\cdot(\varepsilon_{cA}{}^{\kappa-1}-1)$ $w^*_{v1A\_2A}=1.206$

$w^*_{v3A\_4A}:=\delta_{pA\_v}\cdot(1-(\varepsilon_{cA}\cdot\gamma)^{\kappa-1})$ $w^*_{v3A\_4A}=-6.346$

Review of the energy balance on A cycle

$q^*_{2A\_3A}+q^*_{4A\_1O}+w^*_{v1A\_2A}+w^*_{v3A\_4A}+w^*_{v1O\_1A}=0$

$w^*_{v1O\_1A}$ only reduces the discharged heat $q^*_{4A\_1O}$ on A cycle

IFCE, Thermodynamical efficiency of Atkinson-cycle

$w^*_{vA}=w^*_{v1A\_2A}+w^*_{v3A\_4A}$ specific work on A cycle

$w^*_{vA}:=\delta_{pA\_v}-\gamma^{\kappa-1}-(\varepsilon_{cA}\cdot\gamma)^{\kappa-1}\cdot(\delta_{pA\_v}-1)$

$w^*_{vA}=-5.139$

1st evidence for IFCE of Atkinson cycle with isochoric heat release, according to Approach a) and b)

$\eta_{thA\_v}=\dfrac{-w^*_{vA}}{q^*_{2A\_3A}}$

$\eta_{thA\_v}=\dfrac{(\varepsilon_{cA}\cdot\gamma)^{\kappa-1}\cdot(\delta_{pA\_v}-1)-(\delta_{pA\_v}-\gamma^{\kappa-1})}{(\varepsilon_{cA}\cdot\gamma)^{\kappa-1}\cdot(\delta_{pA\_v}-1)}$

2nd evidence for IFCE of Atkinson cycle with isochoric heat release, according to Approach a)

$\eta_{thA\_v}=1-\dfrac{|q^*_{4A\_1O}+w^*_{v1O\_1A}|}{q^*_{2A\_3A}}=1-\dfrac{\delta_{pA\_v}-\gamma^{\kappa-1}}{(\varepsilon_{cA}\cdot\gamma)^{\kappa-1}\cdot(\delta_{pA\_v}-1)}$

The actual heat discharged is lower in A cycle than in O cycle!

$q^*_{4A\_1O}+w^*_{v1O\_1A}=-2.71$

$\eta_{thA\_v}:=1-\dfrac{1}{(\varepsilon_{cA}\cdot\gamma)^{\kappa-1}}\cdot\dfrac{\delta_{pA\_v}-\gamma^{\kappa-1}}{\delta_{pA\_v}-1}$ $\eta_{thA\_v}=0.655$

or, as taken in [27] for $\delta_{pA\_v}=\gamma^{\kappa}$

$\eta_{thA\_v}=1-\dfrac{1}{(\varepsilon_{cA}\cdot\gamma)^{\kappa-1}}\cdot\dfrac{\gamma^{\kappa}-\gamma^{\kappa-1}}{\gamma^{\kappa}-1}$ $\delta_{pA\_v}=4.065$

$1-\dfrac{1}{(\varepsilon_{cA}\cdot\gamma)^{\kappa-1}}\cdot\dfrac{\gamma^{\kappa}-\gamma^{\kappa-1}}{\gamma^{\kappa}-1}=0.655$

2nd evidence for IFCE of Atkinson cycle with isochoric heat release, according to Approach b)

$q_{4A\_1A}=c^{\circ}_{v}\cdot(T_{1A}-T_{4A})=\dfrac{q_{2TC\_3TC}}{\kappa}$ because piston stroke 4A-1A is missing!

$T_{1A}=T_{1O}\cdot\gamma^{\kappa-1}$ $T_{4A}=\dfrac{T_{3A}}{\varepsilon_{eA}{}^{\kappa-1}}=\dfrac{T_{2A}\cdot\delta_{pA\_v}}{(\varepsilon_{cA}\cdot\gamma)^{\kappa-1}}=T_{1O}\cdot\delta_{pA\_v}$

$q^*_{4A\_1A}=\dfrac{c^{\circ}_{v}\cdot(T_{1O}\cdot\gamma^{\kappa-1}-T_{1O}\cdot\delta_{pA\_v})}{c^{\circ}_{v}\cdot T_{1O}}=\gamma^{\kappa-1}-\delta_{pA\_v}$

$q^*_{4A\_1A}:=\gamma^{\kappa-1}-\delta_{pA\_v}$ $q^*_{4A\_1A}=-2.71$ η_{thA_v} results as in **Approach a)**

$\eta_{thA\_p}=1-\dfrac{|q^*_{4A\_1A}|}{q^*_{2A\_3A}}=1-\dfrac{\delta_{pA\_v}-\gamma^{\kappa-1}}{(\varepsilon_{cA}\cdot\gamma)^{\kappa-1}\cdot(\delta_{pA\_v}-1)}$

$\eta_{thA\_v}=1-\dfrac{1}{(\varepsilon_{cA}\cdot\gamma)^{\kappa-1}}\cdot\dfrac{\gamma^{\kappa}-\gamma^{\kappa-1}}{\gamma^{\kappa}-1}$ after $\delta_{pA\_v}=\gamma^{\kappa}$

$q^*_{4O\_1O}:=(1-\delta_{pO\_v})$ $q^*_{4O\_1O}=-3.065$

$q^*_{2O\_3O}:=\varepsilon_{cO}{}^{\kappa-1}\cdot(\delta_{pO\_v}-1)$ $q^*_{2O\_3O}=5.793$

$w^*_{v1O\_2O}:=\varepsilon_{cO}{}^{\kappa-1}-1$ $w^*_{v1O\_2O}=0.89$

$w^*_{v3O\_4O}:=\delta_{pO\_v}\cdot(1-\varepsilon_{cO}{}^{\kappa-1})$ $w^*_{v3O\_4O}=-3.618$

Review of the energy balance on O cycle

$q^*_{4O\_1O}+q^*_{2O\_3O}+w^*_{v1O\_2O}+w^*_{v3O\_4O}=0$

IFCE, Thermodynamical efficiency of Otto-cycle

$w^*_{vO}=w^*_{v1O\_2O}+w^*_{v3O\_4O}$

$w^*_{vO}=(\delta_{pO}-1)\cdot(\varepsilon_{cO}{}^{\kappa-1}-1)$

1st evidence for IFCE of Otto cycle with isochoric heat release

$\eta_{thO\_v}=\dfrac{-w^*_{vO}}{q^*_{2O\_3O}}=\dfrac{-(\delta_{pO\_v}-1)\cdot(\varepsilon_{cO}{}^{\kappa-1}-1)}{\varepsilon_{cO}{}^{\kappa-1}\cdot(\delta_{pO\_v}-1)}$

$\eta_{thO\_v}=\dfrac{-w^*_{vO}}{q^*_{2O\_3O}}=1-\dfrac{1}{\varepsilon_{cO}{}^{\kappa-1}}$

2nd evidence for IFCE of Otto cycle with isochoric heat release

$\eta_{thO\_v}=1-\dfrac{|q^*_{4O\_1O}|}{q^*_{2O\_3O}}=1-\dfrac{\delta_{pO\_v}-1}{\varepsilon_{cO}{}^{\kappa-1}\cdot(\delta_{pO\_v}-1)}$

discharged heat on O cycle

$q^*_{4O\_1O}=-3.065$

$\eta_{thO\_v}:=\left(1-\dfrac{1}{\varepsilon_{cO}{}^{\kappa-1}}\right)$ $\eta_{thO\_v}=0.471$

As is known, IFCE of Otto cycle is not depended on δ_{pO_v}

$\delta_{pO\_v}=4.065$

Note: Even an Otto-cycle with a VCR = $\varepsilon_{cO}\cdot\gamma$, $\varepsilon_{cO}\cdot\gamma=30$ would have the IFCE:

$1-\dfrac{1}{(\varepsilon_{cO}\cdot\gamma)^{\kappa-1}}=0.61$ which is 7.4% less, just for comparison with the A cycle

$q^*_{4TC\_1TC}:=\kappa\cdot\left(1-\dfrac{\delta_{pTC}}{\varepsilon_{cTC}{}^{\kappa-1}}\right)$ $q^*_{4TC\_1TC}=-2.553$

$q^*_{2TC\_3TC}:=\kappa\cdot(\delta_{pTC}-\varepsilon_{cTC}{}^{\kappa-1})$ $q^*_{2TC\_3TC}=3.459$

$w^*_{t1TC\_2TC}:=\kappa\cdot(\varepsilon_{cTC}{}^{\kappa-1}-1)$ $w^*_{t1TC\_2TC}=0.453$

$w^*_{t3TC\_4TC}:=\kappa\cdot\left(\dfrac{\delta_{pTC}}{\varepsilon_{cTC}{}^{\kappa-1}}-\delta_{pTC}\right)$ $w^*_{t3TC\_4TC}=-1.359$

Review of the energy balance on TC cycle

$q^*_{4TC\_1TC}+q^*_{2TC\_3TC}+w^*_{t1TC\_2TC}+w^*_{t3TC\_4TC}=0$

IFCE, Thermodyn. efficiency of Gas-Turbine-cycle

$w^*_{tTC}=w^*_{t1TC\_2TC}+w^*_{t3TC\_4TC}$

$w^*_{tTC}=\kappa\cdot(\delta_{pTC}-\varepsilon_{cTC}{}^{\kappa-1})\cdot\left(\dfrac{1}{\varepsilon_{cTC}{}^{\kappa-1}}-1\right)$

1st evidence for IFCE of Gas-Turbine cycle with isobaric heat release

$\eta_{thTC\_p}=\dfrac{-w^*_{tTC}}{q^*_{2TC\_3TC}}=1-\dfrac{1}{\varepsilon_{cTC}{}^{\kappa-1}}$

The IFCE formulas for Otto and Gas-Turbine cycles are identical, i.e. identical results are obtained for identical $\varepsilon_{cTC}=\varepsilon_{cO}$ compression ratios.

2nd evidence for IFCE of Gas-Turbine cycle with isobaric heat release

$\eta_{thTC\_p}=1-\dfrac{|q^*_{4TC\_1TC}|}{q^*_{2TC\_3TC}}=1-\dfrac{1}{\varepsilon_{cTC}{}^{\kappa-1}}$

$\eta_{thTC\_p}:=\left(1-\dfrac{1}{\varepsilon_{cTC}{}^{\kappa-1}}\right)$ $\eta_{thTC\_p}=0.262$

As is known, IFCE of Gas-Turbine cycle is not depended on δ_{pTC}

$\delta_{pTC}=4.065$

Proof of the relation $\delta_{pA\_v}=\gamma^{\kappa}$ for Atkinson cycle

$\varepsilon_{cA}=\dfrac{v_{2A}}{v_{1A}}$ $\varepsilon_{eA}=\dfrac{v_{4A}}{v_{2A}}$ $\gamma=\dfrac{\varepsilon_{eA}}{\varepsilon_{cA}}=\dfrac{v_{4A}}{v_{1A}}$

On the one hand:

$p_{2A}=p_{1A}\cdot\varepsilon^{\kappa}$ $p_{3A}=p_{2A}\cdot\delta_{pA\_v}$ $p_{3A}=p_{1A}\cdot\varepsilon^{\kappa}\cdot\delta_{pA\_v}$

On the other hand:

$p_{3A}=p_{4A}\cdot\varepsilon_{eA}{}^{\kappa}$ $p_{4A}=p_{1A}$ $p_{3A}=p_{1A}\cdot\varepsilon^{\kappa}\cdot\gamma^{\kappa}$

This results in the desired relation: $\delta_{pA\_v}=\gamma^{\kappa}$

FIGURE A1-4 Thermodynamic background and proof of the Efficiency formulas for **isobaric** heat release. Part 4.

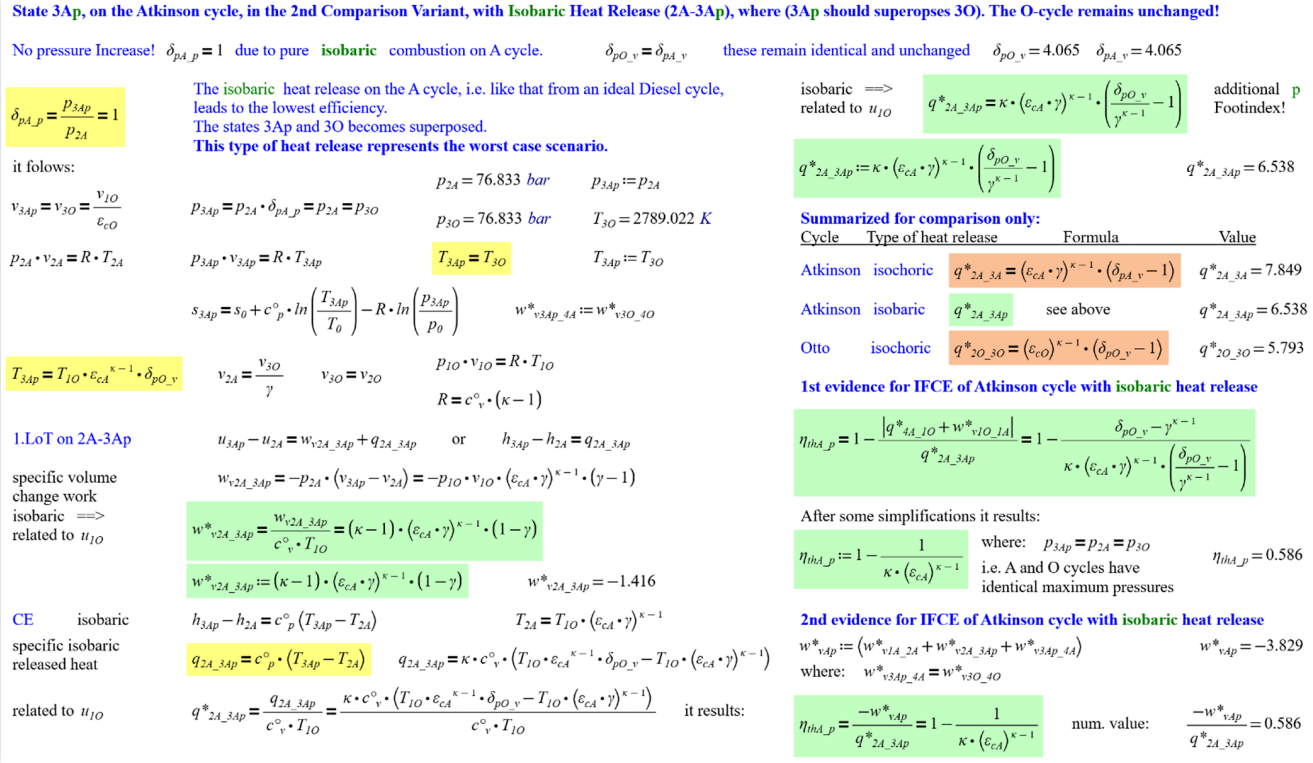

Appendix 2

Comparison of the thermal efficiencies for the real cycles of the true Atkinson (A) and the classic gasoline Otto (O) ICE Seiliger (S), both turbocharged & hydrogen fueled, while maintaining the same VCR values, expansion stroke lengths, maximum gas mass and AFR, λ = 1, (thus under the same conditions).

The classic Otto ICE - considered here - is **hypothetical** because it offers the variation of its volumetric compression ratio (VCR) by means of a symmetrical crank drive (e.g. like that of a CFR octane-testing engine).

The comparison was done using the AVL BOOST simulation tool. The simulation model used below is developed for a 3-cylinder engine with hydrogen-direct-injection GasDI, two stage turbocharging and air intercooling. The displacement volume of this engine is near 1 liter.

FIGURE A2-1 Simulation Model in AVL BOOST tool on the left. The simulated cases (top Table) of the true Atkinson (A) cycles and (bottom Table) of the classical Seiliger (S) cycles are presented on the right side.

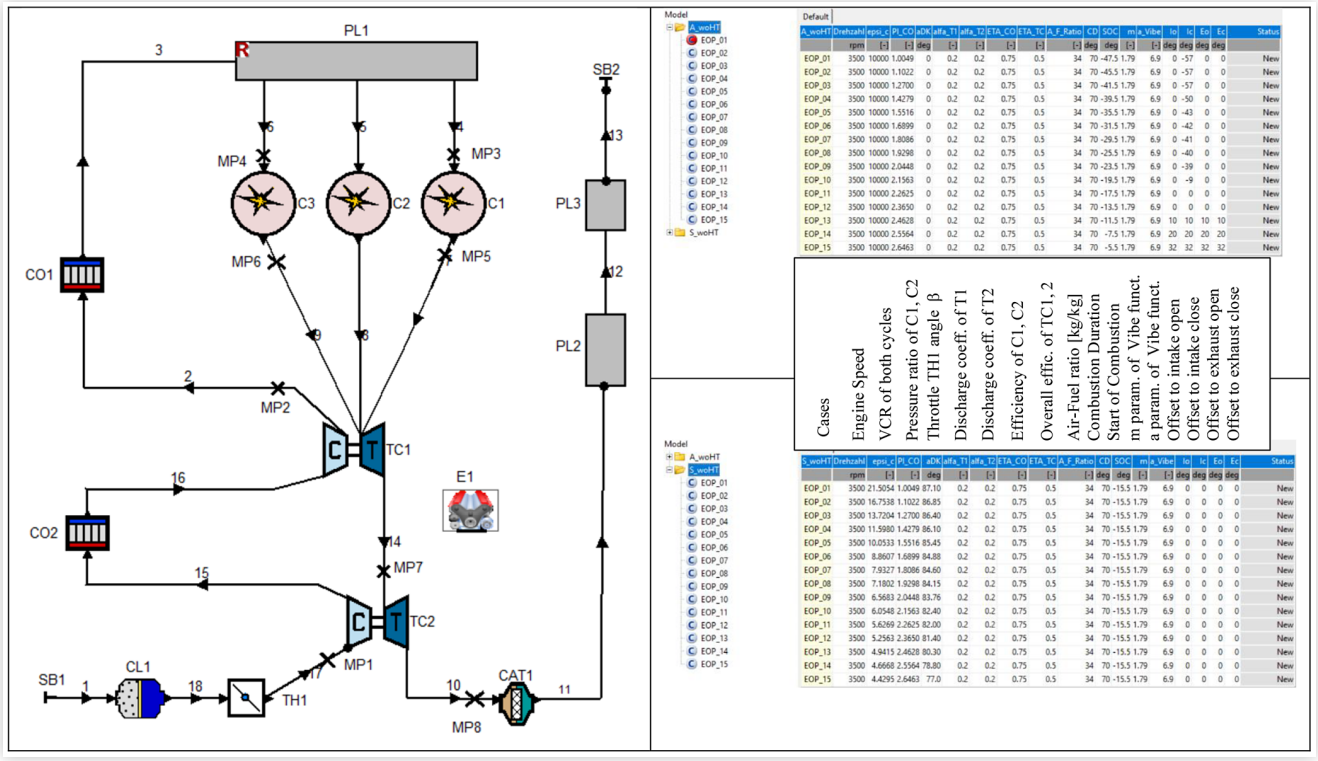

In the top Table of the simulated cases from Fig. A2-1, the VCR values of the true Atkinson cycles are the same as those of the Seiliger cycle. The values 10000 introduced there for (A) are only formal, i.e. they are not effective. The AVL BOOST tool has the possibility to simulate cycles with a user-defined piston motion. This gives the user freedom to simulate an unconventional powertrain, like VCSR. For a user-defined piston motion, the relative piston position should be specified over crank angle. In BOOST, the relative piston position is defined as the distance of the piston from the TDC position relative to the full stroke. Zero degree crank angle corresponds to the Firing TDC of the selected cylinder.

However, the true Atkinson cycle features strokes of various length. The BOOST tool makes in the background a recalculation of the given user-defined piston motions using the set VCR value, the crank mechanism geometry, and modified the user-defined piston motion inadequately. To avoid this alteration of the user-defined piston motion, the VCR is for true Atkinson cycles formally set to 10000 or more. This huge VCR value can by the way influence the computed values for the heat transfer models in the cylinders.

For this reason, **the heat transfer in the cylinders is completely deactivated in this comparison study**, i.e. the simulation is carried out only for **adiabatic** cycles. However, the frictions FMEP in the crank mechanism are considered and set identical in both cycles, as shown in Fig. A2-2.

The VCSR crank mechanism is presented in [2, 10, 11, 5, 16]. The eccentric crank (EC) of the VCSR mechanism for the true Atkinson cycle and the classical crankshaft for the classical Seiliger cycle have the same rotation speed n. The Crank Disks (CD) of the VCSR have only half of it.

The comparison between the true Atkinson and classical Seiliger cycles is presented in the following figures

FIGURE A2-2 Friction values FMEP of the true Atkinson and the Seiliger cycles (on the left side) and Throttle flow coefficients (on the right side) considered in the Simulation Model in AVL BOOST®.

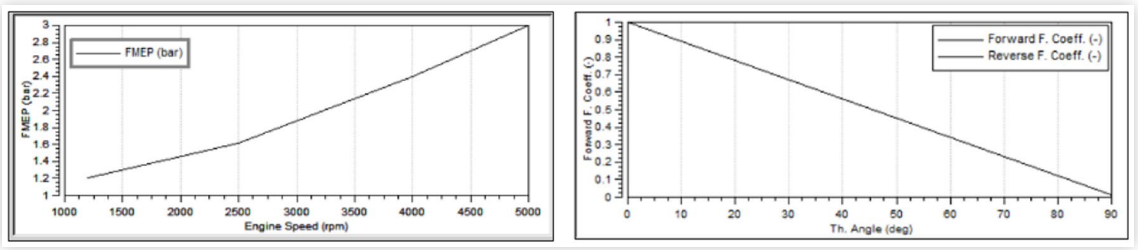

in 15 Engine Operation Points (EOP). The figures demonstrate the new kind, namely Ultra Downsizing (UD), of Load Control (LC) of the VCSR engine – working according to the true Atkinson cycles – from small load 1st EOP to large load 15th EOP. Meanwhile, the engine speed remains unchanged at 3500 rpm.

The load control, at constant speed, of classic motors takes place in the following variants:

a) The quality of the air-fuel mixture AFR of the Diesel ICE is varied for the load control. The sucked air mass with some exhaust gases from EGR remains nearly constant, but the injected fuel mass is varied for load control. The resulting AFR is always higher than one or $\lambda > 1$, i.e. the air-fuel mixture is lean. Lean air-fuel ratios favor the generation of NOx emissions and simultaneously hinder their reduction in the common 3-way catalysts.

b) The quantity of the air-fuel mixture of the Gasoline ICE is varied by means of the throttle valve (see TH1 in the BOOST model of Fig. A2-1) or intake valve throttling for the load control. The quality of the air-fuel mixture remains constant, mostly stoichiometric, i.e. AFR or $\lambda = 1$. Thus, the reduction of NOx emissions in the common 3-way catalysts is assured.

In contrast to the load controls a) and b) of the classic ICE, the UD LC of the VCSR ICE takes place in a new, special way see Patents DE102013003682B4, EP 2 772 624 B1, which tries to retain the advantages of the classic types, while avoiding their disadvantages.

The Ultra Downsizing UD Load Control LC of the VCSR ICE uses the following strategy, see Figure A2-EOPs-01-15 and the Claim 8 of the EP Patent:

a) Only compressed air is sucked into the cylinders.

b) The fuel, preferably hydrogen, but also CNG or other liquid or gaseous fuels in pure or mixed form, are injected or blown in directly and sequentially in the cylinders. A dual fuel injection, with MPI in intake channels only for liquid fuels, like gasoline, methanol or other volatile fuels is also possible.

c) The quality of the air-fuel mixture remains constant, mostly stoichiometric, i.e. AFR or $\lambda = 1$. Thus, the reduction of some possible raw NOx emissions is assured by means of the common 3-way catalysts.

d) The VCR can be varied by means of a rotational adjustment of the Ring Gear RG see [2, 10, 11, 5, 16].

e) High VCR values lead to low loads because the intake stroke becomes shorter and thus less air mass is sucked in. See for example the simulation results of the 1st EOP in Figure A2-EOP-01. In addition, the exhaust stroke is shorter and therefore the emptying of the cylinders remains incomplete. This affords in fact an internal exhaust gas recirculation EGR. The exhaust gases have lower temperature and mass flow values. The turbine produces low power for driving the compressor. Thus, the boost pressure remains at a lower level.

f) Low VCR values lead to high loads because the intake stroke becomes longer and thus more air mass is sucked in. See for example the simulation results of the 15th EOP in Figure A2-EOP-15. In addition, the exhaust stroke is longer and therefore the emptying of the cylinders becomes nearly complete. The exhaust gases have higher temperature and mass flow values. The turbine produces more power for driving the compressor. Thus, the boost pressure reaches a higher level.

Short description of the following Figures.

8. The top-left diagram of each EOP depicts the variations of the displacement volume (V) versus crank angle (CA).
   - The VCR is defined as the quotient of the V in Gasex. BDC to V in TDC.
   - The VER is defined as the quotient of the V in BDC to V in TDC.
   - The Parameter γ is defined as the quotient of VER to VCR and thus of V in TDC to V in Gasex. BDC.
9. The top-right diagram each EOP depicts the variations of the cylinder pressure (p) versus V in natural logarithmic coordinates. Because of the kinematic of the VCSR crank mechanism, the angular positions of the TDC of the true Atkinson cycle migrate in relation to the TDC of the Seiliger cycle. That produces a slow translation of the curves in these diagrams, but the correspondence to the curves from Fig. 4 remains obvious. The variation of the strokes described above under e) and f) for load control is clearly observable.
10. The middle-left diagram of each EOP depicts the variations of the cylinder gas mass (m) versus V. The maximum values on the cycles are indicated there for an easy comparison. The variation of the strokes described above under e) and f) for load control is also clearly observable.
11. The middle-right diagram of each EOP depicts the variations of the indicated fuel conversion efficiency IFCE (i.e. of the volumetric work integral divided by the released heat on the cycle) versus V. These diagrams depict the losses and gains in volumetric work along the strokes. The end values are included. The advantage of a long expansion stroke of the real Atkinson cycle is obvious.
12. The bottom-left diagram of each EOP depicts the variations of the cylinder absolute gas Temperature (T) versus absolute (S = m*s) entropy flow dS/dt. The areas within the diagrams are energy flows in Watt released into the cylinder or exchanged between the gas from the

cylinder and the exterior. The lower consumed power (i.e. exergy flow) on the compression strokes and the greater released power on the expansion strokes of the real Atkinson cycles are clearly shown. The lost energy flow during exhaust is clearly depicted. This energy flow does not produce volumetric work at the piston, but it drives the TC-compressor. The classical T,s diagram from Figure 8 does not work adequately here because of gas mass variation during the exhaust and intake processes. As already discussed in section 2, the classical T,s diagram is only suitable for closed cycles, i.e. with constant mass, or open cycles, with constant mass flow. In the true Atkinson cycle the exergy part of the exhausted energy flow is much lower (indicated by its lower temperature) because of their consumption on the extended expansion, compared with the Seiliger cycle.

13. The bottom-right diagram of each EOP depicts the variations of the cylinder pressure p versus V and the cylinder temperature (T) versus V in the usual coordinates. The summary files for examine the mean values of most cycle parameters are linked in the captions of all EOPs!

FIGURE A2-EOP-01 Simulation results of the true Atkinson and the Seiliger cycles by using the AVL BOOST tool. The Summary files for A & S are linked here, to examine all mean values of the simulation parameters.

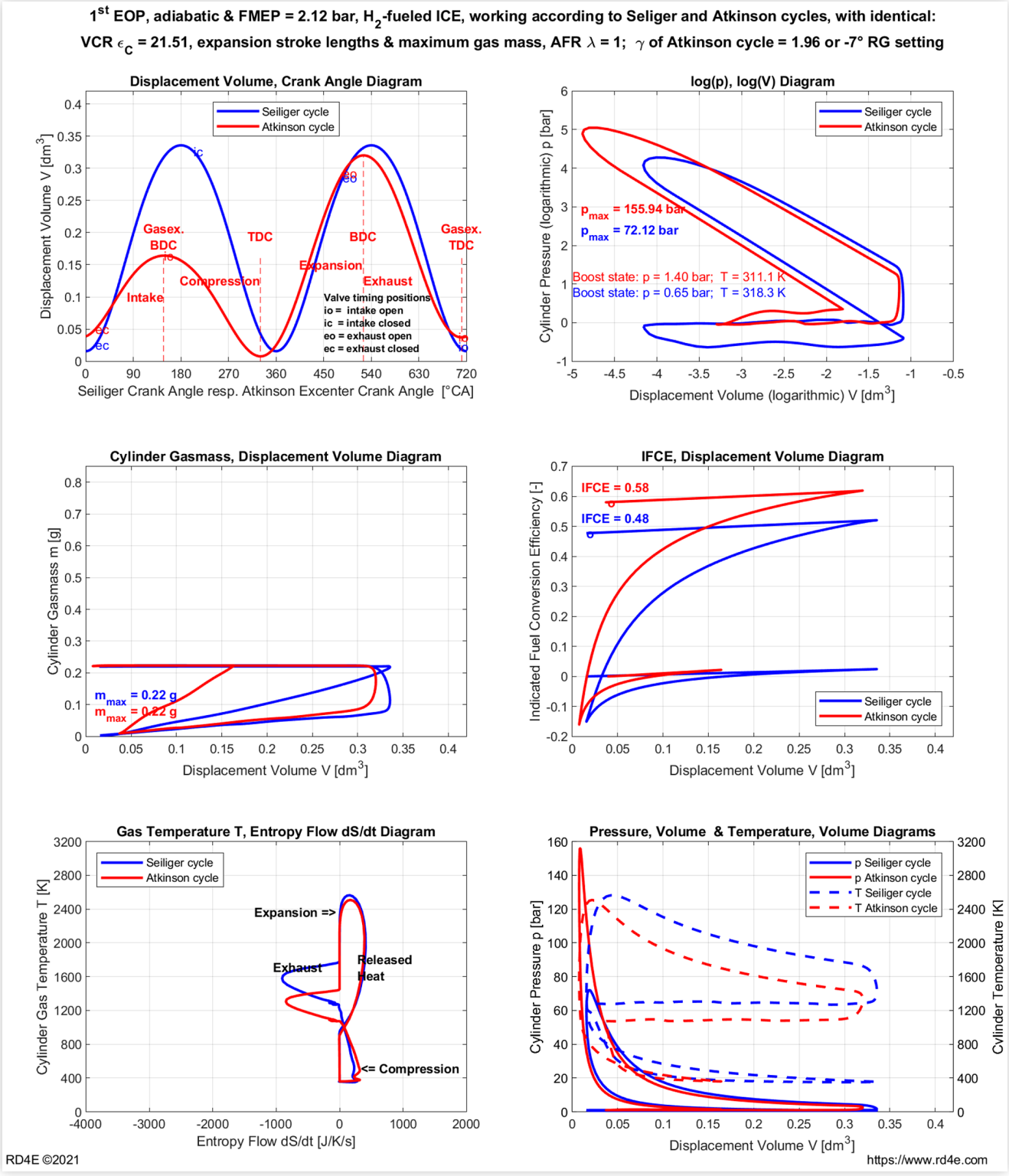

FIGURE A2-EOP-02 Simulation results of the true Atkinson and the Seiliger cycles by using the AVL BOOST tool. The Summary files for A & S are linked here, to examine all mean values of the simulation parameters.

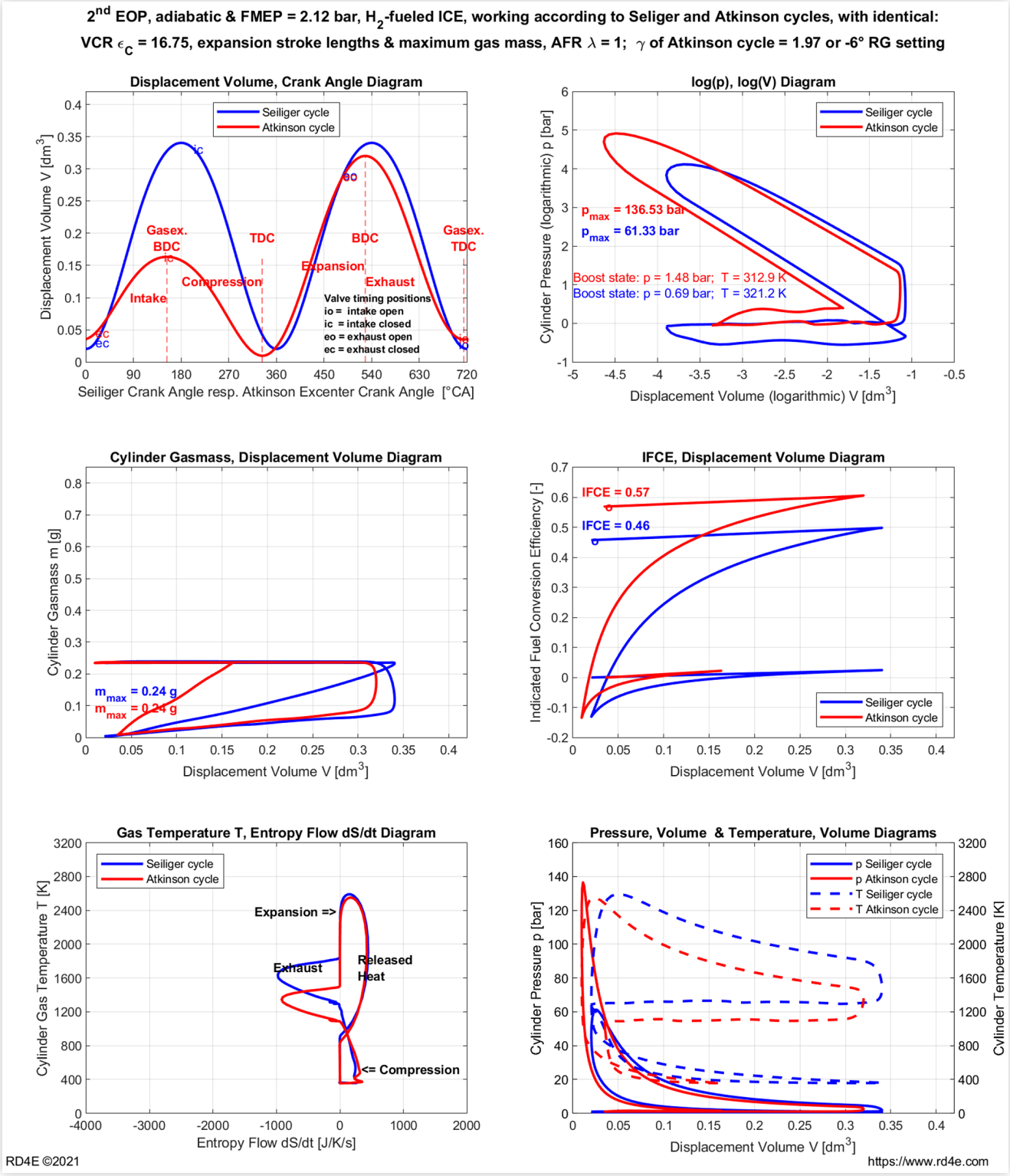

FIGURE A2-EOP-03 Simulation results of the true Atkinson and the Seiliger cycles by using the AVL BOOST tool. The Summary files for A & S are linked here, to examine all mean values of the simulation parameters.

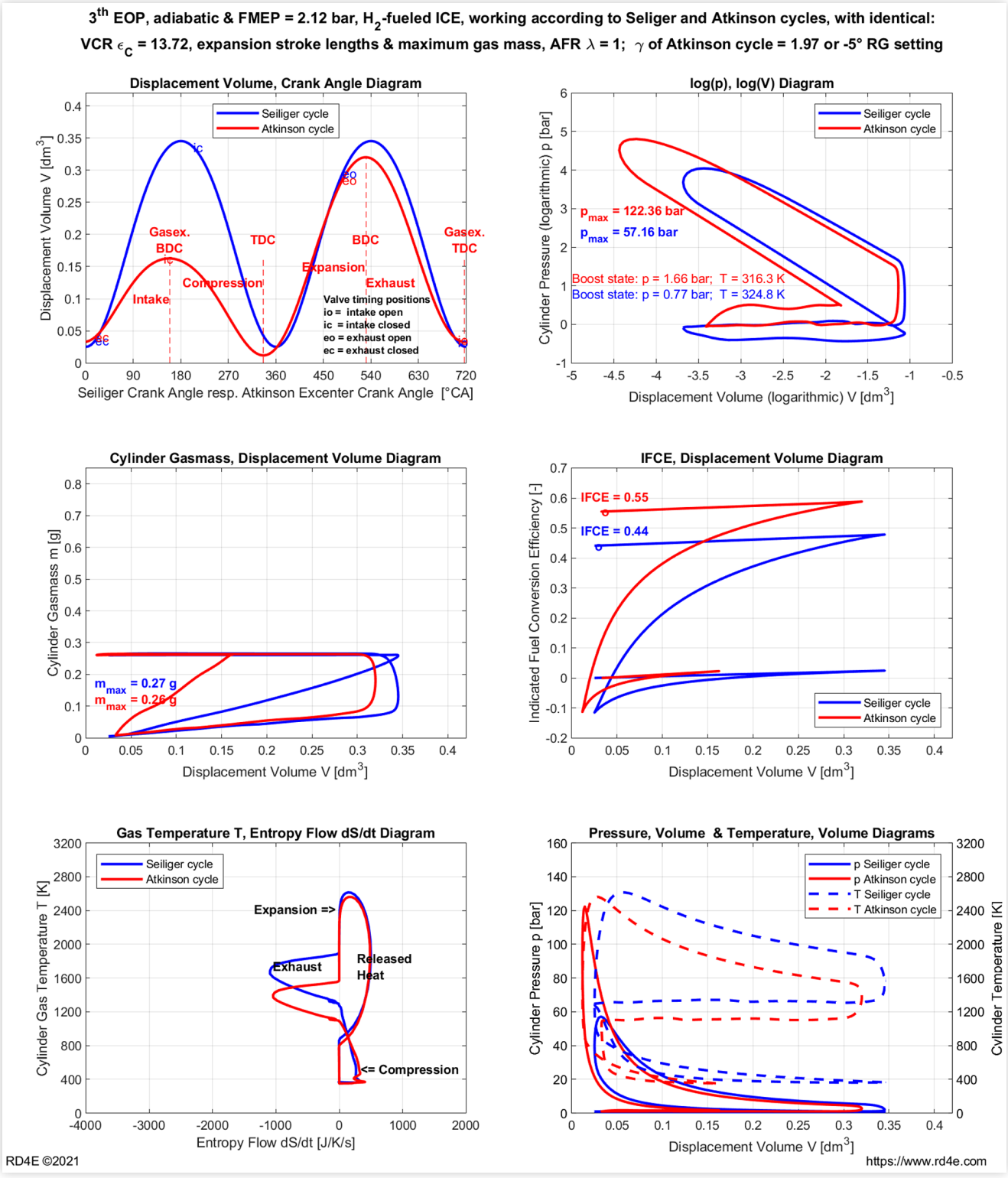

FIGURE A2-EOP-04 Simulation results of the true Atkinson and the Seiliger cycles by using the AVL BOOST tool. The Summary files for A & S are linked here, to examine all mean values of the simulation parameters.

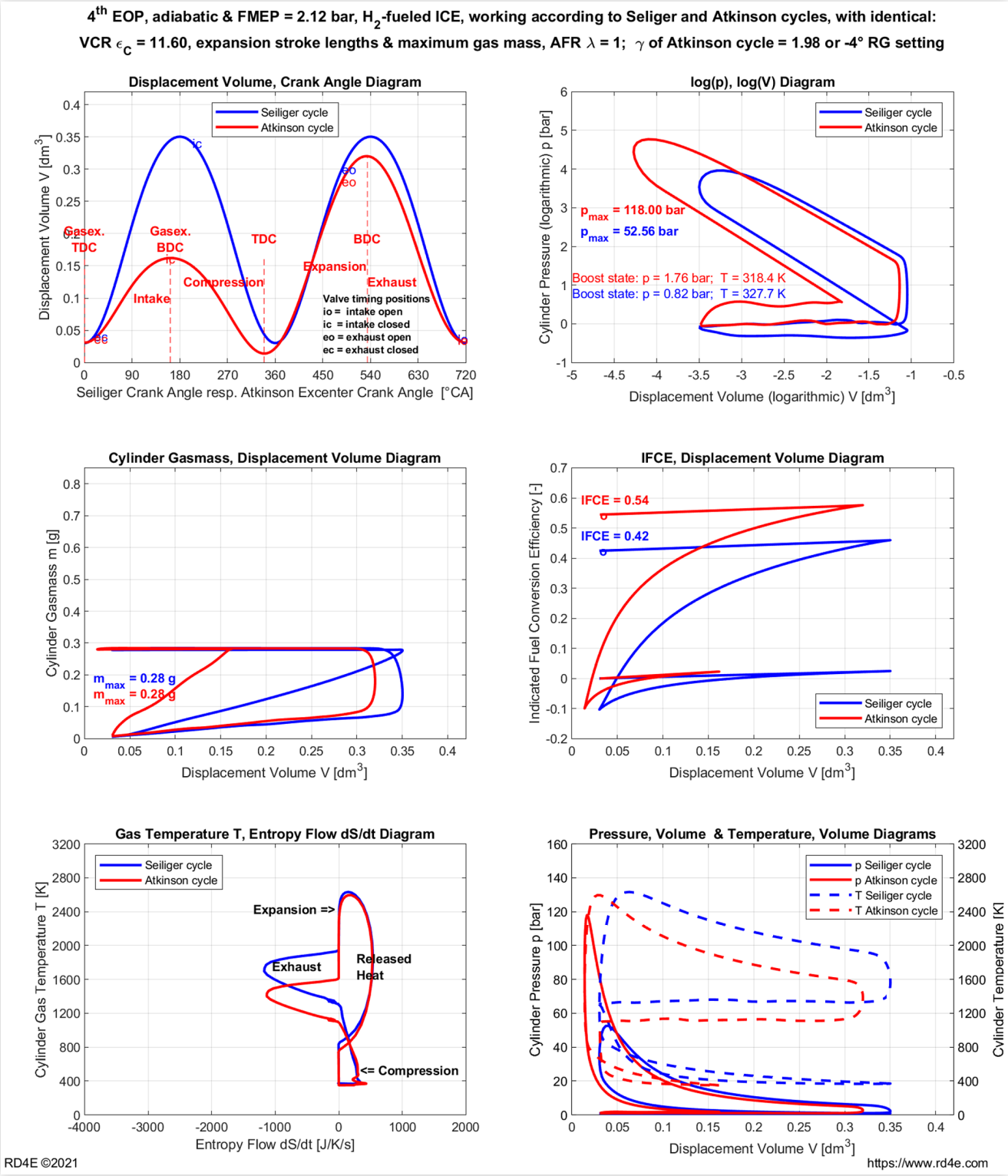

FIGURE A2-EOP-05 Simulation results of the true Atkinson and the Seiliger cycles by using the AVL BOOST tool. The Summary files for A & S are linked here, to examine all mean values of the simulation parameters.

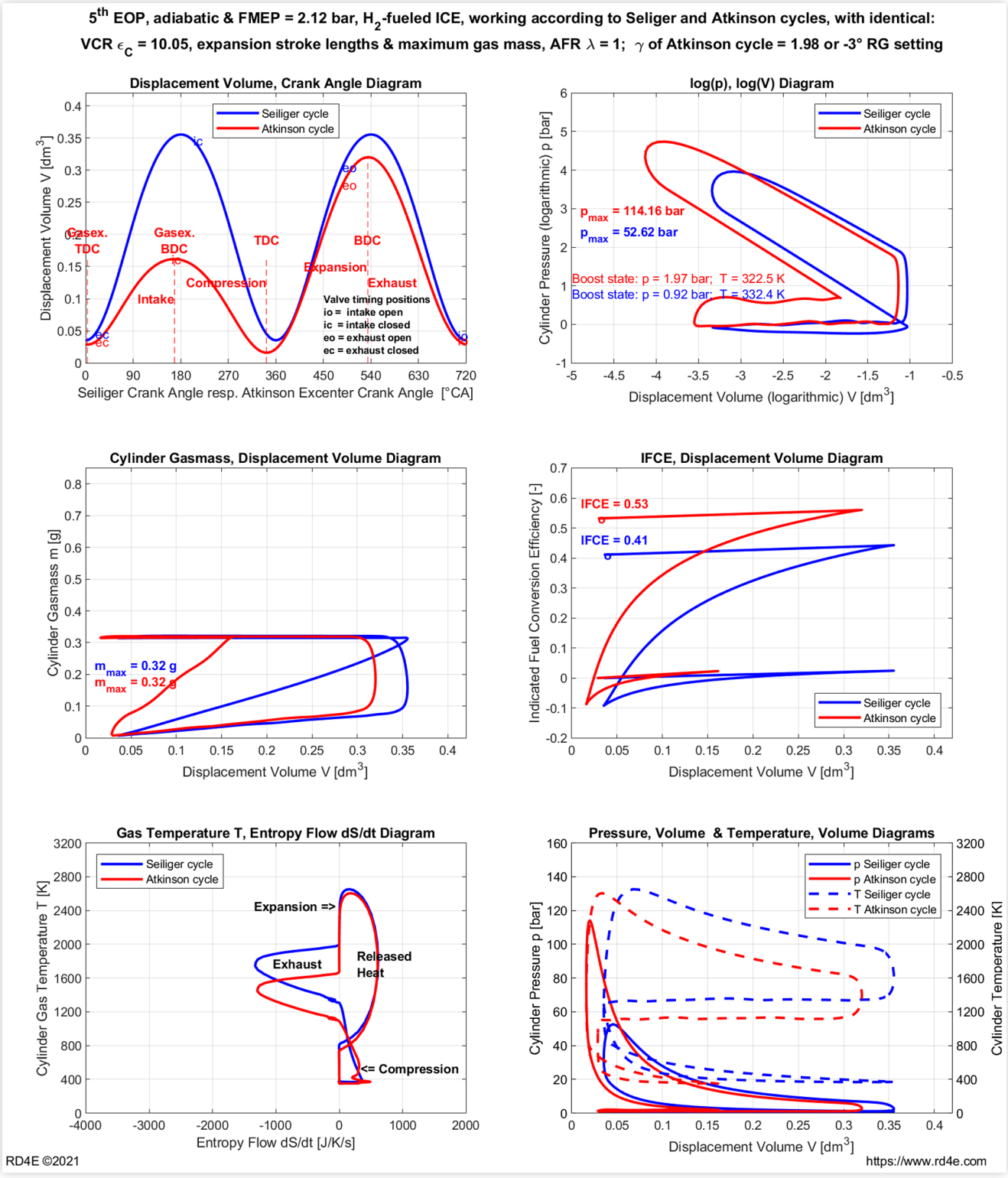

FIGURE A2-EOP-06 Simulation results of the true Atkinson and the Seiliger cycles by using the AVL BOOST tool. The Summary files for A & S are linked here, to examine all mean values of the simulation parameters.

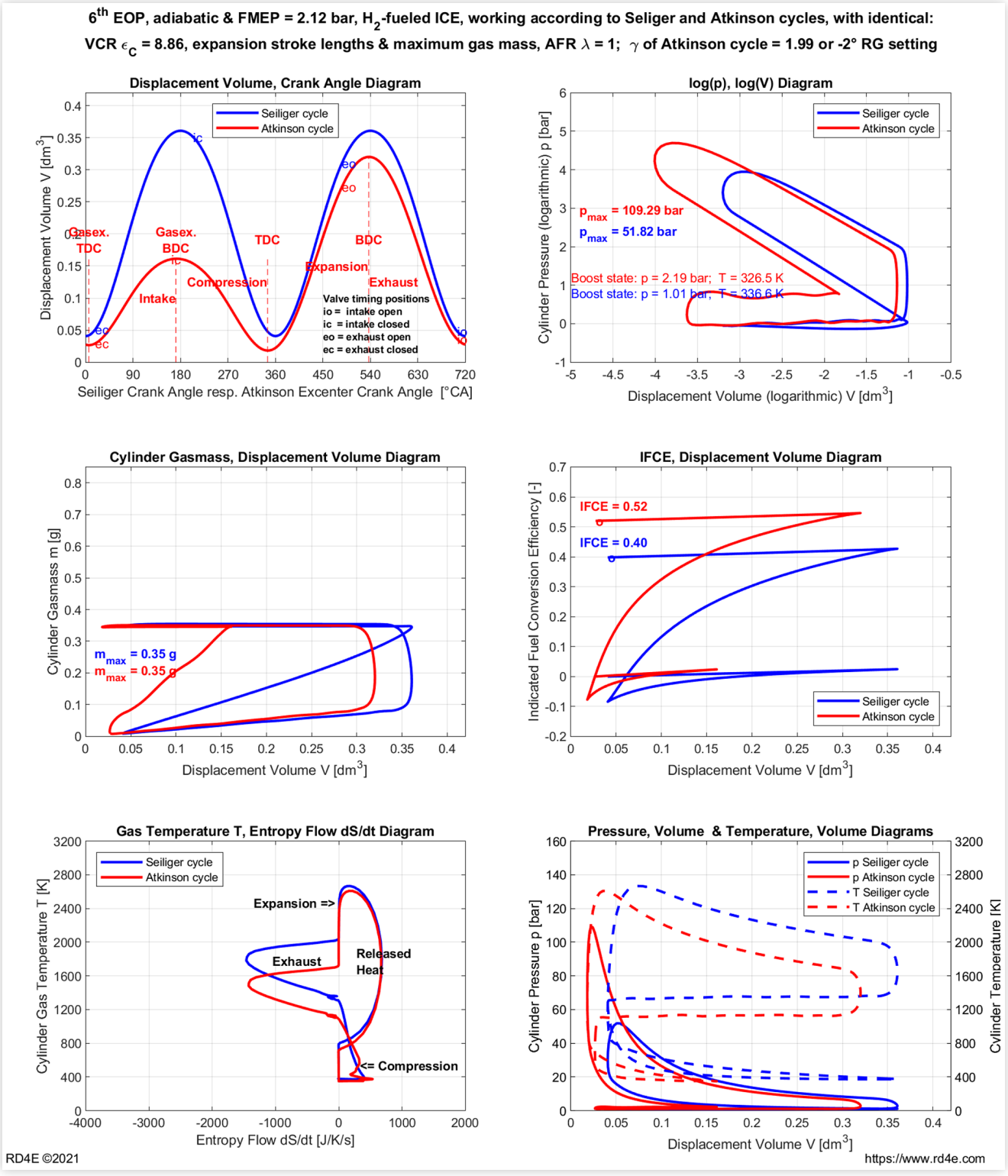

FIGURE A2-EOP-07 Simulation results of the true Atkinson and the Seiliger cycles by using the AVL BOOST tool. The Summary files for A & S are linked here, to examine all mean values of the simulation parameters.

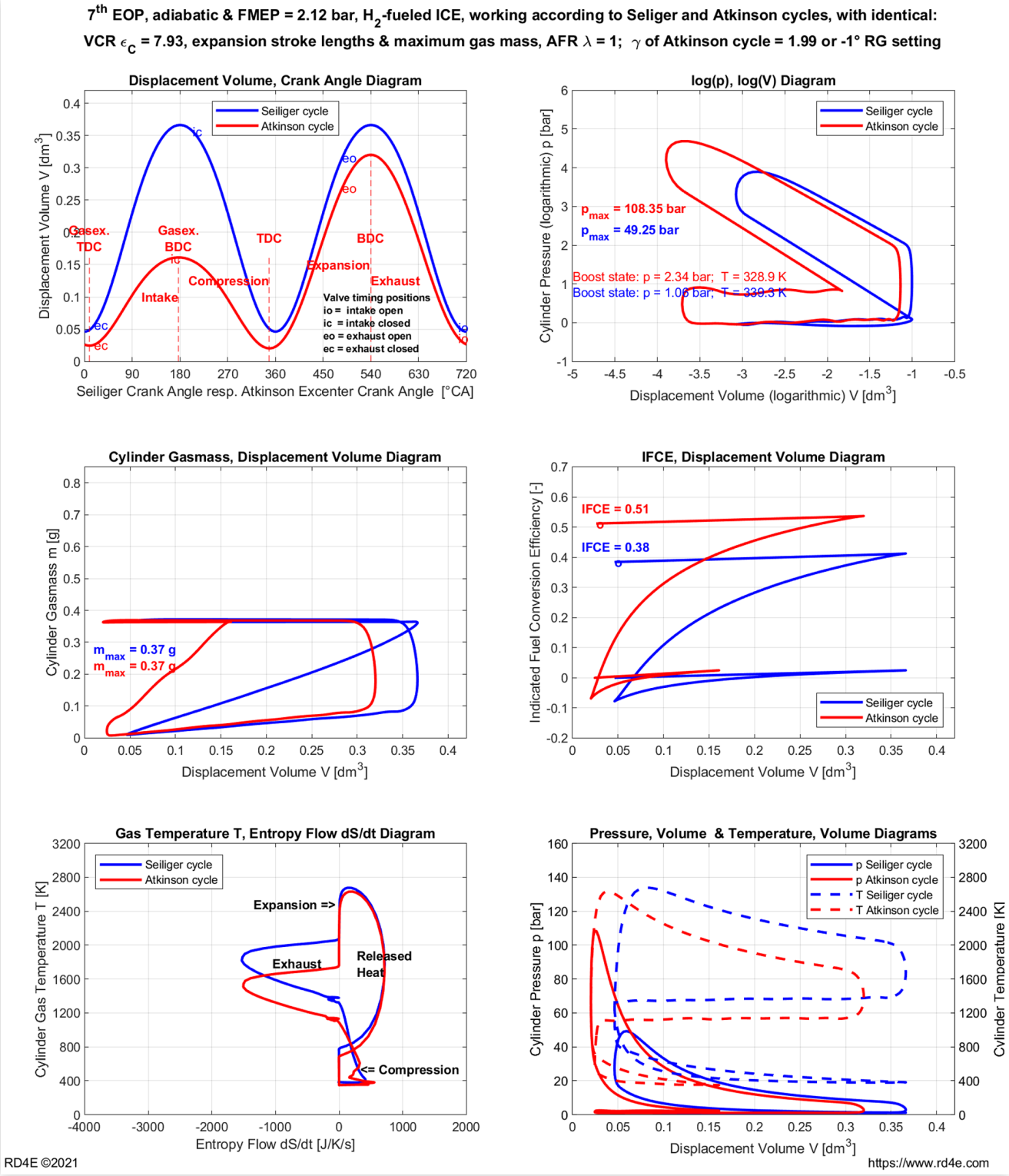

FIGURE A2-EOP-08 Simulation results of the true Atkinson and the Seiliger cycles by using the AVL BOOST tool. The Summary files for A & S are linked here, to examine all mean values of the simulation parameters.

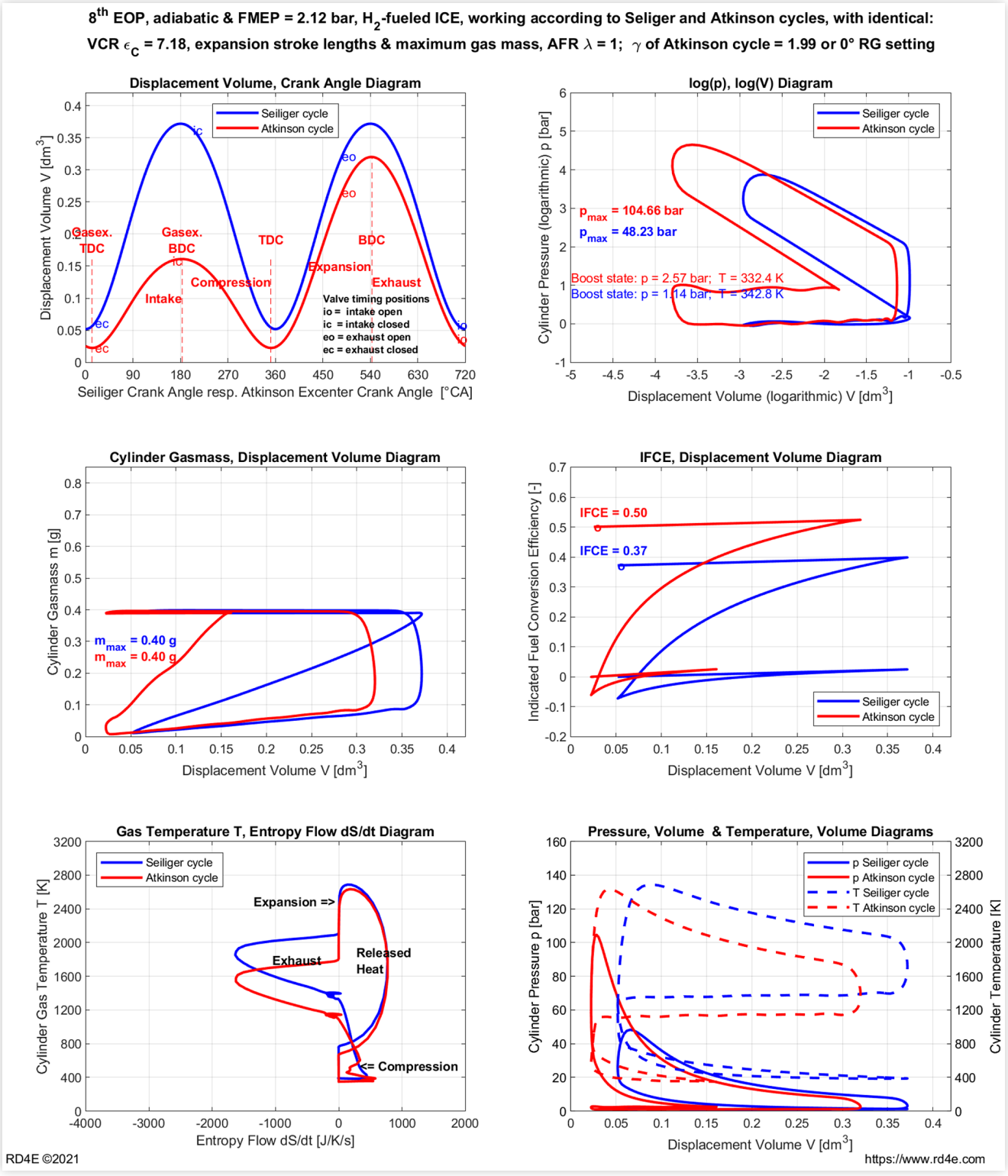

FIGURE A2-EOP-09 Simulation results of the true Atkinson and the Seiliger cycles by using the AVL BOOST tool. The Summary files for A & S are linked here, to examine all mean values of the simulation parameters.

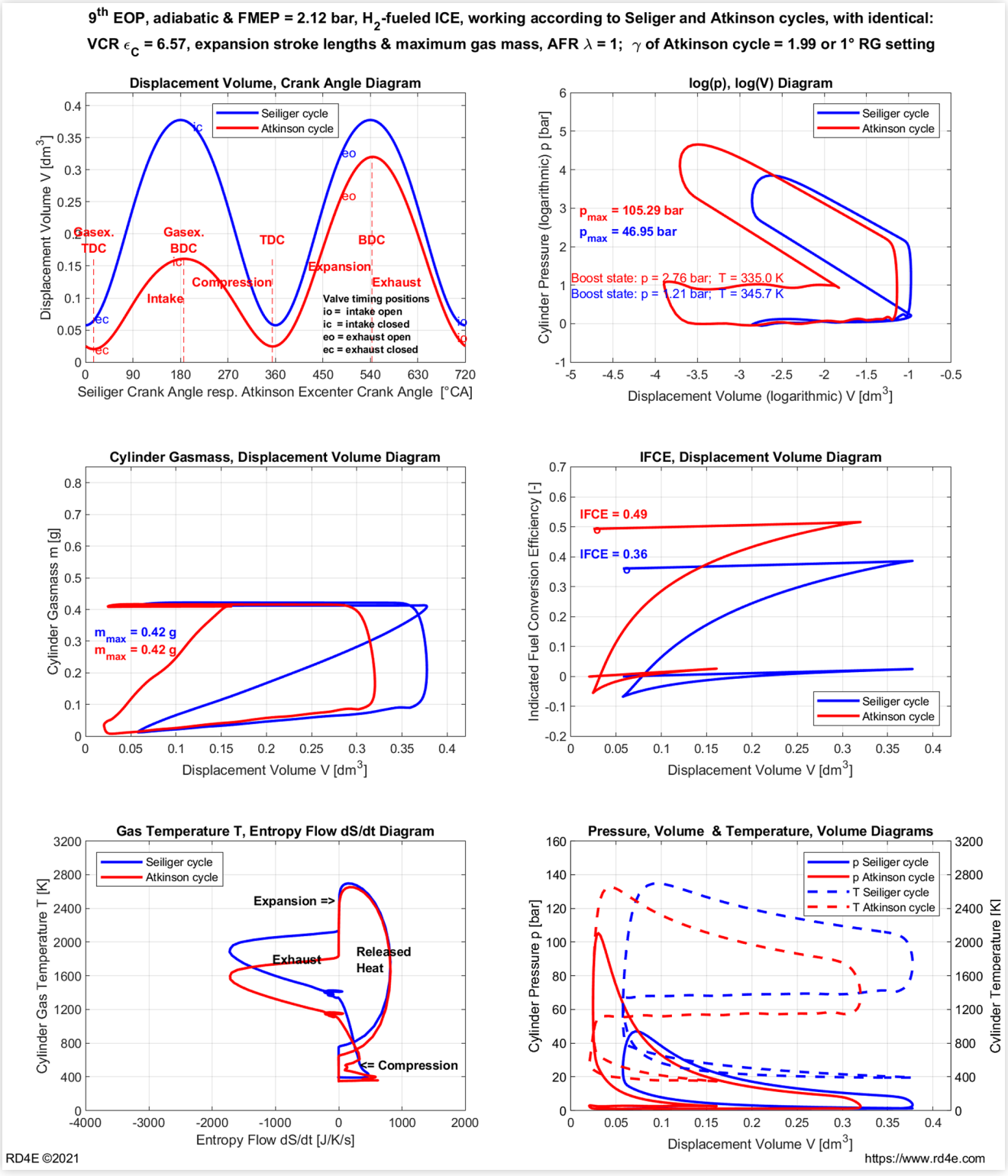

FIGURE A2-EOP-10 Simulation results of the true Atkinson and the Seiliger cycles by using the AVL BOOST tool. The Summary files for A & S are linked here, to examine all mean values of the simulation parameters.

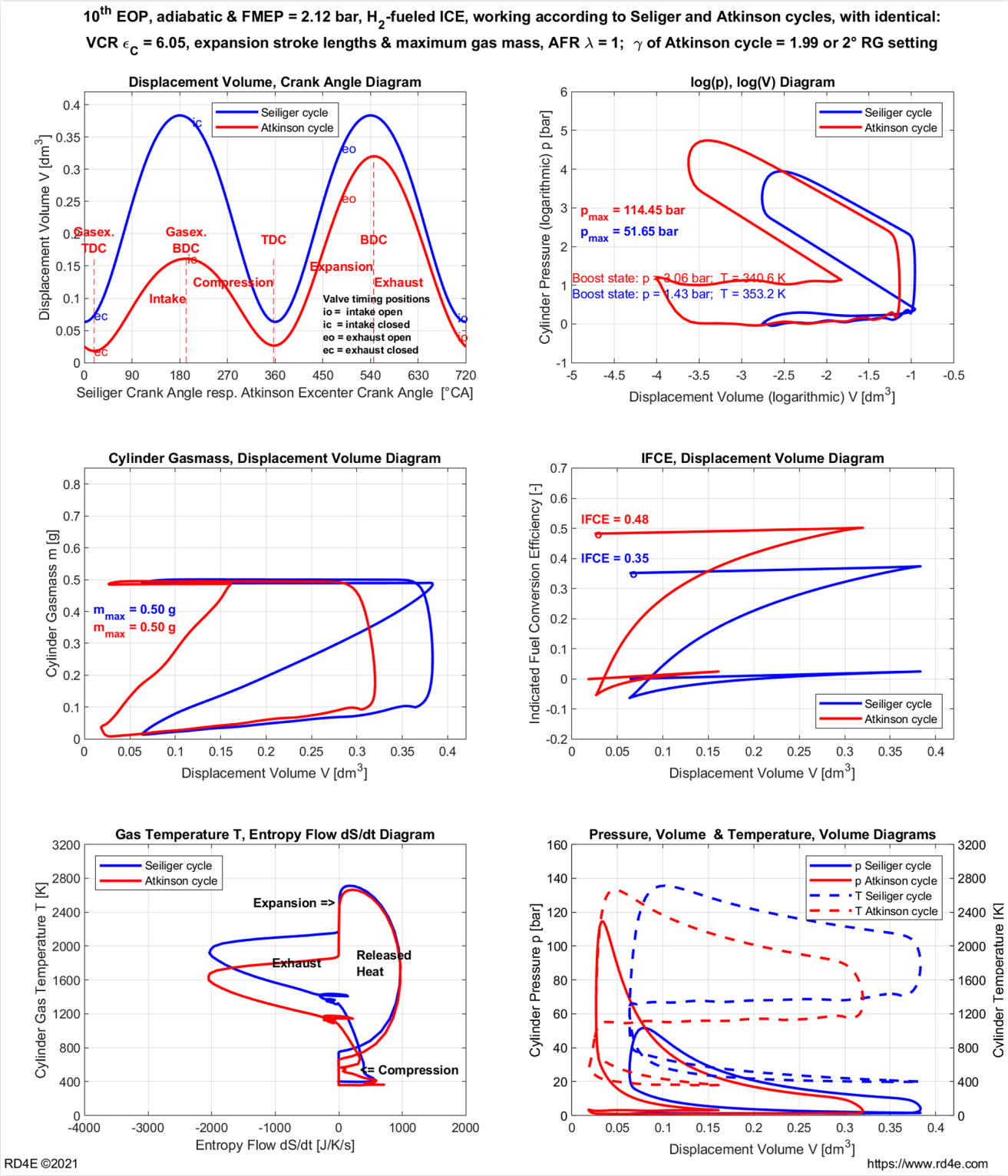

FIGURE A2-EOP-11 Simulation results of the true Atkinson and the Seiliger cycles by using the AVL BOOST tool. The Summary files for A & S are linked here, to examine all mean values of the simulation parameters.

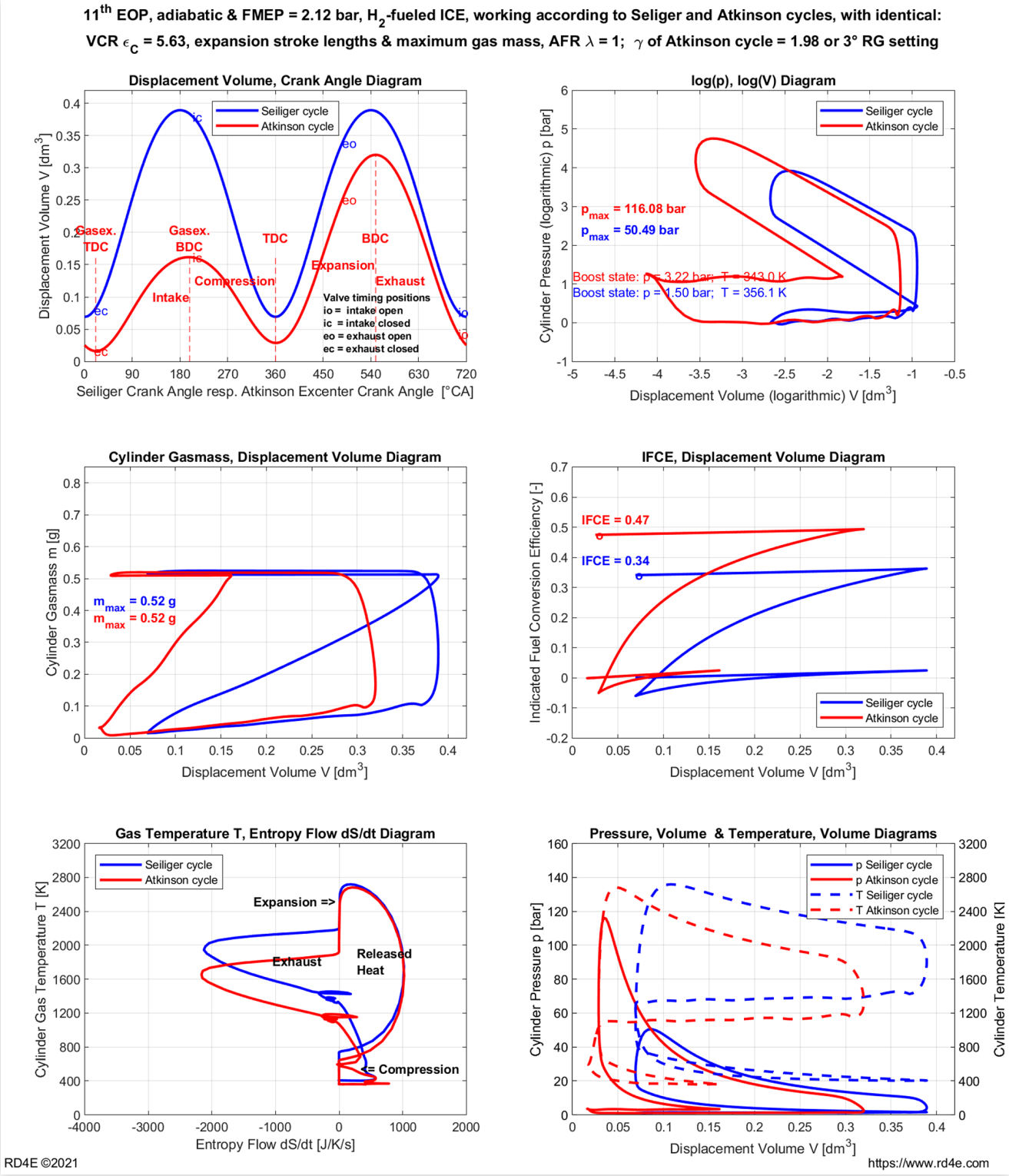

FIGURE A2-EOP-12 Simulation results of the true Atkinson and the Seiliger cycles by using the AVL BOOST tool. The Summary files for A & S are linked here, to examine all mean values of the simulation parameters.

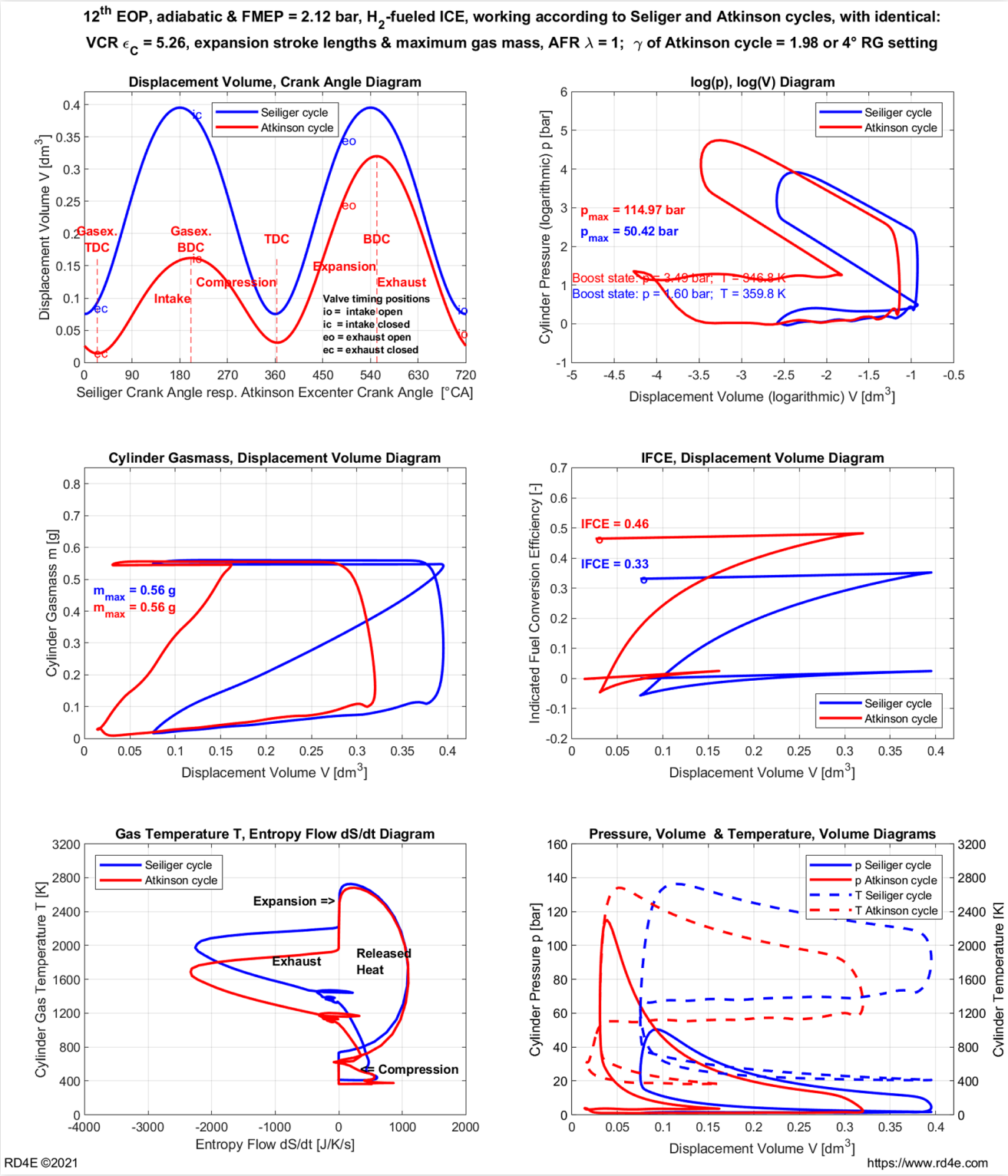

FIGURE A2-EOP-13 Simulation results of the true Atkinson and the Seiliger cycles by using the AVL BOOST tool. The Summary files for A & S are linked here, to examine all mean values of the simulation parameters.

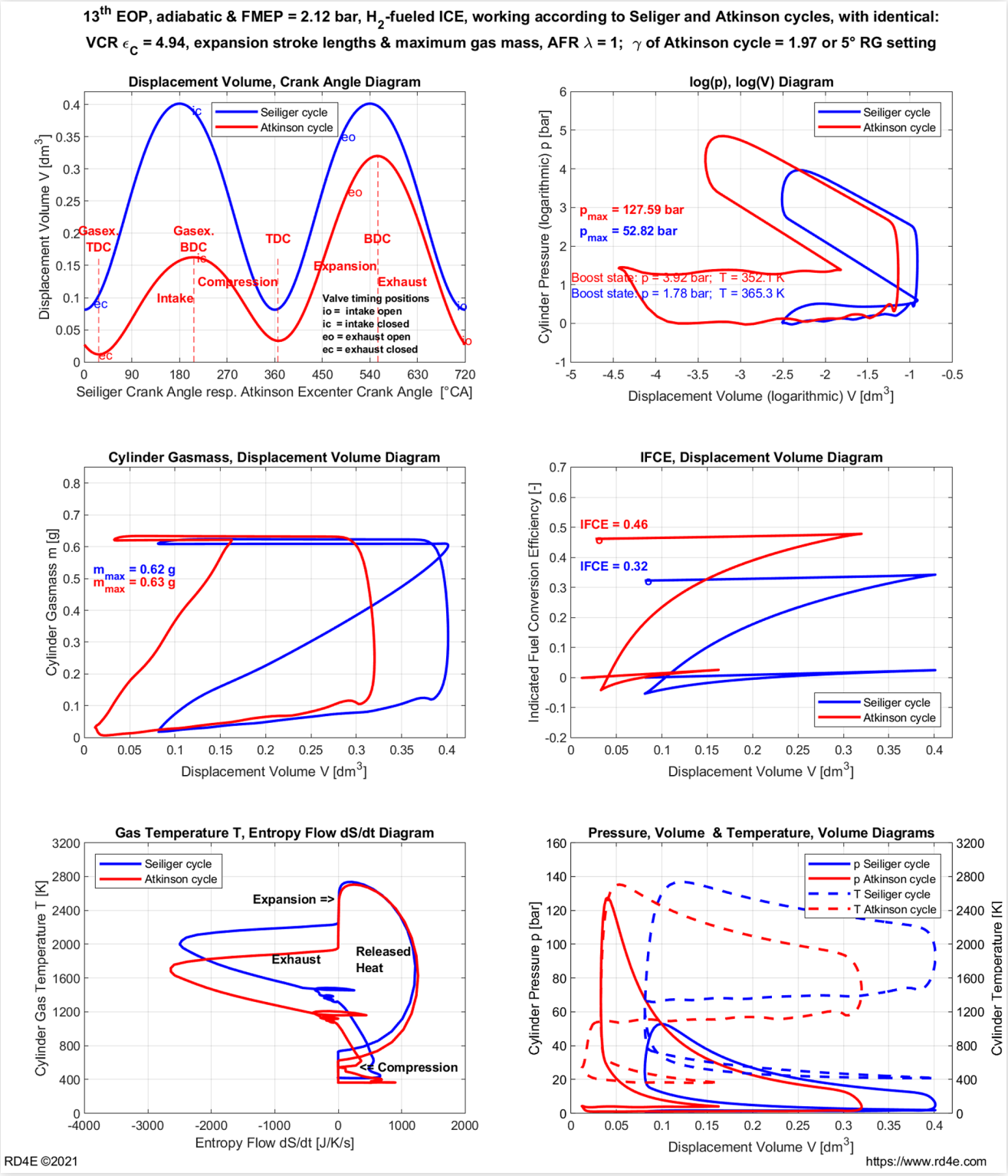

FIGURE A2-EOP-14 Simulation results of the true Atkinson and the Seiliger cycles by using the AVL BOOST tool. The Summary files for A & S are linked here, to examine all mean values of the simulation parameters.

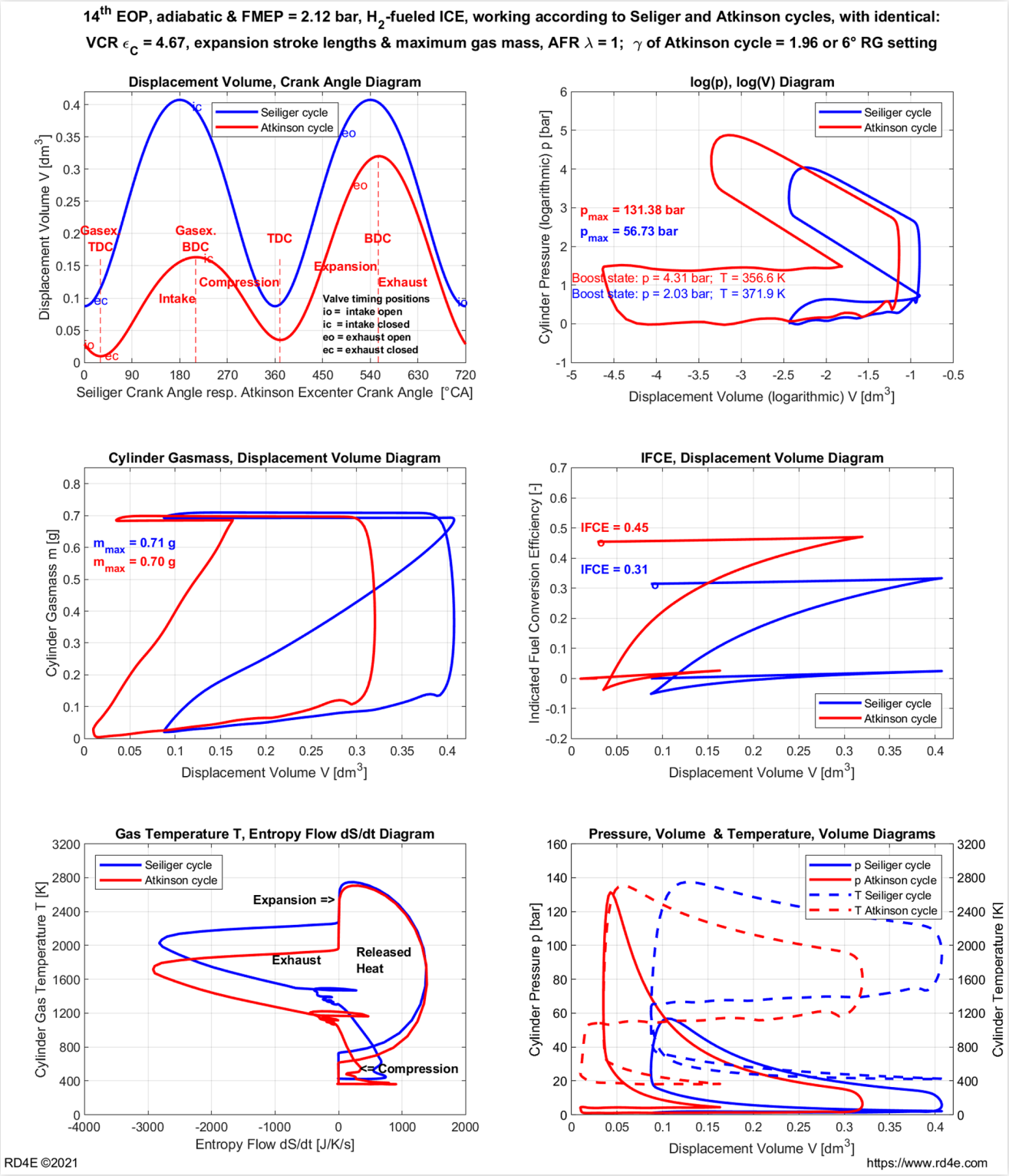

FIGURE A2-EOP-15 Simulation results of the true Atkinson and the Seiliger cycles by using the AVL BOOST tool. The Summary files for A & S are linked here, to examine all mean values of the simulation parameters.

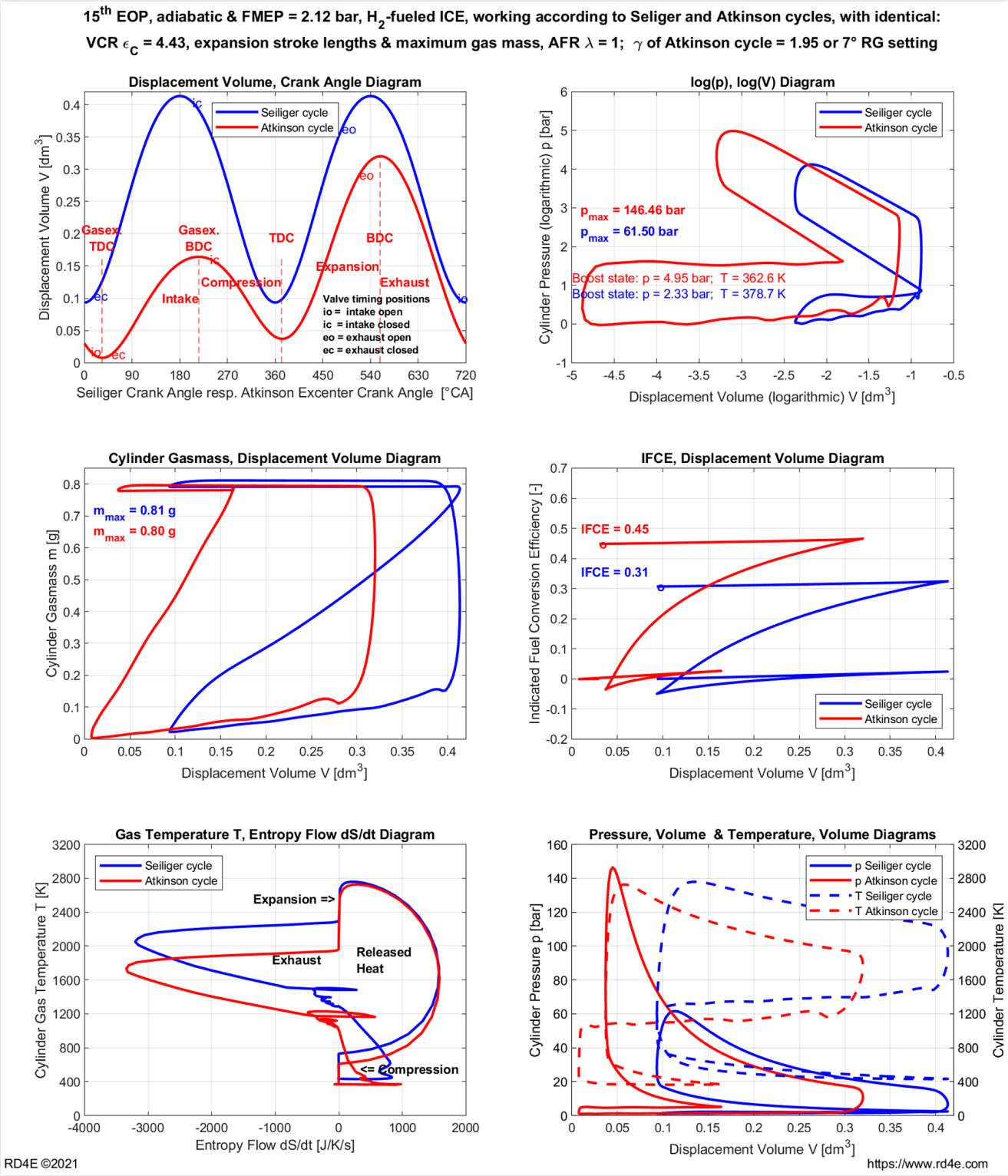

FIGURE A2-EOPS-01-15 Ultra Downsizing (UD) Load Control (LC) example

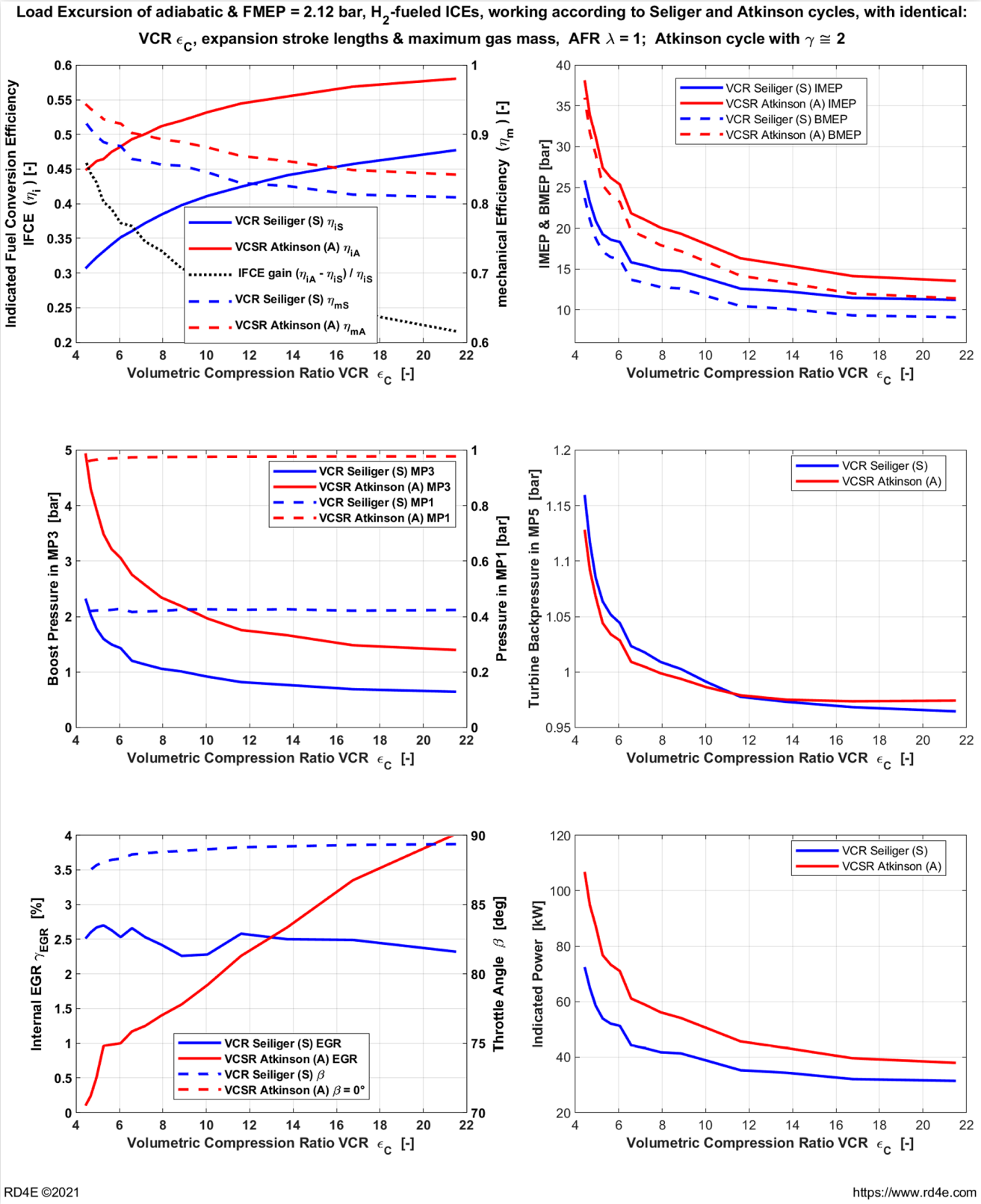

ISSN 0148-7191